排砂バイパストンネルにおける掃流砂間接計測のための信号解析手法の高度化

小柴　孝太

Improvement of Signal Analysis for Surrogate Bedload Monitoring at Sediment Bypass Tunnels

Takahiro Koshiba

Graduate School of Engineering
Kyoto University

This dissertation is submitted for the degree of
Doctor of Philosophy

February 2020

Acknowledgements

Firstly, I would like to express my sincere gratitude to my advisor Prof. Tetsuya Sumi for the continuous support of my study for six years, for his patience, motivation, and immense knowledge. His guidance helped me in all the time of research and writing of this thesis.

Besides my advisor, I would like to thank the rest of my thesis committee: Prof. Yasuhiro Takemon, Prof. Sameh A. Kantoush for their insightful comments and encouragement, but also for the hard question which incented me to widen my research from various perspectives.

I would like to extend my appreciation to Dr. Daisuke Nohara and Dr. Sohei Kobayashi not for their fruitful discussions but also many supports for field survey.

Further thanks go to Prof. Daizo Tsutsumi who aroused my deep interest in the wide research field of bedload surrogate monitoring. The experiment carried at the ETH was designed by him and this study would not be completed without the his support.

My sincere thanks also goes to Prof. Robert Boes, who provided me an opportunity to join their team in Switzerland, and who gave access to the laboratory and research facilities at the Laboratory of Hydraulics, Hydrology and Glaciology (VAW) of ETH Zurich. Without they precious support it would not be possible to conduct this research. A big thanks also goes to Dr. Christian Auel. He spent a great deal of discussion time for me and advised me on my study, field survey, and academic writing. Many thanks also to Dr. Carlos Wyss who supported our flume experiment at ETH.

Many thanks also go to the Public Works Research Institute (PWRI) for fruitful discussion. They also allowed me to conduct flume experiments with incredibly high speed flow.

My thanks also go out to CTI Engineering Co., Ltd. They shared important data obtained with their flume experiments with me.

I thank my labmates in for the stimulating discussions, for the sleepless nights we were working together before deadlines, and for all the fun.

I would like to thank Mr. Michinobu Nonaka. He designed the impact plate used in this study and always found time on every occasion I needed technical support.

Moreover, I am thankful to staffs in Chubu Regional Development Bureau, Tenryu River Office who manage the Koshibu Dam and the SBT. I asked them for a lot of informmation on the SBT and I really appreciate their patience.

This work was supported by JSPS KAKENHI Grant Number 18J14626 and Global Survivability Studies (GSS) Program, Kyoto University.

Last but not the least, I would like to thank my family: my wife and parents for supporting me spiritually throughout writing this thesis and my life in general.

Abstract

Sediment bypass tunnels are a leading technique to mitigate reservoir sedimentation. The method reduces incoming sediment to reservoirs by diverting sediment laden flood to a tunnel and draining directly to the downstream reaches. A major issue that induces their high maintenance cost is the tunnel invert hydro-abrasion caused by a combination of high sediment transport rate and high flow velocity. This study is dedicated to observe bedload transport in the tunnel to unveil the relation between abrasion and bedload transport distribution.

For the observation, we exploited impact plates, one of bedload surrogate monitoring systems, used in the field of erosion control. Impact plates consist of a steel plate embedded on river bed and a microphone and accelerometer backside of the plate. The impact induced by gravel collision to the plate is registered as signals from which we extract bedload information, i.e., grain size and bedload bedload transport rate. The device is already installed at the Koshibu Dam sediment bypass tunnel in Japan and monitoring operations. This study analyzes signals obtained from the operations on the basis of flume and on-site calibration experiments.

The signal analyses followed general signal processing approach composed of three steps: signal cleaning, feature extraction, and modeling. Signal cleaning was done with using Discrete Wavelet Transform by considering the properties of the signals obtained from impact plates, i.e., non-periodicity and abrupt change appearance. Then, a conventional feature quantity called impulses count was employed for feature extraction. For the modeling, we used non-parametric Gaussian process regression, which has both high expressive power and high interpretability by designing kernels that determines regression functions. Essentially, application of models based on flume experiments to field sites involves extrapolation. In order to cope with the weak point, our models were created only using flume experiment data with incorporating background knowledge into kernels. Then, the models were evaluated by the prediction accuracy to on-site experiment data where the prediction also presents extrapolation.

Finally, the best model was utilized for estimating spatiotemporal transition of grain size and bedload transport rate during the Koshibu Dam sediment bypass tunnel operations.

Table of contents

List of figures

List of tables

Chapter 1

Introduction

Today, many dams on which our civilization relies are suffering from reservoir sedimentation. Among a number of measures to meet the situation, the technology of Sediment Bypass Tunnels (SBTs) have been earning attention because of its advantages over others with respect to their efficiency and ecofriendliness. Although SBTs are already operated mainly in Japan, Switzerland, and Taiwan for years, the application worldwide is few. One reason for that is there is no clear guidance to use SBTs safely and sustainably, in particular, the lack of measures to mitigate tunnel invert abrasion cause by a combination of high flow velocity and high sediment flux. We believe that in order to address the abrasion problem, bedload transport monitoring in SBTs is inevitable to see the relation of sediment transport and consequent invert abrasion.

This chapter shortly introduces the reservoir sedimentation problem and SBTs. Then, we argue that, in order to make guidance to use SBTs, the mechanism of tunnel invert abrasion needs to be unveiled and for that, bedload monitoring in SBTs is the important first step. Finally, the chapter provides an outline of the thesis.

1.1 Reservoir sedimentation

The history of dam is incredibly long, it is said that the first dam in the world was built more than 5000 years ago (TATA & HOWARD, 2019, accessed November 2019). Although, at that time, the purposes of dams are only irrigation or flood control, today, dams are built worldwide for a wide range of purposes including irrigation, hydropower, water supply for drinking and industrial use, inland navigation, and flood control

(ICOLD, 2019b, accessed November 2019). Still irrigation accounts for the largest ratio of the global dam use, but the hydropower does the second largest ratio today. ICOLD (2019a) reports that the current gross reservoir storage reaches 6,000 km^3 with 45,000 large dams, dams with a height of 15 metres or greater, and 3,687 dams built after 2000 or under construction. And yet, more dams need to be constructed due to the increase in demand for water. Given their wide range of roles and the tremendous volume, it would be evident that dams contribute to great deal to human beings. Dams are important our resource, therefore we need to keep sustainable use of dams and reservoirs. Then, the question is what is a crucial obstacle for making it possible? The answer is the reservoir sedimentation problem.

With the nature of reservoirs, they store not only water but also sediment coming from upstream reaches. One example in Japan is shown in fig. 1.1. The photos clearly exhibit the progress of reservoir sedimentation in 36 years after dam completion. The current worldwide storage loss and annual sedimentation rate are estimated to be 570 km^3 (12%) and 31 km^3/year(0.52%/year) respectively (Sumi and Kantoush, 2011). This fact implies that without additional measures against the sedimentation problem, the total capacity of reservoirs would be decreased to less than half by 2100. Since a dam becomes useless when the reservoir is filled with sediment completely, stopping or mitigating sedimentation in reservoirs is a major task for long-term use of them.

Beside the storage loss noted above, sedimentation can cause other problems.

1. **Damages to turbines and loss of hydropower production**

   Water with the high sediment or suspended load concentration results in sediment blockage of dam outlet structures, that might impede appropriate dam operation. In addition, sediment makes hydropower turbines damaged (Auel, 2014; Cesare et al., 2001).

2. **Downstream impacts**

   Due to the trap of sediment at reservoirs, downstream reaches suffer from sediment shortage that causes channel erosion and ecosystem deterioration, well known as *hungry water* (Grams et al., 2007; Kondolf, 1997; Kondolf et al., 2014; Ma et al., 2012; Schmidt and Wilcock, 2008; Singer, 2010). Furthermore, the reduction in sediment volume transported to coastal areas lose the balance of sediment budget with coastline recessed (Gaillot and Piegay, 1999).

Japan is one of the countries where is suffering from a severe sedimentation problem. There are roughly 3,000 large dams in Japan, the forth greatest number in the

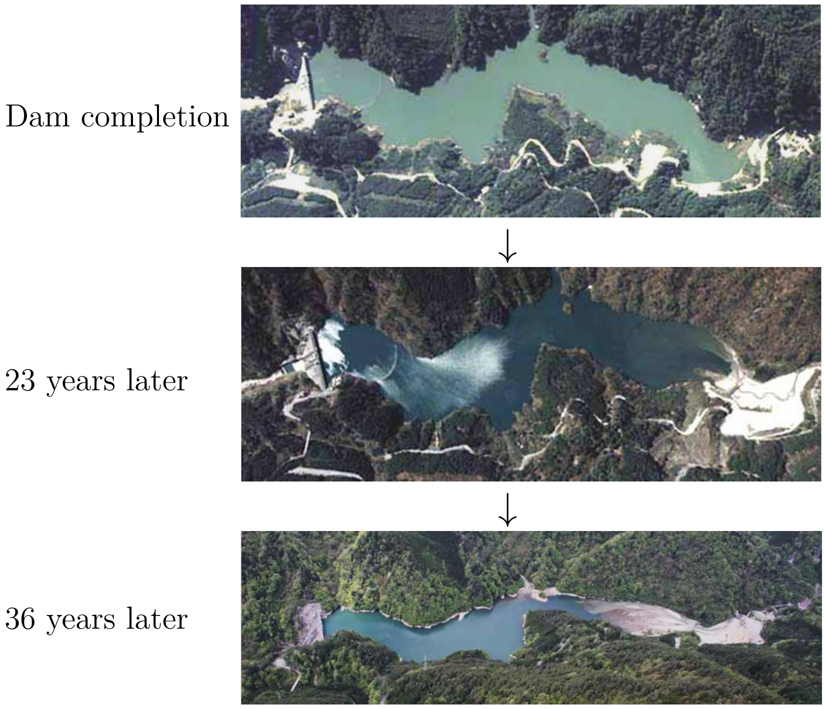

Fig. 1.1 Progress of sedimentation.

world. Due to a high sediment yield associated with the topographical, geological and hydrological conditions, the progress of sedimentation in Japan is severe. Generally, dams in Japan are allocated extra storage for catching sediment for 100 years without limiting their functions. The examination for 974 dams carried out in 2004 by the Japanese Ministry of Land, Infrastructure and Transport (MLIT), reports that the sedimentation rate in average is 8%, and the rate is as expected (Hakoishi and Sakurai, 2013). Even though the rate is expected value, considering the fact that around 50 dams experience their allocated storage for sediment filled (MLIT) and large part of dams were constructed approximately between 1950 and 1960 (period of high economic growth), we are required to take some measures urgently (Sumi et al., 2004).

1.2 Objective and motivation

Sediment bypass tunnels (SBTs) is a leading technique to mitigate reservoir sedimentation. This system connects the upstream and downstream of a dam and bypasses sediment-laden flood to downstream. SBTs are operated mainly in Japan, Switzerland, and Taiwan and regarded as a promising measure in the aspect of sedimentation mitigation efficiency and good impact on the downstream reaches. However, a topical problem on operating SBTs is severe invert abrasion caused by a combination of high flow velocity and sediment transport rate.

This study aims at revealing bedload transport movement inside of SBTs by conducting bedload monitoring. Understanding bedload transport must contribute on elucidation of the relation between bedload transport rate and the consequent invert abrasion. This is useful to predict abrasion depth under the given conditions, i.e., tunnel dimensions, bypass discharge, and invert lining material, and thus to think the better SBTs design, operation, and maintenance.

We used an indirect bedload monitoring system called an impact plate in this study. This is because direct monitoring in SBTs is impossible due to the intensive flow condition there. Impact plates register the acoustic and acceleration signal induced by sediment particles impact as a proxy of bedload transport rate. A large part of the study was dedicated to make a statistical model converting the signals to sediment transport information, i.e., grain size and bedload transport rate.

In this study, for the systematic modeling, I separated the analysis into three phases: signal cleaning, feature extraction, and modeling. This classification makes it easier to chose appropriate methods for analysis. In this process, I used data obtained from several laboratory experiments and on-site experiments at the Koshibu Dam SBT in Japan. Finally, sediment transport movement during the Koshibu Dam SBT operation is unveiled by using the model obtained here.

1.3 Outline of this thesis

The goal of this thesis is to provide guidance for designing, maintaining, and operating SBT appropriately with regard to reduction in the volume of invert abrasion with keeping the bypassing efficiency. For that, we improved existing bedload monitoring systems and output data analyzing methods so that the system works in SBT where sediment flux is extremely high. Then, the relation between spatiotemporal appearance of sediment flow and the consequence abrasion is investigated with actual observation.

Chapter 2 demonstrates the standpoint of SBTs in many measures against the reservoir sedimentation problem. Then, the structure of SBTs and related tasks that should be studies are listed up. I pick up an abrasion problem and explain the importance of bedload monitoring during SBTs operation. Finally, the Koshibu Dam SBT, our study field, is introduced.

Chapter 3 explains the general principle of surrogate bedload monitoring and see the existing systems with literature revews. Also, published methods for analyzing obtained data by the systems are discussed. Then, we introduce the novel device called Impact Plate, which is developed for making high sensitivity and toughness possible. Finally, the direction of our approach of data analyses is stated; making a model that has both high expressivity and interpretability through systematic process.

Chapter 4 consists of two part. The former illustrates measurement setup with impact plates. Laboratory and on-site experimental condition and the data obtained are illustrated.

The latter describes the signal analysis approach in this study. Here, the chapter emphasizes the importance of regarding analyses for surrogate bedload monitoring as not only in *Sedimentology* but also in *Signal Processing*. It enables us to use various techniques created in the field of Signal Processing. In particular, at least, we should aware of and keep a systematic process of signal processing, namely, signal denoising, feature extraction, and then, analysis.

Chapter 5 investigates the data obtained from impact plates for better denoising methods and feature extraction than that currently exploited. Given such characteristics of the signals as non-periodicity and possession of abrupt changes, we applied the *Discrete Wavelet Transform* to denoise signals. For feature extraction, we inherited a conventional one used in Japan called the *Pulse Count* method. The data used in the section was obtained through flume and field experiments.

Chapter 6 models to convert the extracted features to sediment transport rate and grain sizes. In order to make a model that has general applicability including SBTs and various natural rivers, the statistical approach called *Gaussian Processes* (GPs) was chosen. Pronounced advantages of GPs are their high expressivity and interpretability. The section shows models using GPs yield much better performance than that with a conventional simple approach, i.e., linear regression. Additionally, we demonstrate that the high interpretability of GPs makes extrapolation from data of flume experiments to that of actual SBTs operation possible.

In chapter 7, firstly the Koshibu Dam SBT operations in 2016 - 2019 are shown. Then, the model developed in the preceding two chapters is applied to some of the observed data. Results illustrate the temporal change of grain size and bedload transport rate during the SBT operation with the estimate uncertainty. These observation and analysis firstly enabled us to know spatiotemporal movement of sediment transport inside of an SBT.

Chapter 8 discusses two topics: surrogate bedload monitoring and the abrasion problem. About the first topic, we again highlights the advantages of using methods having high expressivity, and improvement to be done in future work. In addition, the expected problems for applying the model to data obtained in natural rivers and required experiments for dealing with that are noted. On the second topic, on the basis of our findings in the last two chapters, we suggest several things for better designing, maintenance, and operation of SBTs.

Chapter 2

Sediment Bypass Tunnels

There are many measures against the reservoir sedimentation problem. In general, the measures are classified into three on the basis of their approaches: sediment yield reduction, sediment routing, and sediment removal. This chapter clarifies the standpoint of SBTs in the classification. Even though SBTs have advantages over others in the aspect of favorable impact to downstream environment and semi-permanent sedimentation mitigation, still there are many unknown issues on them. Among them, the invert abrasion problem is picked up and the importance of bedload monitoring inside of SBTs is argued. At last, the Koshibu Dam SBT in Japan, my study field, is introduced.

2.1 Measures against reservoir sedimentation

There are many techniques for addressing the sedimentation problem for reservoirs (Morris and Fan, 1998, e.g.). In general, those are classified into three groups, also as in fig. 2.1 (Okano, 2005; Sumi et al., 2004).

1. **Sediment yield reduction**

   Measures in this group reduce incoming sediment from upstream reaches to a reservoir. Although nothing is better than reducing sediment yield from the upstream mountains by forestry conservation, this is not easy with regard to economic and technical aspects. Instead of the approach, one standard way is building a check dam at the upstream end of a reservoir. Recently, sediment replenishment with sediment stored in the check dams has been attracting attentions (e.g. Kantoush et al., 2010).

2. **Sediment routing**

   The next approach is routing sediment coming from upstream to downstream areas without letting sediment enter reservoirs. In this group, three major methodologies exist: bypassing sediment coming from upstream to downstream reaches directly with diverting and tunnel structures (sediment bypassing); flushing sediment from dam outlets by decreasing reservoir water level during flood events using the consequent increase of the dragging force (sluicing); flushing flood water with sediment from dam outlets without decreasing the reservoir water level but owing to their high density (venting of turbidity currents).

3. **Sediment removal**

   The last option, in the case that the precede two approaches do not work, is removing sediment from reservoirs. Excavating, dredging, and flushing are possible ways. Excavating and dredging remove sediment from a reservoir with heavy machinery so they are similar, but the target location in a reservoir is different; the former focuses on upstream region of a reservoir where is partially dried up artificially, to the contrary, the latter does middle to downstream area with pump-up apparatus. Flushing, less common than others but effective, output sediment with the same principle as that of sluicing. The difference is attempting to flush not only newly incoming sediment by a flood but also pre-deposited sediment in the reservoir, thus normally complete drawdown is required.

2.2 Sediment bypass tunnels

Although every technology has certain pros and cons and suitable reservoir properties (Sumi, 2013), sediment bypassing using *Sediment Bypass Tunnels* (SBTs) is a promising choice (Auel and Boes, 2012; Kashiwai et al., 1997; Sumi et al., 2004; Vischer et al., 1997). In general, an SBT consists of a tunnel, inlet gate, outlet, and weirs located at the upstream of a dam to divert flood into the tunnel as shown in fig. 2.2 (Auel and Boes, 2011a). The terminology of SBTs is still not clearly defined, it is understood that SBTs are mainly operated in Japan, Switzerland and Taiwan, as listed in table 2.1. Note that the first SBT in the world would be at the Nunobiki reservoir. Just eight years after the dam was completed the SBT was constructed, and this still works

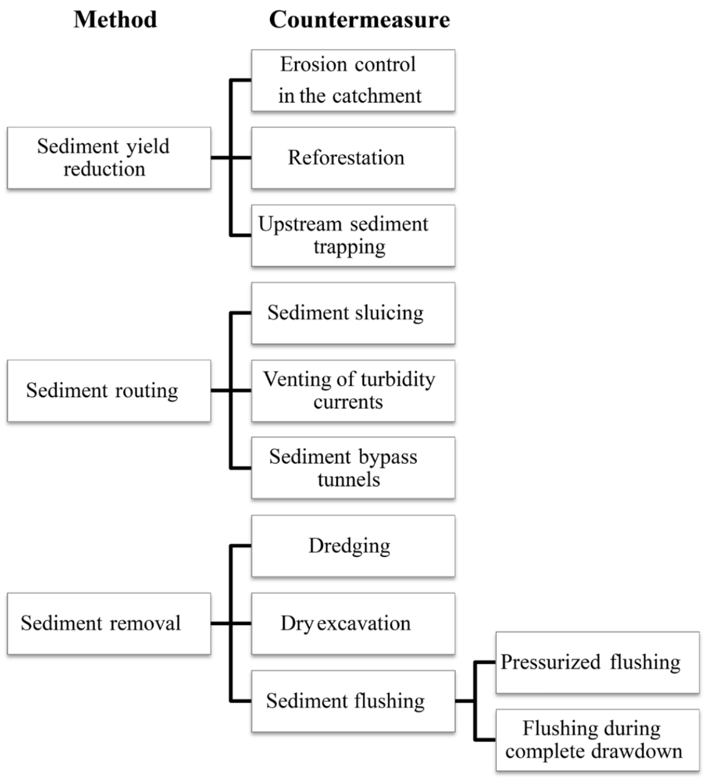

Fig. 2.1 Reservoir sedimentation countermeasures (adapted from Sumi et al. (2004) and Boes et al. (2014)).

effectively. It is estimated that without the SBT, the reservoir would have been filled with sediment by 1925. Another case, the Asahi SBT in Japan reported by Fukuroi (2012), is shown in fig. 2.3. Obviously, a large part of incoming sediment was bypassed by Asahi SBT, hence the accumulated sedimentation volume is lowered. The use of SBT would redistribute approximately 77 to 94% of incoming sediment (Auel et al., 2016).

Table 2.1 Sediment Bypass Tunnels in Japan, Switzerland, and Taiwan

Country	Reservoir name	Completion	Width×Height×Length	Slope	Discharge (Velocity)	Related works
		year	[m]×[m]×[m]	[%]	[m^3/s] ([m/s])	
JP	Nunobiki	1908	$2.9\times2.9\times258^{*}$	1.3	39 (-)	Sumi (2015); Sumi et al. (2004)
JP	Asahi	1998	$3.8\times3.8\times2350^{*}$	2.9	140 (11.4)	Fukuroi (2012); Harada (1997) Auel et al. (2018); Nakajima et al. (2015)
JP	Miwa	2005	$7.8\times7.8\times4308^{**}$	1.0	300 (10.8)	Kantoush et al. (2011); Sumi et al. (2012) Sakurai and Kobayashio (2015)
JP	Koshibu	2016	$7.95\times7.95\times3999^{**}$	2.0	370 (15.8)	Kashiwai and Kimura (2015); Takeuchi et al. (2017)
JP	Matsukawa	2016	$4.7\times4.8\times282^{*}$	4.0	200 (15.0)	Narusawa and Nishimoto (2017)
CH	Pfaffensprung	1922	$2.9\times2.9\times282^{**}$	2.0	220 (14)	Auel and Boes (2012); Hagmann et al. (2015) Müller and Walker (2015)
CH	Runcahez	1962	$3.8\times4.5\times572^{*}$	1.4	110 (9)	Jacobs and Hagmann (2015)
CH	Ual da Mulin	1962	$3.7\times3.7\times268^{***}$	0.043	145 (14.9)	
CH	Egschi	1976	$2.8\times2.8\times360^{***}$	2.6	50 (10)	
CH	Palagnedra	1977	$6.2\times6.1\times1760^{**}$	2.0	250 (13)	Baumer and Radogna (2015)
CH	Rempen	1986	$3.4\times3.4\times450^{**}$	4.0	80 (12)	
CH	Solis	2012	$4.4\times4.7\times968^{*}$	1.9	170 (11)	Martín et al. (2015); Oertli and Auel (2015) Albayrak et al. (2017); Facchini et al. (2015) Martín et al. (2017)
TW	Tsengwen	2017	$9.5\times9.5\times1235^{**}$	5.32	995 (18-30)	
TW	Nanhua	2018	$9.5\times9.5\times1287^{**}$	1.85	1000 (24.5)	Kung et al. (2015)
TW	Shihmen	in plan	$8.0\times9.0\times3685^{*}$	2.86	600 (10-20)	Lai et al. (2015); Lin et al. (2017)

JP : Japan, CH : Switzerland, TW : Taiwan (R.O.C)
* Hood-type shape
** Horseshoe shape
*** Circle shape
General information of every SBTs in Japan and Switzerland is in Auel (2014).

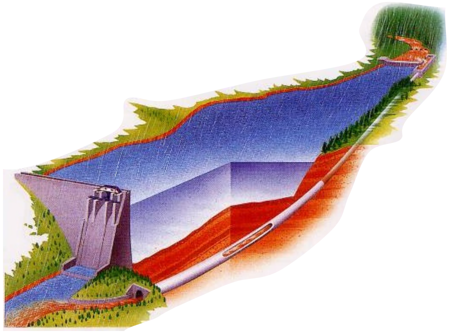

Fig. 2.2 A sketch of a sediment bypass tunnel.

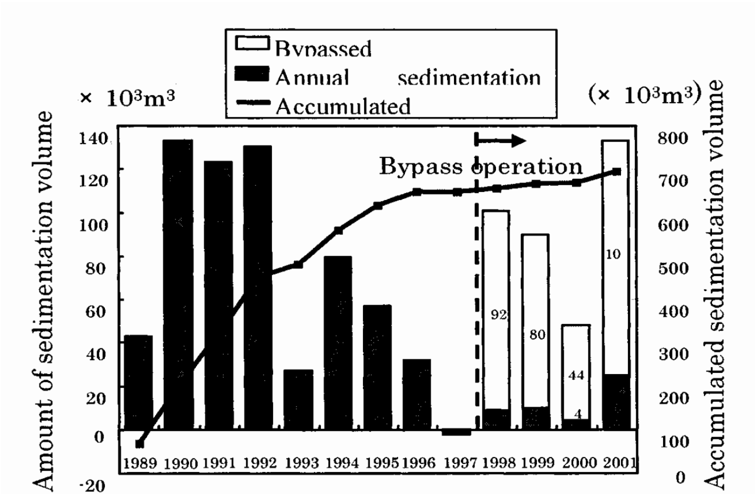

Fig. 2.3 Effect on the reduction of reservoir sedimentation by the use of bypass tunnel (adapted from Kataoka (2003)).

There are technical and ecological benefits in using SBTs over other methods. Technically, we can use SBTs without drawdown thus the economic loss of water users is limited. Although the high initial cost can not be ignored, the technology might be regarded as semi-permanent mitigation of the sedimentation. Furthermore, if a new dam is designed with an SBT from the stage of planning, economic efficiency and equability would be better (Auel et al., 2017b; Facchini et al., 2015; Martín et al., 2015). SBTs are also favorable to downstream ecology because they do not incur sudden change in sediment concentration unlike that by flushing; the downstream reaches receive flood water that presents more natural characteristics. For promoting SBTs and sharing the exiting problems with dam owners and researchers, International Workshop on Sediment Bypass Tunnels is held every two years since 2015 (e.g. Boes, 2015).

Nevertheless the advantages of SBTs over other measures, there are still few applications in the world. The primal reason for that is a lack of knowledge for designing, operating, and maintaining SBTs properly, so is cost effectiveness. Kubota (2017) summarized the research topics and problems related with SBTs as in table 2.2.

Table 2.2 Research topics and problems related with SBTs.

Target	Research topics or problems
Tunnel	Selection of an optimal bypass tunnel route Determination of bypass discharge Design of tunnel the cross section shape Invert abrasion problem
Diversion weir	Determination of diversion rule Necessity of check dams in the immediate upstream reaches Design of the diversion weir Diversion weir abrasion problem
Inlet	Design of inlet structures Inlet abrasion problem
Outlet	Design of outlet structures Outlet abrasion problem
Upstream reaches	Determination of inflow discharge to the reservoir Estimation of inflow sediment volume to the reservoir Grain size distribution of the inflow sediment
Downstream reaches	Monitoring grain size distribution and environmental effect Prediction of impact on downstream environment

2.3 Invert abrasion problem

As in the table, abrasion is severe problem related to most parts of an SBT. In particular, hydro-abrasion on the tunnel invert caused by a combination of high sediment transport rate and high flow velocity is a serious problem on which maintenance cost depend. Figure 2.4 shows severely damaged invert in the Asahi Dam SBT. The owner, Kansai Electric Power Co., Inc., is required annual rehabilitation works to fix it (Nakajima et al., 2015). However, countermeasures are not well established because the relation between sediment transport distribution and the consequent abrasion is not clear.

It is reported that most existing SBTs are affected by invert abrasion. Indeed, in the 2nd International Workshop on SBT held in Kyoto, Japan, the three tasks which should be elucidated for addressing the abrasion problem were identifie:

task1 How bedload is transported in SBTs.

Fig. 2.4 Invert damages at Asahi dam SBT in 2011.

task2 How bedload gives an impact on inverts.

task3 What kind of countermeasures are effective.

To elucidate them, first of all, bedload monitoring in SBTs is important because the volume of abrasion is highly related with the invert strength and bedload transport rate (Auel et al., 2018). Therefore, primary, this thesis is devoted to clarify **task1** by developing a bedlod transport monitoring system and apply this for the Koshibu dam SBTs in Japan. Then, I investigate the relation between the bedload observation and measured invert abrasion to know **task2**. On the basis of above works, finally, I give suggestion to improve SBTs design, operation and maintenance for reducing abrasion with keeping the bypass efficiency. This might contribute to **task3**).

2.4 The Koshibu Dam sediment bypass tunnel

The Koshibu dam is located at the Koshibu river catchment in Nagano prefecture, Japan, and is operated by the Ministry of Land, Infrastructure, Transport and Tourism (MLIT) for flood prevention, water supply and hydropower generation. The dam was built on 1969, and is 105 m high with a crest length of 293.3 m. The catchment area is 288 km^2 and mostly covered by forest and sediment supply prone area. Moreover, the reservoir received enormous severe floods and thus rapid sedimentation rate has been an issue for the dam management. Indeed, on 2015, the sedimentation volume exceeds 15.6 Million m^3almost reaching to 20.0 MCM of original designed sedimentation capacity.

Considering the proceeding Koshibu reservoir sedimentation, MLIT initiated the construction of the Koshibu dam SBT and the first operation was successfully achieved between 21st and 23rd of September 2016. The length of the SBT is 3,982 m with a cross section of circular shape and a plain invert with a slope of 2 %. The width and height are 5.5 m and 7.9 m, respectively. Most of the parts are rectilinear tunnel but the last approximately 600 m from the outlet is curved on the orographic right direction (Radius = 1000 m). Most of the tunnel invert is paved with the high strength concrete (50 N/mm^2), particularly in the first 20 m where is in the inlet facility and the next 30 m where the tunnel inclination is relatively high for accelerating incoming flow are reinforced with rubber-steel and steel-lining material respectively. Figure 2.5 shows the plan view of the Koshibu Dam SBT with location relation of the SBT inlet, outlet, tunnel, diversion weirs, and the Koshibu Dam body. A view from immediately downstream place to the SBT inlet and dam body is shown in fig. 2.6.

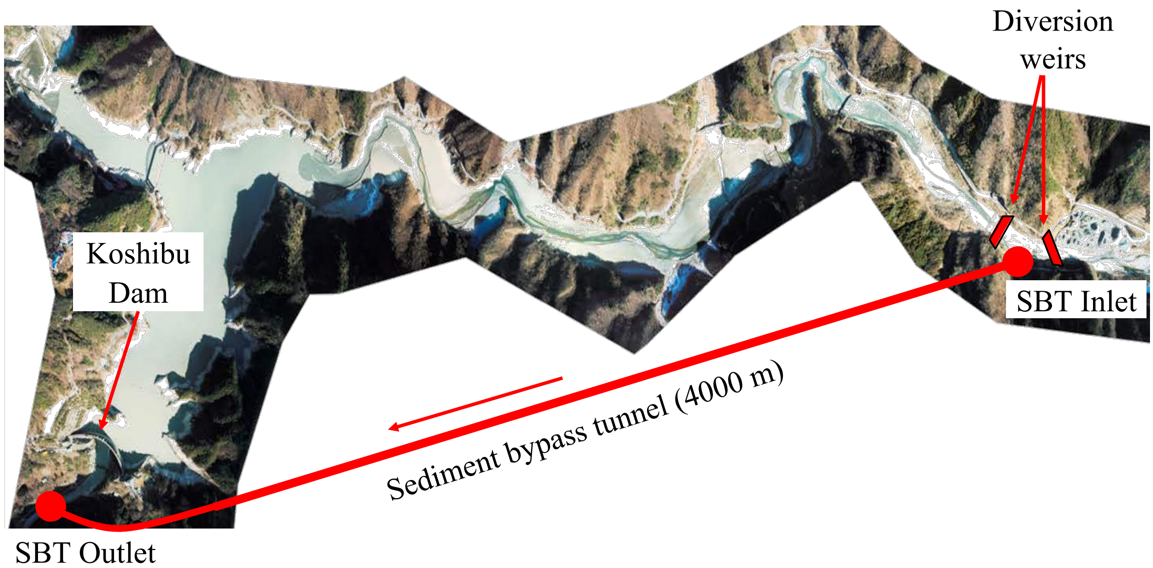

Fig. 2.5 The plan view of the Koshibu Dam SBT.

Fig. 2.6 The Koshibu dam and the SBT outlet.

Chapter 3

Surrogate Bedload Transport Monitoring

In the precede chapter, I highlighted the importance of bedload monitoring in SBTs. For doing that, however, I face a problem, too high sediment flux to monitor them directory. In such a situation, surrogate bedload monitoring is very attractive because they monitor bedload indirectly: via acoustic energy, vibrations caused by sediment impact on the river bed. In this chapter, the newly developed device called the Impact Plate is introduced followed by the introduction of existing surrogate monitoring systems. In addition, I roughly describe the history of Japanese techniques, because despite of the number of studies for decades, few study has published in English.

3.1 Surrogate monitoring

The study on bedload monitoring has been done for more than 100 years for disaster prevention. For the monitoring, the most simple and reliable is direct measurement. As a direct bedload transport rate (hereafter, BTR) measuring system, sediment samplers have been used for decades (Bunte et al., 2004; Helley and Smith, 1971; Reid et al., 1980). Nevertheless, despite the high reliability of the sampling systems, their disadvantages include their time-consuming and laborious nature and their ineffectiveness under conditions of high flow velocity and transportation of coarse sediment. Needless to say, SBTs are one of such places, where the maximum water velocity reaches 10 m/s and a wide diameter range of transported gravel prevails (Auel, 2014). To overcome the inconvenience of samplers, recent studies have attempted to collect indirect bedload transport observations by developing different bedload surrogate monitoring techniques (Gray et al., 2010; Mizuyama et al., 2010a; Rickenmann and McArdell, 2007).

Surrogate monitoring techniques record naturally generated signals caused by moving bedload particles, e.g., acoustic energy and vibration. These techniques generally consist of such sensors as microphones, hydrophone, accelerometer, and geophones placed on a steel box or pipe. Subsequently, they record acoustic or acceleration data generated by particles as they collide with each other, which are used to measure the bedload transportation properties by our analyses. These surrogate monitoring systems yield continuous bedload monitoring, and previous applications have covered a wide range of riverbed conditions. Further advantages include the relatively low maintenance cost and low interference with the water flow or bedload transportation (Rickenmann, 2017b).

Number of studies have been devoted for the improve of surrogate bedload monitoring systems. To know the history and proposed systems, Gray et al. (2010); Rickenmann (2017b) are comprehensive and detailed references. Among the number systems, in the next section, I pick up two, namely Swiss Plate Geophone and Japanese Pipe Microphone because these already apply to many rivers not only for academic but also for practical purposes.

3.2 Existing surrogate monitoring

3.2.1 Swiss Plate Geophone

The Swiss impact plate geophone (hereafter termed SPG) was developed in the early 1980s by a Swiss research group at the Swiss Federal Institute for Forest, Snow and Landscape Research (WSL) and the Laboratory of Hydraulics, Hydrology and Glaciology, Swiss Federal Institute of Technology (VAW). The SPG consists of a 50 cm by 36 cm steel plate with a geophone sensor (Geospace GS-20DX, manufactured by Geospace Technologies, Houston, TX) mounted underneath. The sensor is embedded in a steel frame and installed directly in a riverbed. A similar impact sensor, consisting of a metal plate with an accelerometer, has also been demonstrated to work effectively (Reid et al., 2007; Tsakiris et al., 2014). It is also recommended to make observations using two or more sensors to gain detailed information on bedload transport (Beylich and Laute, 2014; Mao et al., 2016). Recently, validation studies of bedload surrogate monitoring systems in flume experiments have been done, suggesting their usefulness for field observations in natural rivers. Numerous studies have been summarized in several recent reviews (Gray et al., 2010; Rickenmann, 2017a).

In particular, the SPG has been extensively used in European countries, especially in the mountainous areas of Switzerland, Austria, and Italy (Rickenmann, 2017b; Rickenmann et al., 2014). The SPG estimates the BTRs based on the plate vibration caused by passing sediment and recorded by the geophone sensor. At the Erlenbach Stream in Switzerland, field observations were done, and a high correlation between long-term BTRs and the SPG output was confirmed (Rickenmann et al., 2012). Furthermore, the SPG is resistant to the impact of sediment; therefore, installation of an SPG on the invert of an SBT is feasible. An SPG system was installed in an SBT for the first time at the Solis dam and has been in operation since 2012 (Auel and Boes, 2011b; Hagmann et al., 2015). However, it has also been found that the SPG cannot detect fine sediments with diameters smaller than 1 to 2 cm (Rickenmann et al., 2012, 2014; Wyss et al., 2016a,b). To clarify the effects of abrasion on the SBT invert, the grain size of the particles making contact is important, as the amount of abrasion on the invert not only depends on the sediment flux but also on the grain size (Auel, 2014).

3.2.2 Japanese Pipe microphone

In addition to the SPGs in Switzerland, another similar indirect BTR measuring system was developed and is widely used in Japan, namely, the Japanese pipe microphone (hereafter termed JPM) (Mizuyama et al., 2010a,b). The JPM consists of a metal pipe installed directly in a riverbed. When gravel and sand particles pass over the pipe, the number of colliding particles is counted based on the number of impulses in the sound pressure over time. The JPM system is already installed in some rivers in Japan, e.g., the Yodagiri and Koshibu rivers, and bedload transport observation is done at the Hodaka Sedimentation Observatory, DPRI, Kyoto University (Tsutsumi et al., 2010). The studies at the observatory reveal that the JPM can detect sediment with a diameter larger than 2 mm. However, the JPM often underestimates the bedload when particle impacts are successive and overlap. Moreover, the pipe has a small dimension in the flow direction (pipe diameter of 48.6 mm), resulting in particles jumping over the pipe. Additionally, the JPM deforms easily when hit by large stones, which negatively affects the sound collection

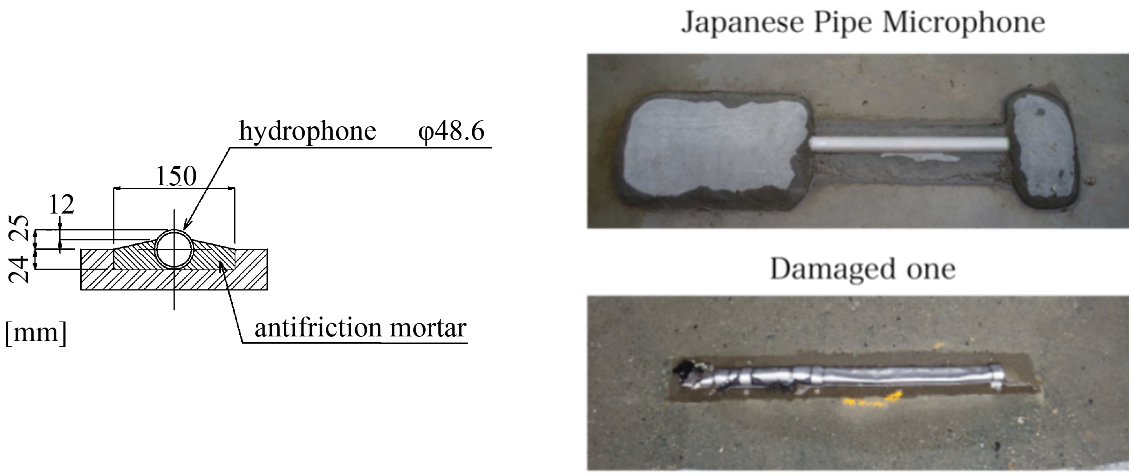

Fig. 3.1 Japanese Pipe Microphone (JPM). *Left*: a cross section of JPM installation. *Right*: A JPM installed on river bed.

3.2.3 The history of surrogate monitoring in Japan

Since the concept of surrogate monitoring was proposed by Taniguchi et al. (1992), many studies have been published in the field of erosion control (Sabo works) headed by JPM (called just *hydrophone* in japan) . In addition, JPMs already apply more than 300 sites for practical purposes. Even though the active studies of surrogate monitoring in Japan, few study has published in English, for example, Goto et al. (2014); Koshiba et al. (2018); Mizuyama et al. (2010a,b); Uchida et al. (2013) and Tsutsumi et al. (2018). In particular, there is no information of the sound pressure integration method in English, which is a de facto standard method in Japan to convert obtained signals to BTR. Therefore, I briefly go over the history and development of surrogate monitoring in Japan in this section.

The first application of a surrogate bedload monitoring system was reported by Kurihara and Miyamoto (1992). Considering several surrogate media of bedload transport, e.g., infrared light, and dielectric constant, they finally decided to use a microphone set in a steel pipe. The signal processing used in the study was already almost same as the current one using impulses with five levels of amplification factors (see section 5.2.1). The study experimentally found that the momentum of sediment and the recorded signal in magnitude has positive correlation. Following the study, JPMs have installed several sites for a long-term continuous observation for example in Mt. Rokko (Mizuyama et al., 1996), and the Joganji River (Mizuyama et al., 2002). They reported JPMs were promising because the temporal variation of relative sediment transport magnitude can be visualized by the inexpensive system. At the same time, however, they faced several difficulties for example in determining the appropriate number of amplification factors and a threshold with regard to water noise removal and finding the best pipe length. In particular, addressing reduction in impulses caused by dense signals in high sediment transport rate, Mizuyama et al. (2008) proposed the use of acoustic pressure. In the study, it was confirmed that the *integrated acoustic pressure*, the mean of acoustic pressure in a second registered every 200 ms, mitigates the problem.

Since the end of 2000s, some studies tried to quantify sediment transport rate. Nakatani (2009) made a regression model to estimate bedload transport rate with impulses with an amplification factor 16 and flow velocity. One method exploited in Japan widely is the *integrated acoustic pressure method* developed by Suzuki et al. (2010, 2013). This method is rather a phenomenological than a statistical approach and this has become a de facto standard to convert impulses by JPMs to sediment transport rate.

Finally, I argue several problems in present circumstances in Japan. Although there are many studies above, the fundamental part, impulse counting, depends on an analog signal processing that is in a black box. Therefore, it does not enable us to reproduce the process on computers and compare with other studies overseas. Also, the process has not improved significantly since the idea was firstly suggested in Kurihara and Miyamoto (1992) notwithstanding the improvement of speed and capability of our computers over the past decade. Another problem is few information on real observation in practical applications. Many sediment transport rates in rivers are reported but the computation processes are unclear.

3.3 Impact plate

For BTR monitoring in SBTs, the grain size distribution of the transported sediment is important because grain size and the number of particles are required elements for calculating the amount of abrasion using Ishibashi's formula, which is widely used in Japan (Auel et al., 2018; Ishibashi, 1983). Moreover, the installation costs should be limited for a surrogate bedload measurement system because the combination of multiple systems can realize a wide spatial bedload distribution in SBT, e.g., the cross-sectional bedload transport distribution. Therefore, an impact plate with a microphone has been selected for this study, considering both the robustness of plate-type systems and the JPM's ability to detect particles of $D_s > 2$ mm. Moreover, an acceleration sensor was mounted to the plate to compare the sensitivity with that of the microphone. The acceleration sensor is different from the traditional geophone sensor mounted on the SPG.

The *Impact Plate* (IP), manufactured by Hydrotech Co., Ltd. (Japan), was developed as an alternate surrogate BTR measurement system to overcome the disadvantages of the Japanese pipe microphone (Koshiba et al., 2018). The impact plate consists of a steel plate with the same dimensions as for the SPG system, a microphone, and an acceleration sensor. The same microphone model as for the JPM is mounted to the plate, and it registers microphone signals produced by the impact of sediment particles on the plate. The impact plate is expected to record the impact of small gravel particles with diameters of approximately 2 mm, which the JPM can detect, to ensure resistance to the impacts of coarse sediment.

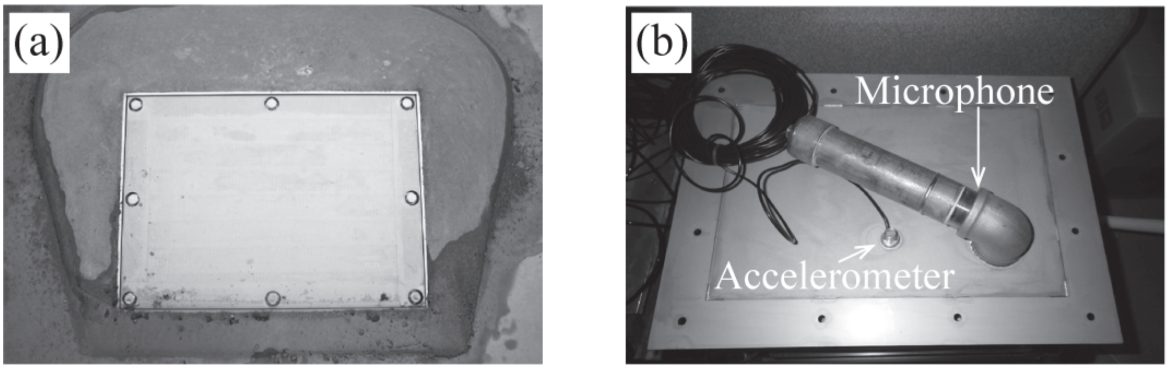

Fig. 3.2 An Impact Plate. *Left*: top view of an IP. *Right*: the back side of an IP with a microphone and accelerometer.

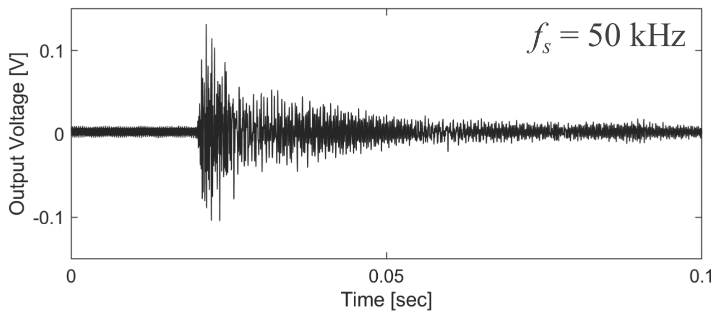

Fig. 3.3 A signal obtained recorded by an IP when a 10 mm gravel hit on the plate.

Another sensor is the acceleration sensor, which has already been used for bedload monitoring in several studies (Beylich and Laute, 2014; Møen et al., 2010; Reid et al., 2007; Rickenmann, 2017b; Rickenmann et al., 2017; Tsakiris et al., 2014). The impact plate also includes an acceleration sensor (GH-313A, which serves as a sensor, and GA-223, which functions as a converter; manufactured by KEYENCE, Japan), which improves the measurement by recording data simultaneously with the microphone. This concept originated from an attempt to replace the SPG 's geophone sensor with a sensor with a higher response frequency. It is likely that a sensor with a higher response frequency is more suitable for use on a rigid steel plate for detecting smaller grains than are detectable by a geophone sensor, which was designed for the observation of low-frequency seismic signals. The geophone sensor (20DX geophones) has a natural frequency of 10 Hz and flat response frequencies in the range of approximately 20 to 500 Hz, which are classified as ultralow frequencies (Roth et al., 2016; Wyss et al., 2016a). The frequency response of the replaced acceleration sensor is much higher, i.e., 0.1 to 80 kHz. Due to this difference, it might be expected that the acceleration sensor is more suitable than the geophone, especially for small bedload sediment fractions, because it has been reported that the dominant frequency of raw data of the signals produced by sediment impact increases as the sediment grain size decreases (Møen et al., 2010; Wyss et al., 2016a).

The impact plate consists of four parts: a steel plate, a microphone, an acceleration sensor, and a data logger. The steel plate is 49.2 cm in width, covering the whole flume width to allow all the test particles to pass over the plate, 35.8 cm in length in the flow direction and 1.5 cm in depth, being identical to the SPG(Rickenmann et al., 2014).

Chapter 4

Methodology

Impact plates are working for bedload monitoring at the Koshibu SBT since 2016. My goal is quantifying bedload transport rate and grain size during the SBT operations. For making a model to accomplish the goal, I carried out several laboratory and on-site experiments. Modeling introduced in the following chapters was done through the data collected in the experiments. This chapter illustrates the detail on the experiments and general findings on the raw data collected .

4.1 Measurement setup

Experimental data were collected by two set of flume experiments and one on-site experiment at the Koshibu dam SBT (about the Koshibu dam SBT, see section 2.4). A series of experiments was done to collect signals produced by various particles colliding with the plate under various flow conditions.

4.1.1 Laboratory flume experiments

Flume experiments were done in a flume facility at the Laboratory of Hydraulics, Hydrology and Glaciology (VAW) of ETH Zurich, Switzerland (Koshiba et al., 2018), and Public Works Research Institute (PWRI), Tsukuba, Japan. On the both tests, an IP was placed at the outlet of a fixed bed flume. In every experiment, gravel particles were transported along a flume, detected by the IP and captured using a basket. Both IPs were the one introduced in section 3.3, having a microphone and an accelerometer. A computer records the signals detected by the acceleration sensor and microphone sensor of the steel plate during each test with a sampling frequency f_s of 50 kHz. The plate was affixed to the flume using four screws and acoustically isolated using a rubber material to minimize the detection of vibrations from the flume structure. Figure 4.1 shows the downward facing side of the plate, where the smaller sensor represents the acceleration sensor and the microphone is connected to the steel pipe by a 90° angle pipe piece.

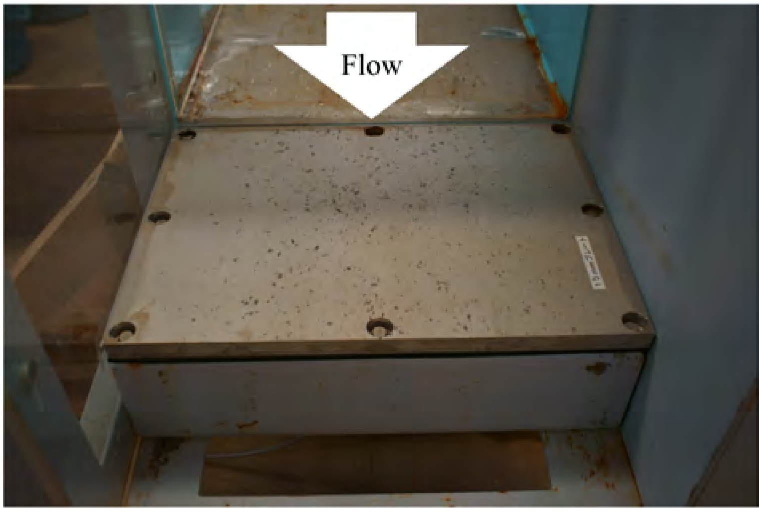

Fig. 4.1 Impact plate mounted below the steel plate in the test flume at ETH.

The experimental conditions conducted at ETH and PWRI are listed in table 4.1 and table 4.2 respectively.

All gravel particles used in the experiments were sampled from natural rivers, and, thus, had various shapes, including round, irregular, and angular shapes. The sediment was sieved in the laboratory to five uniform grain size fractions. According to the average weight and grain size , the sediment particle density can be calculated as ρ_s = 2700 kg/m^3. The number of particles for each release, P_n, in the tables was calculated on the basis of these parameters. A predefined sediment weight, W, was used for two small grain sizes, i.e., D_s = 2 mm and 5 mm. For D_s = 10 mm, 20 mm, 50 mm, and 100 mm, a fixed number of stones was added manually to the flow every five seconds.

Experimental flume at ETH

The experimental setup consisted of an elevated water supply tank that discharges water through a jetbox (Schwalt and Hager, 1992) to a rectangular glass-sided flume with inner width, height, and length dimensions of 0.50, 0.60, and 7.56 m, respectively fig. 4.2. The jetbox enables regulation of the flow depth by vertically moving the

Table 4.1 ETH Experimental conditions (conducted at ETH.

Case	Flow				Sediment			Repeat
	Q	V	h	Fr	D_s	W	P_n	
No.	[m^3/s]	[m/s]	[cm]	[-]	[mm]	[g]	[-]	[times]
E1	0.10	2.5	8.0	2.82	2	50*	3100	50
E2	0.10	2.5	8.0	2.82	5	50*	350	50
E3	0.10	2.5	8.0	2.82	10	40	20*	50
E4	0.10	2.5	8.0	2.82	50	620	20*	50
E5	0.10	2.5	8.0	2.82	100	29376	20*	43
E6	0.18	4.5	8.0	5.08	2	50*	3100	49
E7	0.18	4.5	8.0	5.08	5	50*	350	49
E8	0.18	4.5	8.0	5.08	10	40	20*	50
E9	0.18	4.5	8.0	5.08	50	620	20*	50
E10	0.18	4.5	8.0	5.08	100	29376	20*	48
E11***	0.10	2.5	8.0	2.82	50, 100	1516, 7344	10*, 5*	10
E12***	0.18	4.5	8.0	5.08	50, 100	1516, 7344	10*, 5*	10
E13***	0.10	2.5	8.0	2.82	5, 10	25*, 25*	175, 12.9	10
E14***	0.18	4.5	8.0	5.08	5, 10	25*, 25*	175, 12.9	10
E15***	0.10	2.5	8.0	2.82	5, 10, 50	25*, 25*, 416**	175, 12.9, 3*	10
E16***	0.18	4.5	8.0	5.08	5, 10, 50	25*, 25*, 416**	175, 12.9, 3*	10

* W and P_n with the symbol are accurate measured values, others were calculated.
** Mean weight.
*** Mixed grain size test.

opening. The discharge was controlled using a gate valve, and a magnetic discharge meter was mounted inside the piping unit of the water supply pump. The flow depth, h, was kept constant at 0.08 m, with the jetbox located at the entrance of the flume, whereas the water velocity was varied between two levels by controlling the flow discharge.

Experimental flume at PWRI

A special flume was prepared for conducting experiments with high flow velocities up to 10 m/s. The flume measures 10 m in length and 0.5 m in width and height with an inclination 1/50. Water was supplied from a nozzle with 0.2 m in width and 0.5 m in height.

Table 4.2 Experimental conditions (conducted at PWRI).

Case No.	Flow Q [m^3/s]	V [m/s]	h [cm]	Fr [-]	Sediment D_s [mm]	W [g]	P_n [-]	Repeat [times]
P1	1.0	8.7	23	18.3	2	100*	5300	5
P2	1.0	8.7	23	18.3	2	200*	10600	5
P3	1.0	8.7	23	18.3	2	300*	15900	5
P4	1.0	8.7	23	18.3	2	400*	21200	5
P5	1.0	8.7	23	18.3	10	56.7**	20*	50
P6	1.0	8.7	23	18.3	20	360.1**	20*	50
P7	1.0	8.7	23	18.3	50	2529.5**	10*	50
P8***	0.5	4.8	23	10.5	2, 5, 10 20 , 50	100*, 100*, 100*, 100*, 503	5300, 380, 36, 6, 2*	3
P9***	1.0	8.7	23	18.3	2, 5, 10 20 , 50	100*, 100*, 100*, 100*, 503	5300, 380, 36, 6, 2*	3
P10***	0.5	4.8	23	10.5	20, 50, 100	124.8, 1006, 3340.8	8*, 4*, 2*	3
P11***	1.0	8.7	23	18.3	20, 50, 100	124.8, 1006, 3340.8	8*, 4*, 2*	3

* W and P_n with the symbol are accurate measured values, others were calculated.
** Mean weight.
*** Mixed grain size test.

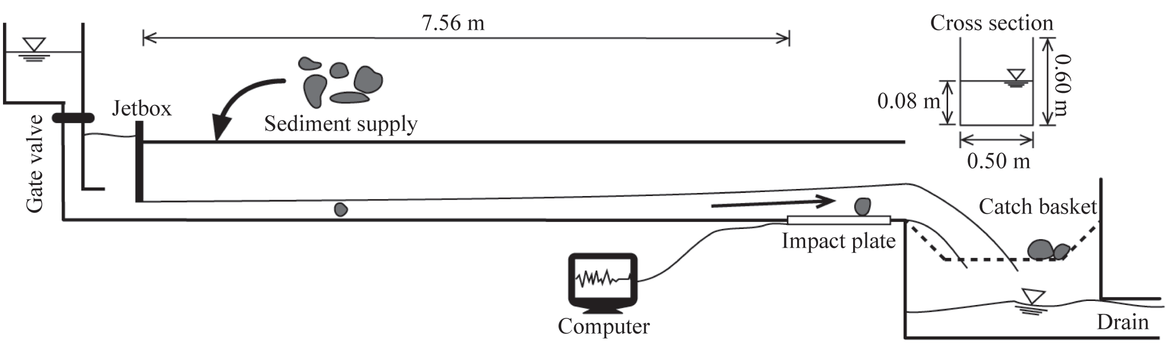

Fig. 4.2 Schematic view of the laboratory test flume at ETH.

4.1.2 Observation at the Koshibu SBT

Figure 4.3 shows the arrangement of measurement devices at the outlet. Five IPs named t15 are mounted in order to measure the cross sectional distribution of transported sediment. Moreover two additional IPs are mounted, t12 and t15 inclined. Original IPs (t15) have the thickness of 15 mm, while t12 stands for that with the thickness of 12 mm. The IPs named t15 inclined has the same dimensions as original one, while the plate is inclined with 10 degree. These were employed for comparative study with the original impact plates to investigate the difference of detection efficiency due to the different thickness and inclination respectively. In particular, the increase of sensitivity by inclining a plate is confirmed in Auel and Boes (2011b). I chose the inclination angle of 10 degree according to the study where the value showed the highest detection rate. In addition, to compare the experimental results with existing studies on JPMs were also employed for the observation. As in fig. 4.3, two JPMs were installed both left and right sides and the geophone sensors were mounted underneath the plate 3, 6, and 7 in addition to the microphone and the acceleration sensor.

Hereafter, IPs numbered one to five, t12, t15 inclined, JPMs numbered one and two are referred as `IP1` to `IP7`, `JPM1`, and `JPM2` respectively.

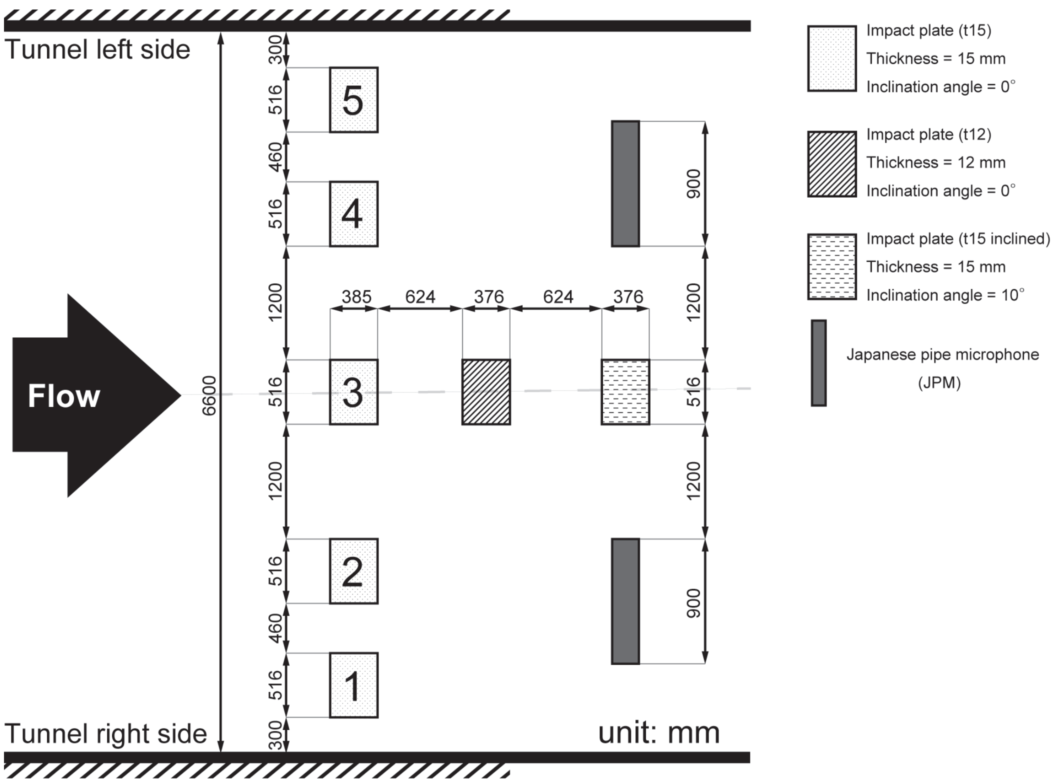

Fig. 4.3 Plan view of the bedload measurement apparatuses on the Koshibu dam SBT.

4.1.3 On-site experiment at the Koshibu SBT

For calibrating the impact plates, a series of field experiments were conducted at the Koshibu SBT by artificially flush sediment over the impact plates. Figure 4.4(a) is a photo taken at the outlet where five impact plates are installed (see also section 2.4). As in table 4.3, 10 cases of experimental conditions were tested varying grain size, sediment volume, and water discharge, fig. 4.4(b) exemplifies sediment placed in the tunnel. At `Case K8` and `Case K10`, sediment consists of mixed grain sizes were tested so that all grain sizes are included with a 3 $m^3$of volume for each. The grain sizes were determined on the basis of the Koshibu SBT's design that only sediment smaller than 100 mm in diameter was planned to be bypassed by collecting larger sediment particles at a divert equipment nearby the inlet. The test sediment was derived from the quarrying area in the immediate downstream of the inlet and carried by a dump truck into the tunnel just before every runs.

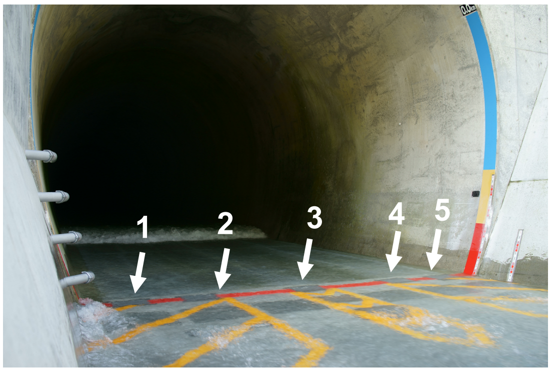

Fig. 4.4 Photos taken during the on-site experiment at the Koshibu SBT. a) Koshibu SBT outlet. White arrows show the impact plates, b) Input sediment (D_s = 10 mm, V = 5 m^3/s).

For observing uneven flow induced by the tunnel curvature, the 600 m from the outlet, sediment was placed 800 m upstream from the outlet. The natural riverine water stored in a pool impounded by diversion equipment was used for the experiment. In order not to allow sediment in the pool pass into the tunnel during the experiment, previous gate open operation was conducted for flushing the deposited sediment. Since the data volume of signals is extremely high and difficult to be stored continuously with the sampling frequency of 50 kHz, raw waveforms were recorded with the cycle of five seconds of recording and ten seconds of interval. Several cameras were also placed at the tunnel inside where sediment was placed and the outlet of the tunnel, flow depth at the outlet was estimated from the video recorded by the camera.

Table 4.3 Experimental conditions (conducted at the Koshibu dam SBT).

Case No.	Q [m^3/s]	V_{mean} [m/s]	D_s [mm]	V_s [m^3]
K1	10	2.60	10	1
K2	5	1.98	10	3
K3	5	1.85	50	3
K4	5	1.67	5	3
K5	5	2.03	10	5
K6	5	1.87	10	9
K7	20	3.66	10	9
K8*	5	1.89	5, 10, 50	3, 3, 3
K9	20	3.34	10	9
K10*	20	3.98	5, 10, 50	3, 3, 3

The value V_{mean} is mean flow velocity calculated from measured flow depths in every second estimated from recorded videos.

* Mixed grain size test.

4.1.4 Examples of raw waveforms obtained

It is important step to see signals obtained prior to analysis for understanding their visual properties. Figure 4.5 shows signals obtained by the impact plate at the flume experiment conducted at ETH. Signals registered by a microphone and accelerometer are shown with five grain sizes. Apparently, the amplitude has an positive correlation with the grain size of impacted gravels. A microphone tends to output signals with longer attenuation time than that by an accelerometer. In addition, microphone signals are affected by water noise especially for small grain sizes. For instance, it is not easy to separate signal with a grain size 2 mm gravel into water noise and sediment impact visually.

Overall, signals obtained from an accelerometer look better to analyze grain size and bedload transport rate. However, this should be evaluated quantitatively through signal processing techniques and analysis. I continue these analyses with using raw signals obtained because it might be reasonable to judge that these signals have a lot of information about sediment transport.

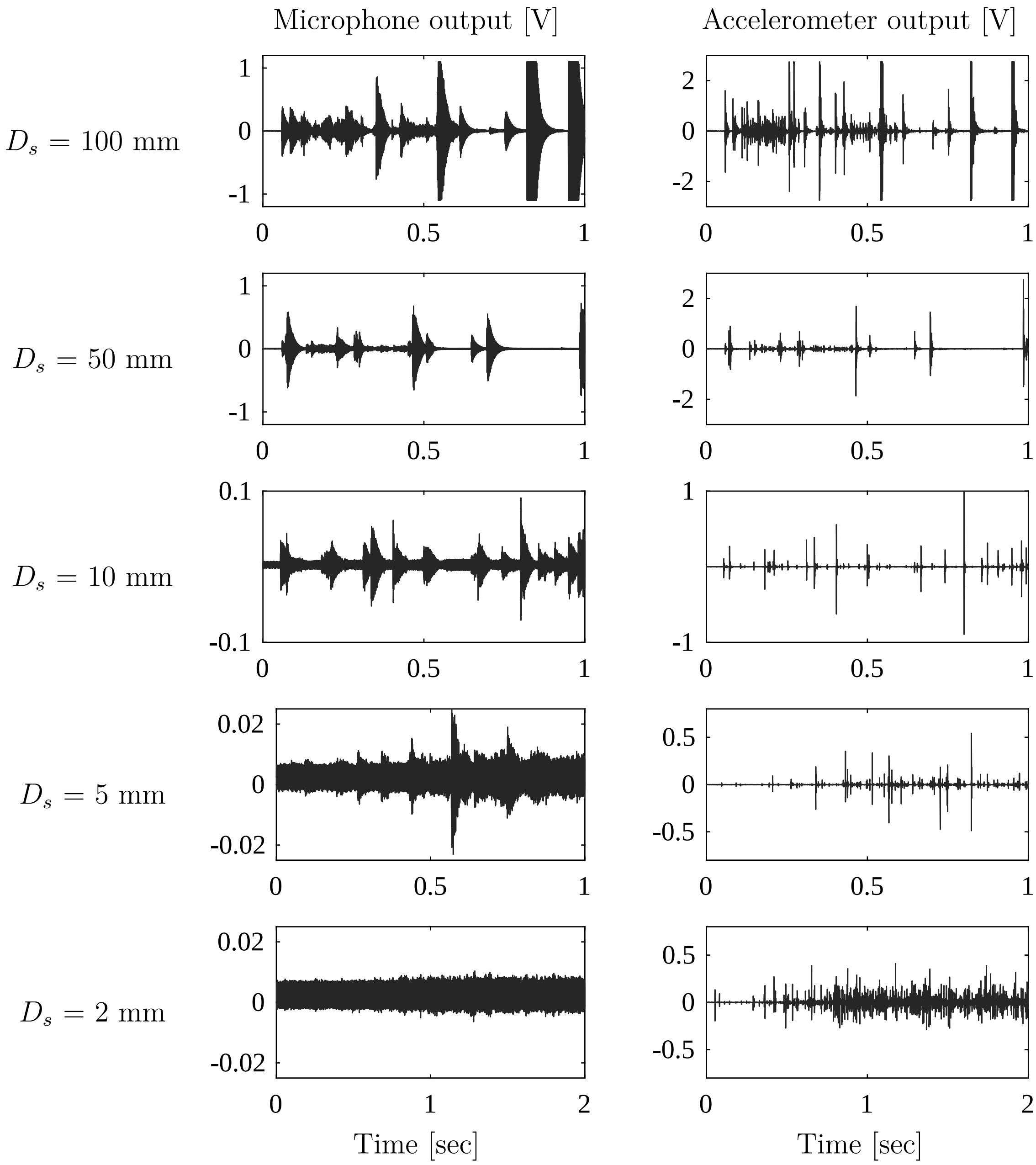

Fig. 4.5 Raw waveform signals obtained by an impact plate with a microphone and accelerometer. Signals were obtained from the flume experiment at ETH with a flow velocity 2.5 m/s.

4.2 Signal analysis approach

4.2.1 General signal analysis approach

This study aims at estimating bedload transport rate and grain size from signals obtained from IPs. Figure 4.6 depicts the general flow for signal processing, which consists of three steps. The first step is signal cleaning to get rid of noise riding on raw signals. For surrogate bedload monitoring, the noise is often produced from flow turbulence, hydrostatic pressure fluctuations, and bed-load noise Rickenmann (2017b). The second step is feature extraction. Here, denoised signals are converted to quantities presenting an analyzable data size, at the same time, the essence of the data. Impulses can be regarded as one of feature quantities from sediment signals. Finally, in the third step, some models are developed to estimate target information from the feature quantity. Statistical model is major technique for the step including simple linear regression and machine learning also often called AI (artificial intelligence). Although this procedure is common to all kinds of data science (e.g. Bishop, 2006; Zheng and Casari, 2018), studies in surrogate monitoring does not seem to follow that explicitly.

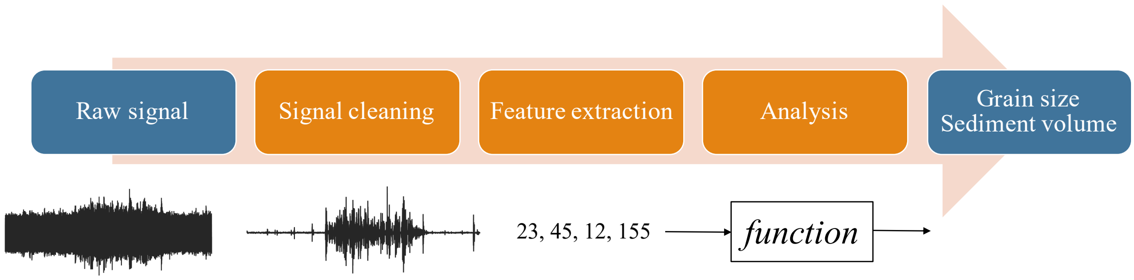

Fig. 4.6 The flow of signal processing.

4.2.2 Literature reviews from the view of signal analysis

I summarized some of existing surrogate bedload monitoring studies from the view of the above three steps table 4.4. I picked up several studies which were performed with calibration. This means that I excluded studies which use surrogate monitoring system without quantifying bedload transport rate and grain size. In the table, cleaning, feature quantity, and reported correlation are corresponding to the process in fig. 4.6.

For cleaning, band-pass filtering (BPF) and low-pass filtering (LPF) were major approach. These are methods to remove high frequency region in signals which are generally regarded as noise. Both filtering are performed using the Fourier Transform essentially. This should be noted that close to half the number of studies in the table did not process signal cleaning. Signal cleaning is an important step for effective signal processing. In fact recent studies on surrogate monitoring emphasize the possibility that this step would improve the bedload transport estimate accuracy (Geay et al., 2017; Krein et al., 2008; Mao et al., 2016; Wyss et al., 2016a). However, this step is often omitted or carried out with simple methods in the field of surrogate monitoring due to difficulty in recording raw signals continuously.

For feature extraction, mainly information on spikes, amplitude, and frequency are used. In table 4.4, I stands for features counting the number of spikes being over a prefixed threshold allowing for some differences. Some of the studies used I with several levels of threshold values to obtain information on amplitude distribution. The symbol A means methods computing mean, max, or integrated amplitude. These might be represent the energy of a signal caused by impacted gravels. Some representative values on frequency spectrum F have also used for estimating grain size recently. Generally, F and grain size present a negative correlation, and this is theoretically supported by Hertz's contact theory (Buttle and Scruby, 1990; Tsunoda et al., 1986; Uher and Beneš, 2012).

For analysis, in general, linear or power law regressions was employed to connect bedload transport rate or grain size and feature quantities. These were based on physical knowledge, and thus, highly understandable. A problem is that these regressions are not generally applicable and require calibrations at each field to estimate site-dependent parameters. In addition, the number of feature quantities used in the analyses were also few. It is reported that the bedload transport rate and grain size depend on many elements, e.g., bedload transport mode (saltation, rolling, sliding), bedload material, and transmission process of gravel impact through the material enclosing the sensor. These highly uncertain environment in estimation might cause the low accuracy if the analysis is done with few parameters or simple regression alone.

Table 4.4 Analysis procedures in existing studies.

Reference	Medium	Sensor	Study in	Cleaning	Feature quantity	Reported correlation
Taniguchi et al. (1992)	Pipe	Mic	Labo	BPF	I	$V_s \sim I$(LR)
Krein et al. (2008)	Plate	Mic	Labo, Field	ϕ	F	$D_s \sim F$(negative correlation)
Møen et al. (2010)	Plate	Acc	Labo, Field	BPF	A	$V_s \sim A$ (LR)
Mizuyama et al. (2010a)	Pipe	Mic	Field	ϕ	I	$V_s \sim I$(PR)
Mizuyama et al. (2010b)	Pipe	Mic	Field	LPF	A	$V_s \sim A$ (LR)
Rickenmann et al. (2012)	Plate	Geo	Field	ϕ	I, many others	$V_s \sim I$(LR)
Tsakiris et al. (2014)	Plate	Geo	Labo, Field	BPF	I	$V_s \sim I$(log-linear regression)
Beylich and Laute (2014)	Plate	Acc	Labo, Field	ϕ	A	$V_s \sim A$ (LR), $D_s \sim A$ (LR)
Goto et al. (2014)	Pipe	Mic	Labo	BPF	I, A	$D_s \sim A$ (LR), $N_p \sim I$(LR)
Dell'Agnese et al. (2014)	Pipe	Mic	Field	BPF	I	$V_s \sim I$(PR)
Rickenmann et al. (2014)	Plate	Plate	Field	ϕ	I, A_{abs}, A_{max}, A^2, many others	$V_s \sim I$(LR, PR), $V_s \sim A_{abs}$ (PR) $V_s \sim A_{max}$ (PR) , $V_s \sim A^2$ (PR)
Barrière et al. (2015)	Plate	Mic	Labo, Field	FAAD signal decomp.	I	$D_s \sim \{A, F\}$ (PR)
Mao et al. (2016)	Pipe	Mic	Labo, Field	BPF	I	$V_s \sim$ {combination of several I}(PR)
Wyss et al. (2016a)	Plate	Geo	Field	ϕ	I, F, A_{max}	$V_s = k\ I$, $k \sim D_s$ (Frechet distribution) $D_s \sim F$, A_{max} (PR)
Geay et al. (2017)	Plate	Geo	Field	ϕ	I, F	$D_s \sim F$(negative correlation)
Koshiba et al. (2018)	Plate	Mic	Labo	BPF	I, A_{max}	$V_s \sim I$(positive correlation) $D_s \sim A_{max}$ (PR)
This study	Plate	Mic, Acc	Labo, Field	DWT	I	$D_s \sim I$(GPR), $V_s \sim \{I, D_s\}$ (GPR)

Mic: Microphone or Hydrophone, Geo: Geophone, Acc: Accelerometer
Labo: Laboratory flume
LPF: Low-pass filter, BPF: Band-pass Filter, ϕ: No signal cleaning
I: Impulses, F: Representative frequency, A: Signal amplitude or integrate signal amplitude
$A \sim B$ (C) means the relation A and B is explained with method C
D_s : Grain size, V_s: Bedload transport rate, N_p: The number of particles
LR: Linear regression, PR: Power law regression

4.2.3 Signal analysis in this study

Notice that it is unfeasible to choose analyzing techniques from the tremendous number of combinations. Therefore I attempted to narrow them with some criteria. In this study, I attempted to improve mainly signal cleaning and analysis parts to estimate bedload transport rate and grain size. As in table 4.4, I used Discrete Wavelet Transform (DWT) for cleaning signals considering the characteristics of signals provided by gravel impact. This will be introduced in chapter 5. In feature extraction, the number of impulses (one of I in the table) was inherited from studies in Japan. For analysis (modelling), Gaussian Process Regression (GPR) was chosen. For explaining the reason to select (GPR), the inductive and deductive approaches in analysis should be noted here.

As demonstrated in fig. 4.7, every data analyses approach has inductive and deductive aspects (Higuchi, 2012). For long time, it has been regarded that science is supposed to be deductive, in other words, data analysis should be done on the basis of a combination of fundamental equations. Indeed, in the field of erosion control in Japan, proposed methods were strongly based on physics of particle movement and hydraulic. For instance, impulses were assumed to have proportional relation with the energy induced by particle collision. Regardless of the high interpretability of the approach, the adherence to deduction limited the generality and expressiveness of models particularly in surrogate monitoring on which a great deal of uncertainty involved.

In contrast, inductive approaches have been booming recently as the increase of data volume. The representative ones are machine leaning and deep learning which have high expression power thus we can extract complicated structure in data to predict information from new data. However, the structure tends to be a black box that is beyond our understanding. Accordingly, this study attempted to mix both approaches. Considering some extend of mechanism on sediment movement and hydraulics are known, I tried to incorporate them into a model. Akaike (1997, chap. 2) and Akaike et al. (2007) give more detailed and deep insight on modelling, prediction and knowledge discovery. They highlights the importance in using sufficiently flexible model to capture the data structure and regarding a priori background knowledge on the data as a part of the data.

In the following two chapters, I developed a model to estimate sediment transport rate and grain size with following fig. 4.6. Chapter 5 focuses on signal cleaning and feature extraction. Then, chapter 6 works on modelling with considering both flexible expression and interpretability.

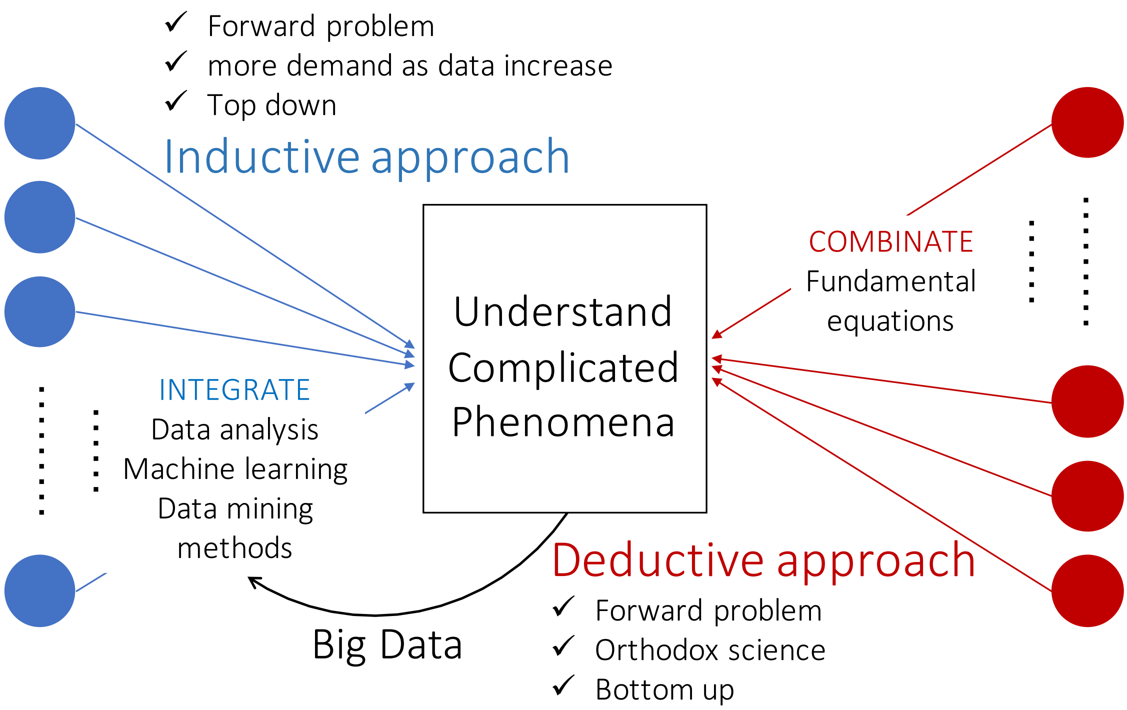

Fig. 4.7 The deductive and inductive approaches in the interpretation of phenomena. Adapted and modified from Higuchi (2012).

4.3 Data use

Note that signals obtained at real SBT operations in magnitude are often much greater than that from flume experiments. It implies that application of a model based on the experiments to real operations might involve extrapolation with much uncertainty presented. Furthermore, not having accurate sediment volume transported in real operations, I cannot verify the accuracy of a model. Accordingly, considering that signals in flume experiments were generally smaller than that in on-site experiments, I made a model using flume experimental data alone. In this step, an important thing is adding some a priori knowledge into a model in order to make it possible to use the model even if extrapolation needed. Then, the ability for extrapolation was verified by applying the model to data from on-site experiments.

Chapter 5

Signal Denoising and Feature Extraction

In the preceding chapter, the process of signal analysis was separated into three steps, namely, signal cleaning, feature extraction, and analyses. This chapter focuses on the signal cleaning and feature extraction. Regardless of few studies on signal cleaning, this is an important step to reveal signals' potential information. According to a particular feature of signals induced by gravel collision, I employed Discrete Wavelet Transform for denoising. Finally, I visually check the effect of denoising by drawing denoised signals and applying dimension reduction with principal component analysis. The procedure developed in this and the next chapters was applied for data obtained during the Koshibu dam SBT operations in chapter 7.

5.1 Signal Denoising

5.1.1 Conventional denoising

Signal denoising for surrogate monitoring needs to be concerned with the several kinds of noise as listed below.

- **Water noise**

  Signals produced by water noise sometimes hinder that by small particle impact, e.g., (Rickenmann, 2017b). Figure 5.1(a) shows a signal obtained by 50 g of gravels with a grain size of 2 mm under the flow of 4.5 m/s. Although signal increase in magnitude can be slightly seen in the middle part, signals are largely drown out by water noise.

- **Long echo**

  It is reported that signal overlapping due to long echo (reverberation) time causes the underestimation of transported sediment (Mizuyama et al., 2010b). Signals in fig. 5.1(b), induced by several gravels with a grain size of 100 mm under the flow of 4.5 m/s, markedly provide overlapping. This phenomenon is more pronounced in microphone signals than in accelerometer signals (Koshiba et al., 2018). Signal denoising should reduce the echo signals for enabling us to separate them precisely.

- **Signal saturation**

  When a large gravel hit on a plate, the consequent signal often saturates as in the first signal in fig. 5.1(b). Evidently, it causes the difficulty of distinguishing large sediment in grain size. In the use of IPs, Koshiba et al. (2018) found that gravels having grain sizes of larger than 50 mm are difficult to be distinguished due to saturation.

Fig. 5.1 Signals with noise. *Left*: Signals hindered by water noise, $D_s = 2$ mm, $W =$ 50 g, and $V = 4.5$ m/s. *Right*: Signals with overlapping and saturation. $D_s = 100$ mm, and $V = 4.5$ m/s.

The most common denoising approach might be the use of filtering with Fourier Transform (FT). This is the case even in surrogate monitoring, the use of low-/band- pass filtering are popular. For instance in Japan, an analog data converter loading a band-pass filter is used to extract signals around 4.5 kHz in the frequency domain. Recent technology has allowed us to apply more advanced signal processing techniques. Nevertheless, the filter has been used for more than 20 years without modifications. Furthermore, essentially, FT is especially suitable for periodical signals such as cardiogram.

In this study, I suggest the use of *Wavelet transform* (WT) istead of FT. The operation WT was developed for overcoming disadvantages of the FT. The noteworthy feature of WTs is the congeniality with signals containing non-periodical, noisy, and transient features. Therefore, with the advantage, WT is often used for anomaly detection and non-destructive test (Baydar and Ball, 2003; Figlus et al., 2014; Lin, 2001; Markalous et al., 2008). Given the signals by IPs contain the aforementioned features, WT seems to be a suitable choice to improve denoising.

5.1.2 Wavelet transform

In this section the principle of WT is briefly introduced. Firstly, the *continuous wavelet transform* (CWT) is presented with contrasting *short-time Fourier transform* (STFT)., then the *discrete wavelet transform* (DWT), used in the present study, is explained. The most standard and comprehensive textbook on WT is Daubechies (1992). Kim and Aggarwal (2000) is one of the easiest but practical tutorial for WT based on the comparison with FT. Suzuki et al. (1996) gives clear compare of WT and STFT with focusing on their role as a window function. Depczynski et al. (1997) demonstrates rather complicated and fundamental theories than others, but helpful due to it's practical information.

The operation STFT is a technique to overcome a disadvantage of the Fourier transform (FT) that the time information is lost in the frequency domain (frequency spectrum). STFT of function $x(t), x = x_0$ is defined as :

$$f\left(t_0, \omega\right) = \int_{-\infty}^{\infty} e^{-i\omega t} w\left(t - t_0\right) x(t) dt \tag{5.1}$$

where ω is a frequency and $w(t - t_0)$ is a window function. This equation means that the signal $x(t)$ is split by the window function defined by t_0 and the splitted signal is Fourier transformed. Therefore, STFT can give the frequency spectrum of $x(t)$ around at $t = t_0$.

Although STFT makes it possible to analyze time variation of frequency spectrum, it does not allow to obtain both good time and frequency resolutions. This causes, for example, setting the window short for observing time variation in detail inevitably invites the reduction of the frequency resolution. This trade-off relationship between time and frequency resolutions is known as *Heisenberg uncertainty principle*.

WT is a technique developed based on the idea to expand and contract the window function for avoiding the problem in STFT. The CWT is defined as:

$$\mathrm{CWT}(a,b) = \int_{-\infty}^{\infty} \psi_{a,b}(t)x(t)dt \tag{5.2}$$

$$\psi_{a,b}(t) = \frac{1}{\sqrt{a}}\psi\left(\frac{t-b}{a}\right) \tag{5.3}$$

where continuous parameters a and b are dilation and translation factors, respectively, and $\psi_{a,b}$ defined as eq. (5.3) is a function called the mother wavelet. Comparing with eq. (5.1), STFT can be interpreted as a method to express a signal with the superposition of sine and cosine curves, whereas CWT expresses that with the superposition of $\psi_{a,b}$. The mother wavelet, dilated by a and shifted by b, is corresponding to $e^{-i\omega w}(t-t_0)$ in STFT. The dilation and shift of $\psi_{a,b}$ make it possible to apply long time resolution to low frequency components of the signal and vice versa, hence CWT realizes both good time and frequency resolutions.

For the preparation of $\psi_{a,b}$, many functions have been suggested and all of them have different pros and cons, convenient list of wavelets in Rucka and Wilde (2006). In this study, *Daubechies wavelet*, one of the most widely used mother wavelets, was selected to analyze IP signals.

In DWT, the dilation and translation factors (a and b) have discrete values. The discrete wavelet is defined by discretizing $a = 2^j$ and $b = 2^j k$ in Eq. 5.1 as :

$$\psi_{j,k}(t) = 2^{-j/2}\psi\left(2^{-j}t-k\right) \tag{5.4}$$

here, j is a parameter called level which scales the wavelet by every 2 times and k plays a role of shifting. A remarkable benefit of DWT is the availability of multiresolution analysis when $\psi_{j,k}$ is an orthogonal wavelet (Addison, 2017; Daubechies, 1992). In this instance, a signal can be expanded in terms of discrete wavelets. This expansion is equivalent to the decomposition of a signal as :

$$x(t) = \sum_{j=1}^{j=J} d_j(t) + a_J(t) \tag{5.5}$$

here, d_j is called detail at level j and a_j is approximation at level j. Equation 5.5 illustrates a signal is decomposed into $d_1 + a_1$, then the a_1 is decomposed into $d_2 + a_2$, and this process is repeated until $j = J$. Literally, a_j provides an approximative component of $x(t)$ and the approximation becomes coarser as j increases. Therefore, respective d_j and a_j are corresponding to high-pass and low-pass filters. The detailed information of the multiresolution analysis is introduced in e.g., Addison (2017).

5.1.3 Denoising with DWT

For finding well denoised raw signals, each raw signal was once decomposed using DWT with Daubechies 6 wavelet at level 5. The original signal was decomposed into five levels of details and one approximation (residual). Then, each detail coefficient was shrinked, so called *soft-thresholding* (Donoho and Johnstone, 1994). The threshold was the maximum value of detail coefficients at each level, that appeared in a signal produced by water flow of $V = 4.5$ m/s without any sediment. This procedure meant to reduce noise caused by water flow. Finally, each coefficient was reconstructed to the time domain signal. Figure 5.2 exemplifies the DWT decomposing procedure. The original signal (s) is decomposed into five levels of high-passed signals d_j after soft thresholding, here d_j illustrates level j reconstructed signals ($j = 1, \ldots, 5$). The signal a_5 is a residual of the decomposition and corresponding to the most approximative (low-passed) composition of the original signal. In contrast, d_1 shows the most detailed (high frequency) component of the original signal.

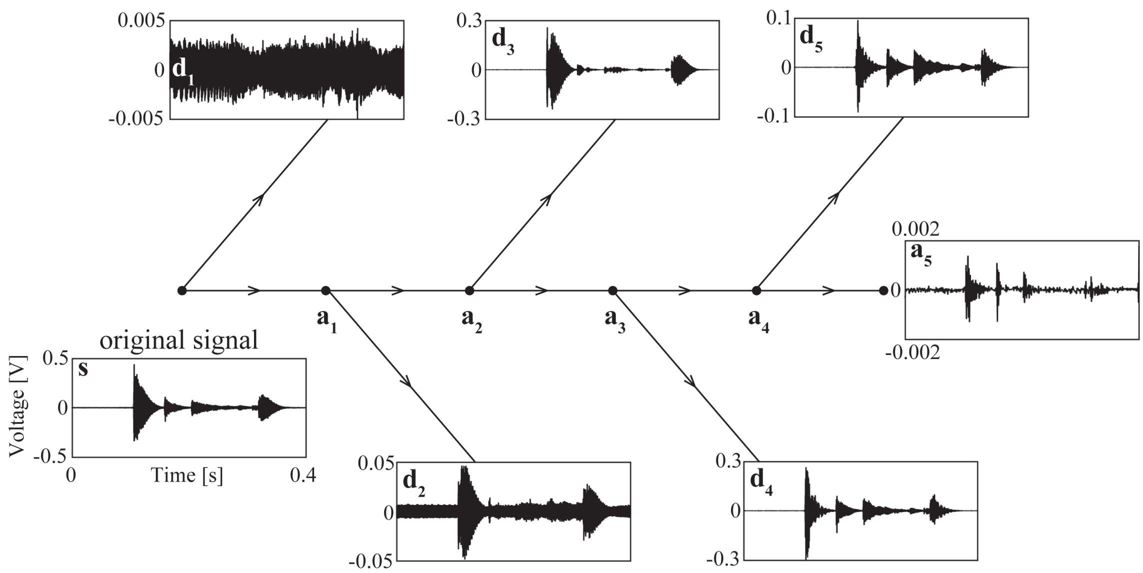

Fig. 5.2 A schematic chart illustrating the signal decomposition process, the original signal (s) is decomposed with DWT into high-pass filtered signals (d_1-d_5) and the residual (a_5).

5.2 Feature Extraction

5.2.1 The number of impulses

Since the recording raw signals requires a huge volume of storage and electricity, a data compression method called the number of impulses (I_{ps}) has been widely used for sediment monitoring with JPM (Mizuyama et al., 2010a). Impulses are counted simultaneously with the raw signal recording through analog signal processing in a data logger (fig. 5.3). Firstly, the raw signal (fig. 5.3a) is sent through a band-path filter to extract a frequency of around 4.6 kHz, which was previously computed as the most effective frequency by the manufacturer (fig. 5.3b). Subsequently, the filtered raw signal is transformed into absolute values hence all the negative values are changed to positive ones (fig. 5.3c). Then, an envelope curve is generated and the enveloped signal is exported to 6 different channels in which the wave is amplified by factors of 2, 4, 16, 64, 256, and 1024 times.

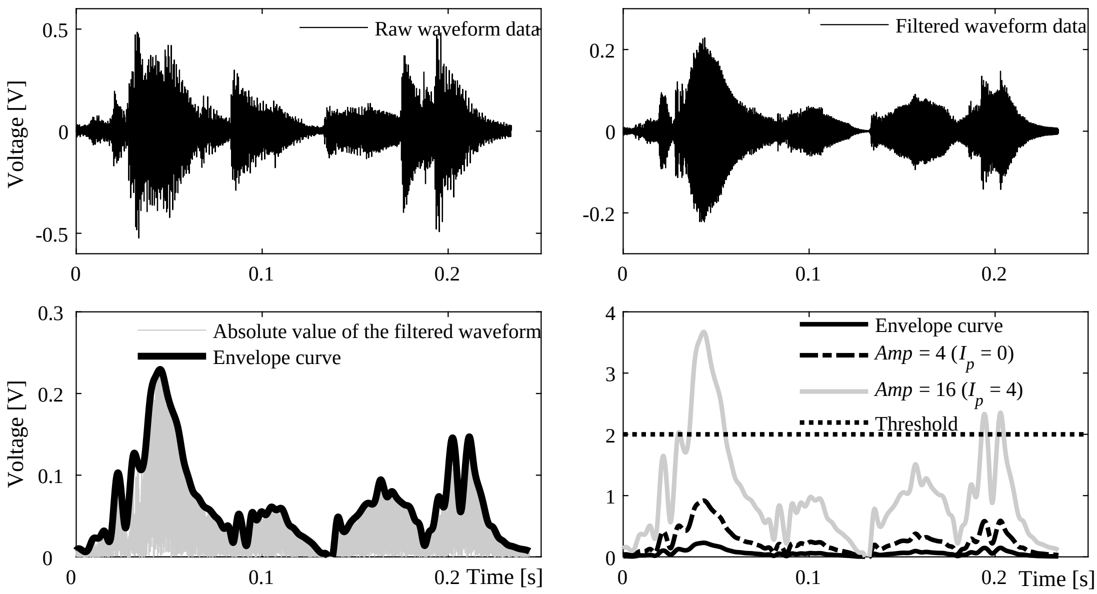

Fig. 5.3 Process to count the number of impulses. (a) A recorded raw signal, (b) The band-pass filtered signal, (c) Transformation into absolute value and enveloping, (d) Amplification and impulse count.

5.2.2 Denoising with DWT

From one original signal, totally 31 patterns of signals were generated as a combination of five signals (d_1-d_5). Then, impulses were counted from the generated denoised signals in the same manner as the conventional impulse count (fig. 5.3cd). Here, 11 levels of amplification factors (Amp), $Amp = 2^0, \ldots, 2^{10}$, were employed. The threshold was set to 0.5 V, which is equivalent to threshold for a non amplified signal ($Amp = 2^0$), through try and error.

5.3 Evaluation of the denoising

The goodness of denoising and feature extraction should be evaluated quantitatively by applying models. However, we are worth visually checking denoised signals to know whether the process was done as expected or not. In this section, some of the denoised signals are picked up to see the effect of denoising using DWTs. In addition, principal component analysis (PCA) was exploited to reduce the dimension of impulses from 11 to 2 and see their potential to distinguish grain sizes.

5.3.1 Comparison of denoised signals denoised by FT and WT

The denoised signals by DWT and a band-pass filter around 4.6 kHz using FT of noised signals in fig. 5.1 are shown in fig. 5.4. The signals in the last row are the sum of decomposed singnals $d_2 + d_3 + d_4 + d_5$ and $d_1 + d_5$ respectively given in fig. 5.2. Apparently, in both waveforms, water noise was removed well by using DWT. Also for echo and saturation, DWT seemed to mitigate them. However, it is also possible that DWT weakened signals too much. Suitable combination of d_1-d_5 is decided according to model precision in the next chapter.

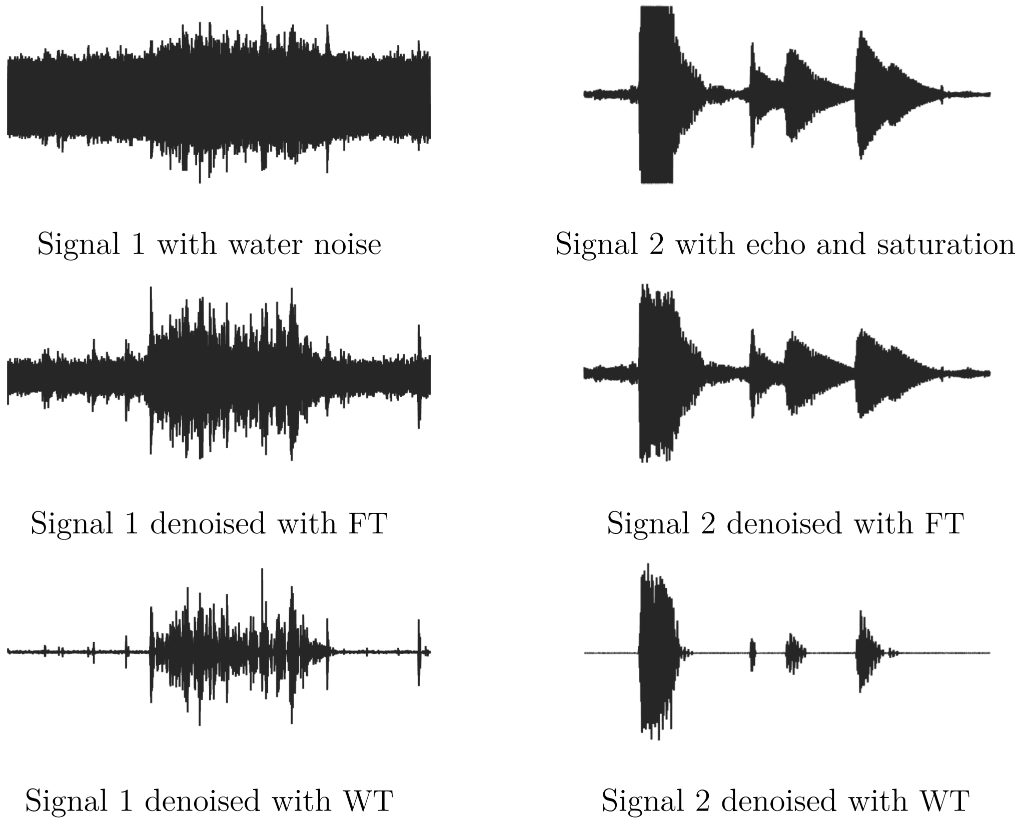

Fig. 5.4 *First column* and *Second column* are denoised results of signals shown in fig. 5.1(a) and fig. 5.1(b) respectively. *First row*: Original signals. *Middle row*: Denoised by a band-pass filter around 4.6 kHz. *Last row*: Denoised by DWT, $d_2 + d_3 + d_4 + d_5$ and $d_1 + d_5$.

5.3.2 Visualize the number of impulses with PCA

The dimension of the number of impulses at `Case E1 - E10` were reduced from eleven to three by using PCA. By this technique, the data is converted to be able to visualized in three dimension space as in fig. 5.5. Overall, the DWT makes it easier to group them by grain size, composing clearer clusters for each grain size than that data denoised by FT. In particular, focusing on data with grain sizes of 50 mm and 100 mm, impulses from denoised signals by FT is mixed and hard to distinguish. It might be resulted from the insufficient reduction of signal saturation. In contrast, denoising with DWT significantly solved the problem.

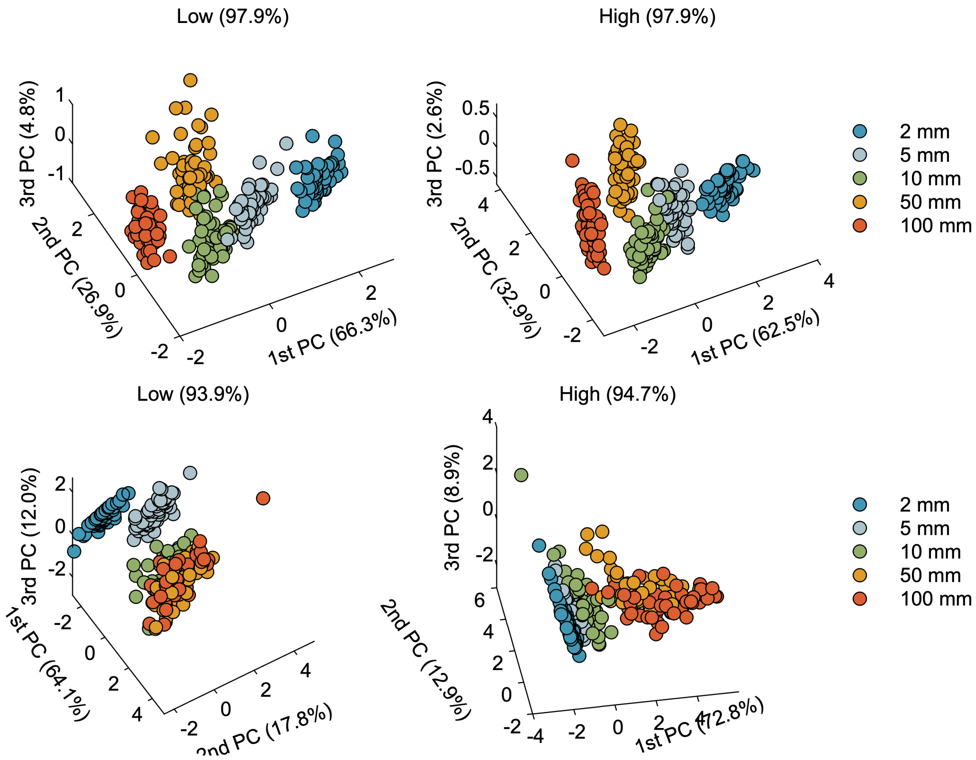

Fig. 5.5 The dimension of the number of impulses for test `Case E1 - E10` after denoised by FT and FT are reduced to three by PCA. The *top row* and *bottom row* are under the $V = 2.5$ and 4.5 m/s respectively. The *left column* and *right column* are denoised results by FT and WT respectively. Each axis is corresponding to ith principal component with the contribution ratio. The value on the top of each plot is the sum of contribution ratios.

5.4 Notation

Hereafter, feature quantities are denoted by following notation. Note that accelerometer signals were not denoised because no denoising method changed the original signal significantly.

Symbol	Feature quantity
`VP`	Impulses $\boldsymbol{I_{ps}}$ $(= (I_{ps}^2, I_{ps}^4, \cdots, I_{ps}^{1024}))$ obtained from an accelerometer without denoising.
`LF`	Impulses $\boldsymbol{I_{ps}}$ obtained from a microphone denoised with conventional band-pass filter around 4.6 kHz.
`WT*****`	Impulses $\boldsymbol{I_{ps}}$ obtained from a microphone denoised with DWT. The combination of decomposed signals are expressed in binary. For example, `WT10101` $= d_1 + d_3 + d_5$.

Chapter 6

Regression Model

I obtained candidates of feature quantities in the preceding chapter. In this chapter, I make a model to convert the feature quantities to my target information, namely, bedload transport rate and grain size. Considering the interpretability and enough expressive power as a desired condition of the model, I chose the use of Gaussian Process Regression (GPR) in this step. At first, I selected several promising feature quantities on the basis of their prediction accuracy with a naïve model for the flume experiments. Then, the model was improved to have the ability of extrapolation to real observation data with applying the on-site experiment data.

6.1 Introduction of Gaussian Process

For converting feature quantities to some real numbers such as bedload transport rate and grain size, I need to make regression models. Many models use linear, exponential, and polynomial regression or their combinations. However, their assumption, linearity, exponential, and polynomial, are often too strong, and thus, they restrict the expressive power of the models. For improving the expressiveness, many recent studies have exploited techniques having advanced methods such as Support Vector Machines, (Deep) Neural Networks, but they tend to be a black box and lose their interpretation.

The Gaussian Process (GP) allows us to make a model with a more light assumption resulting in having high expressive power and interpretability. The intractability is attributed kernel functions that specify the form of regression function. We can incorporate a priori knowledge into a kernel to reflect them on the model. In addition, since the GP is Bayesian approach, the predicted value is provided as a distribution. This feature allows us to know the uncertainty of the prediction.

Intuitive and simple example of GPs application is presented in fig. 6.1. Figure 6.1(a) shows four sample functions from a GP by a predefined kernel and the mean function zero with the doubled standard deviation depicted as the shaded region. After two data are given, the mean function is modified and the shaded area is restrained according to the data as in fig. 6.1(b). Four sample functions from the posterior are given as dashed lines. The posterior can be interpreted as predictions for next new data. The shaded area gives the uncertainty of the prediction, closer width is higher confidence, and vice versa.

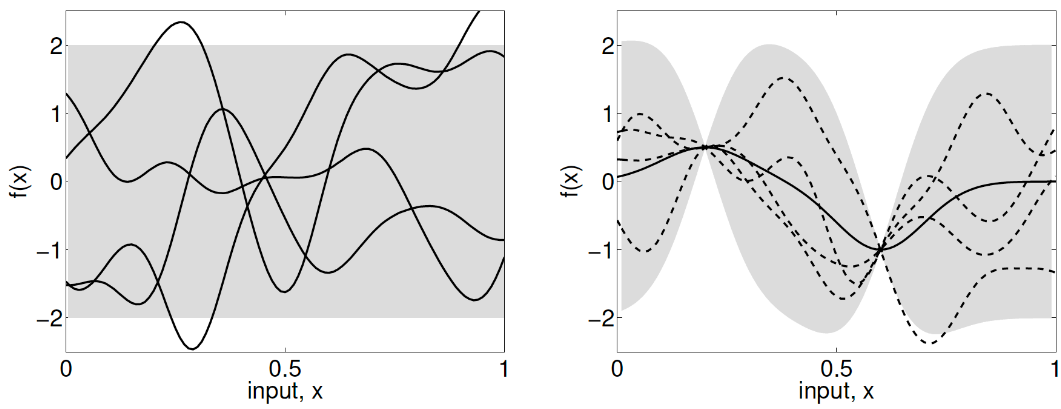

(a), prior (b), posterior

Fig. 6.1 An intuitive example of GPR. (a) shows the samples before data are given. (b) shows the samples after two data points are given. The solid line indicates the mean values and shaded region denotes the double standard deviation ($\pm 2\sigma$). (adapted from Rasmussen and Williams (2006))

In Duvenaud (2014), advantages of using GPs for regression are summarized as follows:

Analytic inference.
Given a kernel function and some observations, the predictive posterior distribution can be computed exactly in closed form. This is a rare property for nonparametric models to have.

Expressivity.
Through the choice of covariance function, we can express a wide range of modeling assumptions.

Integration over hypotheses.
The fact that a GP posterior, given a fixed kernel, lets us integrate exactly over a wide range of hypotheses means that overfitting is less of an issue than in comparable model classes. For example, compared to neural networks, relatively few parameters need to be estimated, which lessens the need for the complex optimization or regularization schemes.

Model selection.
A side benefit of being able to integrate over all hypotheses is that we can compute the marginal likelihood of the data given a model. This gives us a principled way of comparing different models.

Closed-form predictive distribution.
The predictive distribution of a GP at a set of test points is simply a multivariate Gaussian distribution. This means that GPs can easily be composed with other models or decision procedures.

Easy to analyze.
It may seem unsatisfying to restrict ourselves to a limited model class, as opposed to trying to do inference in the set of all computable functions. However, simple models can be used as well-understood building blocks for constructing more interesting models.

6.2 Gaussian Process Regression

In this section, the theory of GPR is demonstrated started from linear regression with which we are familiar.

6.2.1 Preliminary information

The multivariate Gaussian distribution

When a D-dimensional vector $\mathbf{x}$ follows a multivariate Gaussian distribution, the probability density function is given by

$$\Pr(\mathbf{x}|\boldsymbol{\mu},\boldsymbol{\Sigma}) = \frac{1}{(2\pi)^{\frac{n}{2}}|\boldsymbol{\Sigma}|^{\frac{1}{2}}} \exp\left(-\frac{1}{2}(\mathbf{x}-\boldsymbol{\mu})^T\boldsymbol{\Sigma}^{-1}(\mathbf{x}-\boldsymbol{\mu})\right), \tag{6.1}$$

where $\boldsymbol{\mu}$ and $\boldsymbol{\Sigma}$ are the mean vector and covariance matrix. Note that the covariance is calculated as

$$\boldsymbol{\Sigma} = \mathbb{E}[\mathbf{x}\mathbf{x}^{\mathsf{T}}] - \mathbb{E}[\mathbf{x}]\mathbb{E}[\mathbf{x}]^{\mathsf{T}}. \tag{6.2}$$

Marginalization of a multivariate Gaussian distribution

Suppose a D-dimensional $\mathbf{x}$ follows a multivariate Gaussian distribution

$$\mathbf{x} \sim \mathcal{N}(\boldsymbol{\mu},\boldsymbol{\Sigma}). \tag{6.3}$$

Let the first L dimensions of $\mathbf{x}$ and the other $D-L$ dimension be $\mathbf{x}_1$ and $\mathbf{x}_2$ respectively, $\mathbf{x}$ can be denoted by

$$\mathbf{x} = \begin{bmatrix} \mathbf{x}_1 \\ \mathbf{x}_2 \end{bmatrix} \tag{6.4}$$

here, $\mathbf{x}_1$ and $\mathbf{x}_2$ are a L-dimensional and $(D-L)$-dimensional vectors respectively. Parameters $\boldsymbol{\mu}$ and $\boldsymbol{\Sigma}$ are segmented as the same manner, and eq. (6.3) is denoted by

$$\mathbf{x} = \begin{bmatrix} \mathbf{x}_1 \\ \mathbf{x}_2 \end{bmatrix} \sim \mathcal{N}\left(\begin{bmatrix} \boldsymbol{\mu}_1 \\ \boldsymbol{\mu}_2 \end{bmatrix}, \begin{bmatrix} \boldsymbol{\Sigma}_{11} & \boldsymbol{\Sigma}_{12} \\ \boldsymbol{\Sigma}_{21} & \boldsymbol{\Sigma}_{22} \end{bmatrix}\right). \tag{6.5}$$

Now, the distribution of $\mathbf{x}_1$ obtained from marginalizing $p(\mathbf{x}) = p(\mathbf{x}_1,\mathbf{x}_2)$ over $\mathbf{x}_2$ is given as

$$\Pr(\mathbf{x}_1) = \int \Pr(\mathbf{x}_1,\mathbf{x}_2)d\mathbf{x}_2 = \mathcal{N}(\boldsymbol{\mu}_1,\boldsymbol{\Sigma}_{11}). \tag{6.6}$$

Conditional multivariate Gaussian distribution

Assume that a vector $\mathbf{x}$ follows eq. (6.5). If $\mathbf{x}_1$ is given, the conditional random variable $\mathbf{x}_2|\mathbf{x}_1$ also follows the following multivariate Gaussian distribution:

$$\mathbf{x}_2|\mathbf{x}_1 \sim \mathcal{N}\left(\boldsymbol{\mu}_2 + \boldsymbol{\Sigma}_{21}\boldsymbol{\Sigma}_{11}^{-1}\left(\mathbf{x}_1 - \boldsymbol{\mu}_2\right), \boldsymbol{\Sigma}_{22} - \boldsymbol{\Sigma}_{21}\boldsymbol{\Sigma}_{11}^{-1}\boldsymbol{\Sigma}_{12}\right). \tag{6.7}$$

Linear transformation of a multivariate Gaussian distribution

Let $\mathbf{x}$ be a vector following a multivariate Gaussian distribution with a mean vector $\mathbf{0}$ and a covariance function $\boldsymbol{\Sigma}$

$$\mathbf{x} \sim \mathcal{N}(\mathbf{0}, \boldsymbol{\Sigma}). \tag{6.8}$$

If $\mathbf{x}$ is transformed by a matrix $\mathbf{A}$ as

$$\mathbf{y} = \mathbf{A}\mathbf{x} \tag{6.9}$$

$\mathbf{y}$ also follows a multivariate Gaussian distribution

$$\mathbf{y} \sim \mathcal{N}(\mathbf{0}, \boldsymbol{\Lambda}^{-1}). \tag{6.10}$$

Here, $\boldsymbol{\Lambda} = (\mathbf{A}^{-1})^{\mathsf{T}}\boldsymbol{\Sigma}^{-1}\mathbf{A}^{-1}$.

6.2.2 Linear regression

Regression is to predict an output y when the input $\mathbf{x}$ is given. If we assume linear relation between the input and output, the regression is called linear regression. Here I explain linear regression when the input $\mathbf{x}$ is D-dimensional data, so called multiple regression. For example, if $\mathbf{x}^{\mathsf{T}} = \{I_{ps}^{2}, \cdots, I_{ps}^{1024}\}$, the input is 11-dimensional data.

When we have N data $\mathcal{D} = \{(y_1, \mathbf{x}_1), (y_2, \mathbf{x}_2), \cdots, (y_N, \mathbf{x}_N)\}$, by selecting a good weight parameter vector $\mathbf{w}$, a predicted output $\hat{y}$ is expressed by

$$\hat{y} = \mathbf{w}^{\mathsf{T}}\mathbf{x}. \tag{6.11}$$

Then, expressing $\hat{\mathbf{y}}^{\mathsf{T}} = (\hat{y}_1, \hat{y}_2, \cdots, \hat{y}_N)$, $\mathbf{X} = (\mathbf{x}_1^{\mathsf{T}}, \mathbf{x}_2^{\mathsf{T}}, \cdots, \mathbf{x}_N^{\mathsf{T}})^{\mathsf{T}}$, we can obtain

$$\hat{\mathbf{y}} = \mathbf{X}\mathbf{w}. \tag{6.12}$$

Next, we optimize the weight vector $\mathbf{w}$ by minimizing the error

$$E = \sum_{n=1}^{N} (y_n - \hat{y_n})^2 = \sum_{n=1}^{N} (y_n - \mathbf{w}^\mathsf{T}\mathbf{x}_n)^2 = (\mathbf{y} - \mathbf{X}\mathbf{w})^\mathsf{T}(\mathbf{y} - \mathbf{X}\mathbf{w}). \tag{6.13}$$

For that, solving $\partial E/\partial \mathbf{w} = 0$, we can obtain, if $\mathbf{X}^\mathsf{T}\mathbf{X}$ has the inverse,

$$\mathbf{w} = (\mathbf{X}^\mathsf{T}\mathbf{X})^{-1}\mathbf{X}^\mathsf{T}\mathbf{y}. \tag{6.14}$$

This is the solution of a multiple regression, and eq. (6.14) is called *normal equation*.

The expressive power of linear regression model can be improved by introducing a function $\boldsymbol{\phi}(\mathbf{x})$ which converts the data to higher dimension. Now, eq. (6.12) has changed to

$$\hat{y} = \mathbf{w}^\mathsf{T}\boldsymbol{\phi}(\mathbf{x}). \tag{6.15}$$

Therefore, as the same derivation above, the minimum square solution of $\mathbf{w}$ is given as

$$\mathbf{w} = (\boldsymbol{\Phi}^\mathsf{T}\boldsymbol{\Phi})^{-1}\boldsymbol{\Phi}^\mathsf{T}\mathbf{y}. \tag{6.16}$$

Here, $\boldsymbol{\Phi} = (\boldsymbol{\phi}_1^\mathsf{T}, \boldsymbol{\phi}_2^\mathsf{T}, \cdots, \boldsymbol{\phi}_N^\mathsf{T})^\mathsf{T}$.

6.2.3 Linear regression to Gaussian process

Suppose $\mathbf{w}$ is generated by a Gaussian with a mean $\mathbf{0}$ and a covariance $\lambda^2\mathbf{I}$

$$\mathbf{w} \sim \mathcal{N}(\mathbf{0}, \lambda^2\mathbf{I}). \tag{6.17}$$

which implies $\mathbf{y} = \boldsymbol{\Phi}\mathbf{w}$, and $\mathbf{y}$ also follows a Gaussian as in eq. (6.9). The mean is $\mathbb{E}[\mathbf{y}] = \mathbb{E}[\boldsymbol{\Phi}\mathbf{w}] = \boldsymbol{\Phi}\mathbb{E}[\mathbf{w}] = 0$, the covariance is

$$\boldsymbol{\Sigma} = \mathbb{E}[\mathbf{y}\mathbf{y}^\mathsf{T}] - \mathbb{E}[\mathbf{y}]\mathbb{E}[\mathbf{y}]^\mathsf{T} = \mathbb{E}[(\boldsymbol{\Phi}\mathbf{w})(\boldsymbol{\Phi}\mathbf{w})^\mathsf{T}] = \boldsymbol{\Phi}\mathbb{E}[\mathbf{w}\mathbf{w}^\mathsf{T}]\boldsymbol{\Phi}^\mathsf{T} = \lambda^2\boldsymbol{\Phi}\boldsymbol{\Phi}^\mathsf{T}, \tag{6.18}$$

and thus, the distribution of $\mathbf{y}$ is a multivariate Gaussian distribution

$$\mathbf{y} \sim \mathcal{N}(\mathbf{0}, \lambda^2\boldsymbol{\Phi}\boldsymbol{\Phi}^\mathsf{T}) \tag{6.19}$$

Notice that $\mathbf{y}$ is no more governed by $\mathbf{w}$, but just done by the covariance $\lambda^2\mathbf{\Phi}\mathbf{\Phi}^\mathsf{T}$. Hereafter, $\lambda^2\mathbf{\Phi}\mathbf{\Phi}^\mathsf{T}$ is referred as K, and then

$$K_{nn'} = \lambda^2 \boldsymbol{\phi}(\mathbf{x}_n)^\mathsf{T}\boldsymbol{\phi}(\mathbf{x}'_n). \tag{6.20}$$

As $K_{nn'}$ is an element of the covariance, larger $K_{nn'}$ means the higher correlation between y_n and $y_{n'}$. Also, as $\boldsymbol{\phi}(\mathbf{x}_n)^\mathsf{T}\boldsymbol{\phi}(\mathbf{x}_{n'})$ is the inner product of $\mathbf{x}_n$ and $\mathbf{x}_{n'}$, eq. (6.19) means that the similar input $\mathbf{x}$ involves the similar output y.

GP is the case when the covariance can express for any input $\mathbf{x}$, in other words, infinite-dimensional multivariate Gaussian distribution. At that time, the out put y is a function and the covariance determines the property of the function.

Definition 1. *Gaussian Process If for any natural number N, the output vector to the inputs $\mathbf{x}_1, \mathbf{x}_2, \cdots, \mathbf{x}_N \in \mathcal{X}$*

$$\mathbf{f} = (f(\mathbf{x}_1), f(\mathbf{x}_2), \cdots, f(\mathbf{x}_N)) \tag{6.21}$$

follows a Gaussian distribution $\mathcal{N}(\boldsymbol{\mu}, \mathbf{K})$ with the mean $\boldsymbol{\mu} = (\mu(\mathbf{x}_1), \mu(\mathbf{x}_2), \cdots, \mu(\mathbf{x}_N))$, and the covariance $\mathbf{K}$ with every element is denoted by $K_{nn'} = k(\mathbf{x}_n, \mathbf{x}_{n'})$, f can be said to follow a Gaussian process. Here, this is written as

$$f \sim \mathcal{GP}(\mu(\mathbf{x}), k(\mathbf{x}, \mathbf{x}')). \tag{6.22}$$

In this study, I set $\boldsymbol{\mu}$ as $\mathbf{0}$ by assuming the mean is subtracted in advance.

6.2.4 Kernel trick

According to eq. (6.19), the distribution of $\mathbf{y}$ is determined only by the elements of covariance $\mathbf{K}$

$$K_{nn'} = \boldsymbol{\phi}(\mathbf{x}_n)^\mathsf{T}\boldsymbol{\phi}(\mathbf{x}_{n'}) \tag{6.23}$$

Kernel trick is obtaining $K_{nn'}$ without calculating $\boldsymbol{\phi}(\mathbf{x}_n)^\mathsf{T}\boldsymbol{\phi}(\mathbf{x}_{n'})$ explicitly but using *kernel function* k which satisfies

$$k(\mathbf{x}_n, \mathbf{x}_{n'}) = \boldsymbol{\phi}(\mathbf{x}_n)^\mathsf{T}\boldsymbol{\phi}(\mathbf{x}_{n'}) \tag{6.24}$$

According to section 6.2.3, it can be said that the kernel function k gives the closeness of data $\mathbf{x}_n$ and $\mathbf{x}_{n'}$.

One of the most popular kernel functions is a *radial basis function (RBF) kernel*

$$\mathrm{RBF}(\mathbf{x}_n, \mathbf{x}_{n'}) = \theta_1 \exp\left(-\frac{|\mathbf{x}_n - \mathbf{x}_{n'}|^2}{\theta_2}\right) \tag{6.25}$$

here, θ_1 and θ_2 are hyper-parameters that govern the kernel feature. This kernel outputs 1 when $|\mathbf{x}_n - \mathbf{x}_{n'}| = 0$, hence $\mathbf{x}_n = \mathbf{x}_{n'}$, and the output decreases as $|\mathbf{x}_n - \mathbf{x}_{n'}|$ increases. It implies that for the closer pair of inputs, the covariance of $\mathbf{y}$ also becomes higher, hence the output is also close value.

Samples from GPs with a RBF kernel are shown in fig. 6.2 with varying the hyperparameters θ_1 and θ_2. As in the figure, the outputs from GPs with RBF kernel are smooth functions. The variance is governed by θ_1 and the smoothness is done by θ_2. The advantage of GPs are the ability to express complicated regression functions by selecting suitable kernels.

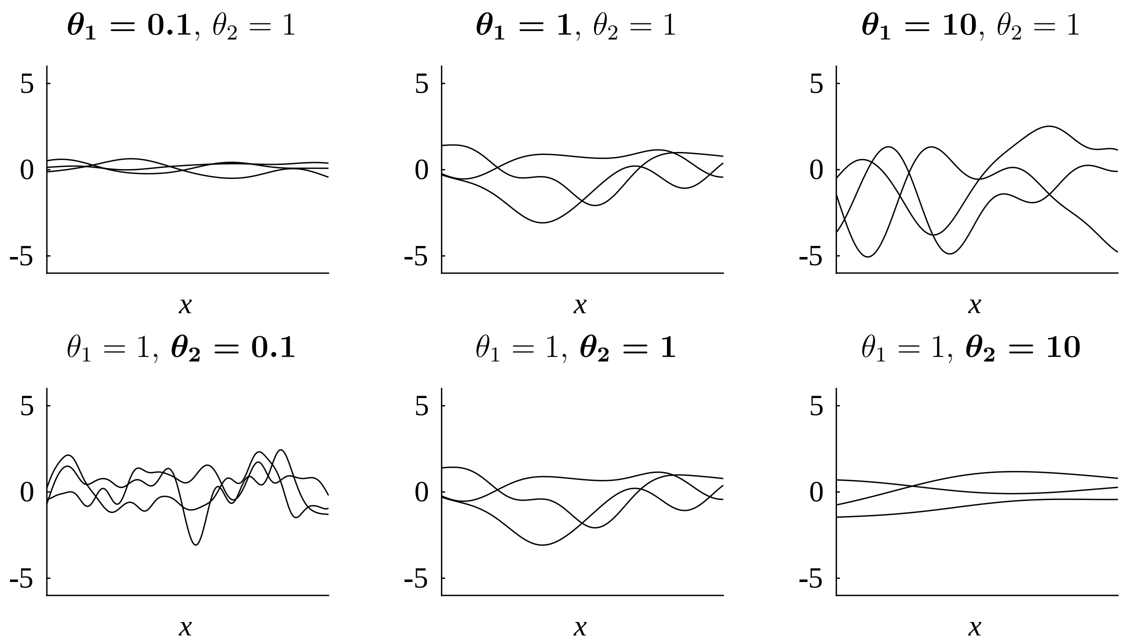

Fig. 6.2 Samples from GPs with a RBF kernel (eq. (6.25)) with varying the hyper-parameters θ_1 and θ_2.

Four other kernels used in this study are shown here. Many kernels, not only real number inputs but also non-numeric inputs, are proposed (e.g., Lodhi et al., 2002; Rasmussen and Williams, 2006).

Linear kernel

$$\mathrm{LIN}(\mathbf{x}_n, \mathbf{x}_{n'}) = \mathbf{x}_n^{\mathsf{T}} \mathbf{x}_{n'} \tag{6.26}$$

GPa with this kernel are equivalent to multiple linear regression since the kernel implies the feature vector is identity

$$\boldsymbol{\phi}(\mathbf{x}) = \mathbf{x}. \tag{6.27}$$

Automatic Relevance Determination (ARD) kernel

$$\mathrm{ARD}(\mathbf{x}_n, \mathbf{x}_{n'}|\boldsymbol{\theta}) = \exp\left(-\sum_{d+1}^{D} \eta_d (x_{id} - x_{jd})^2\right) \tag{6.28}$$

Here, I suppose an observation is D-dimensional vector $\mathbf{x}_i = (x_{i1}, \cdots, x_{iD})$, and the kernel hyperparameters $\boldsymbol{\theta} = (\eta_1, \cdots, \eta_D)$. Therefore, optimizing hyperparameter $\boldsymbol{\theta}$ means selecting efficient vector components in $\mathbf{x}$. Simultaneously, we can know the relevance of each vector element to the output by the optimized $\boldsymbol{\theta}$.

Observation noise

$$\mathrm{WN}(\mathbf{x}_n, \mathbf{x}_{n'}|\boldsymbol{\theta}) = \sigma^2 \delta(n, n') \tag{6.29}$$

This kernel allows a model to involve observation noise. GPs using a kernel function k for a model

$$y_n = f(\mathbf{x}_n) + \epsilon_n, \quad \epsilon_n \sim \mathcal{N}(0, \sigma^2) \quad (n = 1, \cdots, N) \tag{6.30}$$

is equivalent to using the following kernel k'.

$$k'(\mathbf{x}_n, \mathbf{x}_{n'}) = k(\mathbf{x}_n, \mathbf{x}_{n'}) + \sigma^2 \delta(n, n'). \tag{6.31}$$

A powerful advantage in using GPs come from the following properties of kernels.

Kernel combination

Let $k_1(\mathbf{x}, \mathbf{x}')$ and $k_2(\mathbf{x}, \mathbf{x}')$ be kernel functions, then the sum and product of them $k(\mathbf{x}, \mathbf{x}')$ are also kernel functions.

$$k(\mathbf{x}, \mathbf{x}') = k_1(\mathbf{x}, \mathbf{x}') + k_2(\mathbf{x}, \mathbf{x}') \tag{6.32}$$

$$k(\mathbf{x}, \mathbf{x}') = k_1(\mathbf{x}, \mathbf{x}') \times k_2(\mathbf{x}, \mathbf{x}') \tag{6.33}$$

For instance, the sum of a RBF kernel, a linear kernel, and a noise kernel

$$\mathrm{RBF} + \mathrm{LIN} + \mathrm{WN} = \theta_1 \exp\left(-\frac{|\mathbf{x}_n - \mathbf{x}_{n'}|^2}{\theta_2}\right) + \mathbf{x}_n^{\mathsf{T}}\mathbf{x}_{n'} + \sigma^2\delta(n, n') \tag{6.34}$$

can provide a regression to "a function with smooth connection of data and trend having observation noise". Therefore, the kernel design based on feature and background of the data is important to make an effective model.

6.2.5 Gaussian process regression and prediction

Here we think of solving regression problem with GPs. Suppose we have N observations, pairs of inputs $\mathbf{x} \in \mathcal{X}$ and outputs $y \in \mathbb{R}$

$$\mathcal{D} = \{(y_1, \mathbf{x}_1), (y_2, \mathbf{x}_2), \cdots, (y_N, \mathbf{x}_N)\}. \tag{6.35}$$

Then, we design some kernel function $k(\mathbf{x}, \mathbf{x}')$ and assume y follows a GP

$$y \sim \mathcal{GP}(\mathbf{0}, k(\mathbf{x}, \mathbf{x}')). \tag{6.36}$$

Note that the mean of y is subtracted in advance for simplicity. Denoting $\mathbf{y} = (y_1, y_2, \cdots, y_N)^{\mathsf{T}}$, $\mathbf{y}$ follows a Gassian distribution

$$y \sim \mathcal{N}(\mathbf{0}, \mathbf{K}) \tag{6.37}$$

here, an element of $\mathbf{K}$ is expressed by $K_{nn'} = k(\mathbf{x}_n, \mathbf{x}_{n'})$.

Next we calculate an output $y^\star$ when a new input $\mathbf{x}^\star$ is given, $\mathbf{y}' = (y_1, \cdots, y_N, y^\star)$ also follow a Gaussian distribution (Definition 1).

$$\mathbf{y}' = \begin{pmatrix} \mathbf{y} \\ y^\star \end{pmatrix} \sim \mathcal{N}\left(\mathbf{0}, \begin{bmatrix} \mathbf{K} & \mathbf{k}_\star \\ \mathbf{k}_\star^{\mathsf{T}} & k_{\star\star} \end{bmatrix}\right). \tag{6.38}$$

Here,

$$\mathbf{k}_\star = (k(\mathbf{x}^\star, \mathbf{x}_1), k(\mathbf{x}^\star, \mathbf{x}_2), \cdots, k(\mathbf{x}^\star, \mathbf{x}_N))^\mathsf{T} \tag{6.39}$$

$$k_{\star\star} = k(\mathbf{x}^\star, \mathbf{x}^\star) \tag{6.40}$$

Finally, to get the distribution of $y^\star$, $\Pr(y^\star|\mathbf{x}^\star, \mathcal{D})$, we can use the formula of conditional multivariate Gaussian distribution (eq. (6.7)).

$$\Pr(y^\star|\mathbf{x}^\star, \mathcal{D}) = \mathcal{N}(\mathbf{k}_\star^\mathsf{T}\mathbf{K}^{-1}\mathbf{y},\ k_{\star\star} - \mathbf{k}_\star^\mathsf{T}\mathbf{K}^{-1}\mathbf{k}_\star) \tag{6.41}$$

To compute eq. (6.41), $\mathbf{K}^{-1}$ must be known. The calculation of matrix inverse takes $\mathcal{O}(N^3)$ time, which limits the application when N is larger than several thousands. Although, for addressing this barrier many approximate schemes are proposed (Hensman et al., 2013; Quiñonero-Candela and Rasmussen, 2005; Wilson and Nickisch, 2015), I was able to obtain exact distribution since the number of datapoints was less than 1000 in this study.

6.2.6 Hyperparameter optimization

Hyperparameters $\boldsymbol{\theta}$ are optimized by maximizing marginal likelihood $\Pr(\mathbf{y}|\mathbf{X}, \boldsymbol{\theta})$. In this study, GP parameter optimization was performed by using the `GPML toolbox` (Rasmussen and Nickisch, 2010). Note that the optimization is not a convex optimization problem. Therefore, I ran the toolbox for changing initial hyperparameters several times randomly.

6.3 Notation

In the analysis, I assume observation noise for all cases, therefore I omit writing WN explicitly. The data I used for the analysis is the number of impulses $\boldsymbol{I_{ps}} = (I_{ps}^2, I_{ps}^4, \cdots, I_{ps}^{1024})$, flow velocity V, Froude number Fr, and water depth h. For specifying kernels used in model, I use the following notation. A kernel $k(\mathbf{x}_n, \mathbf{x}_{n'})$ for data $\mathcal{D}$ is denoted by

$$\mathrm{Ker}(k(\mathbf{x}_n, \mathbf{x}_{n'});\ \mathcal{D}) \tag{6.42}$$

For example, Ker(RBF $\times$ LIN; Fr, $\boldsymbol{I_{ps}}$) means the following kernel

$$k(\mathbf{x}_n, \mathbf{x}_{n'}) = \underbrace{\theta_1 \exp\left(-\frac{|\mathbf{x}_n - \mathbf{x}_{n'}|^2}{\theta_2}\right)}_{\text{RBF}} \times \underbrace{\mathbf{x}_n^\mathsf{T}\mathbf{x}_{n'}}_{\text{LIN}} \tag{6.43}$$

where, $\mathbf{x}_n = (\mathrm{Fr}_n, I_{ps,n}^2, I_{ps,n}^4, \cdots, I_{ps,n}^{1024})$.

6.4 Feature selection

In this section, I select several feature quantities from those prepared in the preceing chapter. Each feature is evaluated for their ability to predict grain size and bedload transport rate per a second for laboratory flume experiments data (`E1 - E16`, and `P1 - P11`) with K-Fold cross validation ($K = 5$ in this study). For regression, GPR and linear regression are carried out. The kernel used for the GPR is Ker(RBF; $V, \boldsymbol{I_{ps}}$). Impulses $\boldsymbol{I_{ps}}$ were normalized by I_{ps}^{1024} and signal duration ([sec]) for grain size and sediment transport rate models respectively. Their performance were evaluated by MSE (mean square error).

The top 10 feature quantities are listed in table 6.1 and table 6.2. Evidently, GPR provided much better performance than linear regression overall. In the results if GPR, feature quantities that appears in both tables are in boldface. It connotates that feature quantities `WT10110`, `WT11111`, `WT11011`, and `VP` are promising. Following studies use `WT10110`, which gave high performance both for grain size and sediment transport rate prediction.

Table 6.1 Regression mean squared error for D_{50}

	GPR		LR	
Rank order	Feature name	MSE	Feature name	MSE
1	`WT11010`	0.0465	`WT01011`	0.2681
2	`WT00110`	0.0568	`WT11010`	0.2731
3	`WT01010`	0.0593	`WT11001`	0.2814
4	`WT11110`	0.0613	`WT01001`	0.2835
5	`WT01110`	0.0666	`WT01010`	0.2857
6	**`WT10110`**	0.0686	`WT11011`	0.2886
7	**`VP`**	0.0718	`WT00101`	0.2919
8	**`WT11111`**	0.0740	`VP`	0.2921
9	`WT10111`	0.0760	`WT10101`	0.3137
10	**`WT11011`**	0.0770	`WT10111`	0.3279

Table 6.2 Regression mean squared error for sediment transport rate

	GPR		LR	
Rank order	Feature name	MSE	Feature name	MSE
1	**VP**	0.0801	VP	0.1538
2	WT10011	0.1814	WT11011	0.2311
3	**WT10110**	0.1966	WT01011	0.2322
4	**WT11011**	0.2019	WT00010	0.2334
5	WT00111	0.2065	WT10010	0.2373
6	**WT11111**	0.2120	WT10011	0.2377
7	WT01111	0.2185	WT00011	0.2411
8	WT00010	0.2186	WT01010	0.2512
9	WT01001	0.2186	WT11010	0.2555
10	WT10001	0.2187	WT10001	0.2610

6.5 Model construction

This section makes models with GPR to predict grain size and sediment transport. Models were optimized using flume experimental data and then, evaluated by applicability to the on-site experiment data. Assume that estimation of grain size is easier than that of bedload transport rate, I first made grain size prediction model then bedload transport model. This is because that the grain sizes employed in the on-site experiments are as in the same order as that used in flume experiments.

6.5.1 Grain size prediction

Naïve GPR

I call GPR using RBF kernel alone as *naïve GPR* because this is the simplest application. This approach simply finds a regression function which connects among data smoothly, in other words, tries to find structure only from data itself. Two kernels were tested, Ker(RBF; $\boldsymbol{I_{ps}}$) and Ker(RBF; $\boldsymbol{I_{ps}}, V$). The results are in fig. 6.3 and fig. 6.4 respectively. Although predictions in fig. 6.3 overestimated grain size, it is mitigated in fig. 6.4. This fact implicates that not only impulses but also flow velocity should be accounted for. This is consistent with other studies stating that the signal magnitude increases as particle motion velocity increases (Taniguchi et al., 1992).

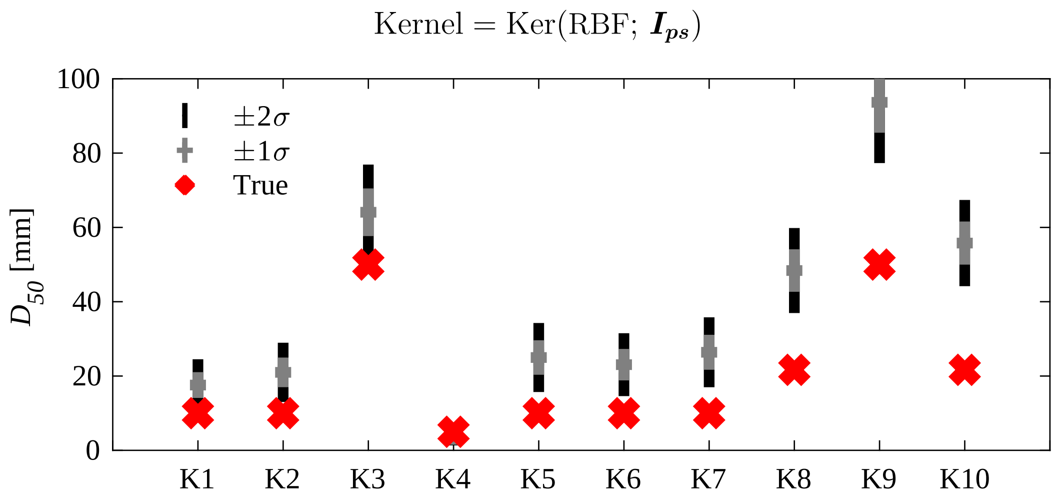

Fig. 6.3 True and estimated D_{50} at the on-site experiment with Ker(RBF; $\boldsymbol{I_{ps}}$).

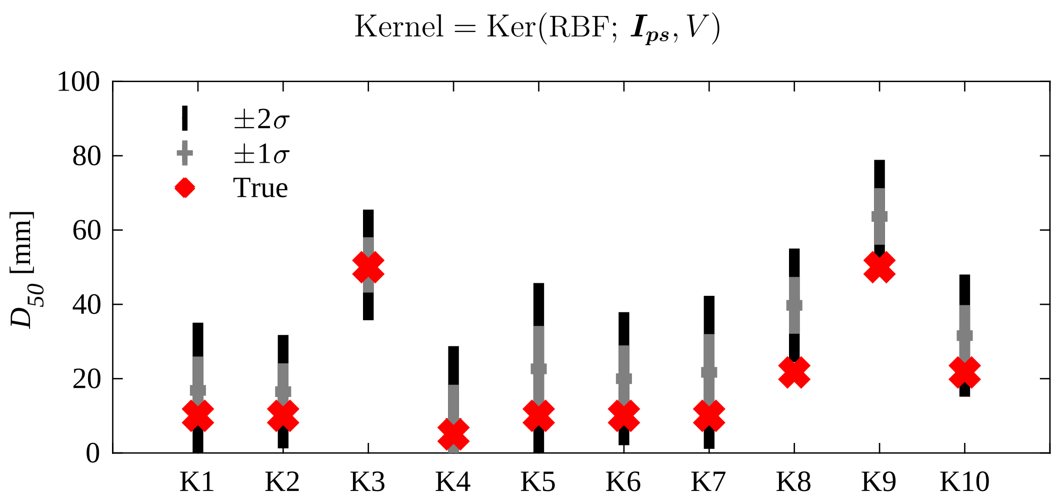

Fig. 6.4 True and estimated D_{50} at the on-site experiment with Ker(RBF; $\boldsymbol{I_{ps}}, V$).

Advanced GPR

According to the discussion above, I explicitly added V^{-1} into the kernel. In addition, I introduced linear kernel by assuming that the impulses increase as D_{50} increases. The result (fig. 6.5) exhibits that the overestimation is mitigated. Although the estimate variance increased comparing with fig. 6.4, I decided to uses this kernel for D_{50} estimate because the mean value is accurate.

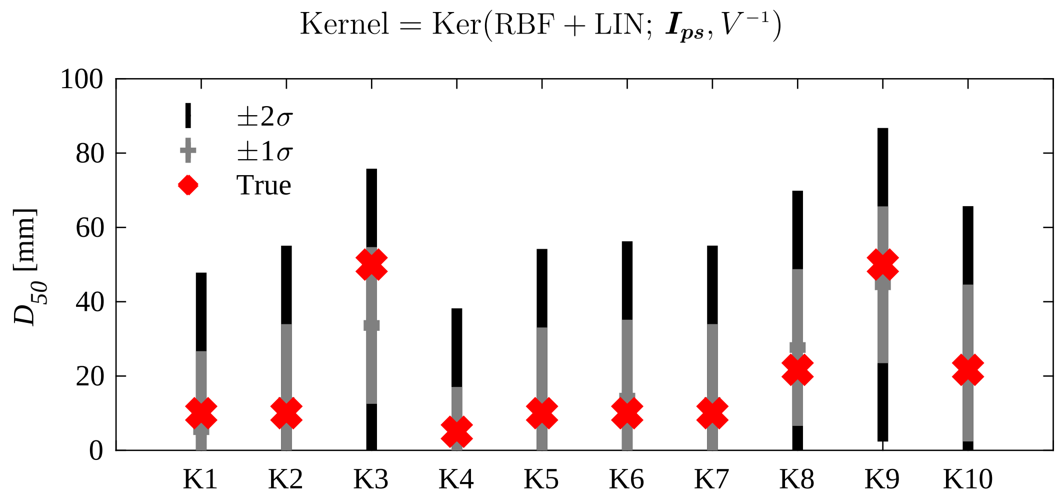

Fig. 6.5 True and estimated D_{50} at the on-site experiment with Ker(RBF + LIN; $\boldsymbol{I_{ps}}, V^{-1}$).

6.5.2 Bedload transport rate prediction

Naïve GPR

In the same as D_{50} estimate, RBF kernel is used with $\boldsymbol{I_{ps}}$. The results in fig. 6.6 are highly under estimated. This tendency is significant for `K7`, `K9`, and `K10` where flow discharge is 20 m^3/s. This implicates that the reduction in the number of hitting gravels on the plate due to high flow velocities. Also it is possible that much higher water depth than that of flume experiments caused the same phenomenon.

For comparing estimated value to tested sediment volume in m^3, all the estimated value in gram were firstly summed and converted into volume with sediment density $\rho_s = 2700$ kg/m^3. Then, the summed value was multiplied by duration that sediment was recorded by IPs and the reciprocal of the ratio of the total plates width to the tunnel width r_p ($r_p = 2.7$ at the Koshibu Dam SBT). Finally, the computed volume was converted the fed volume with assuming a porosity 0.7.

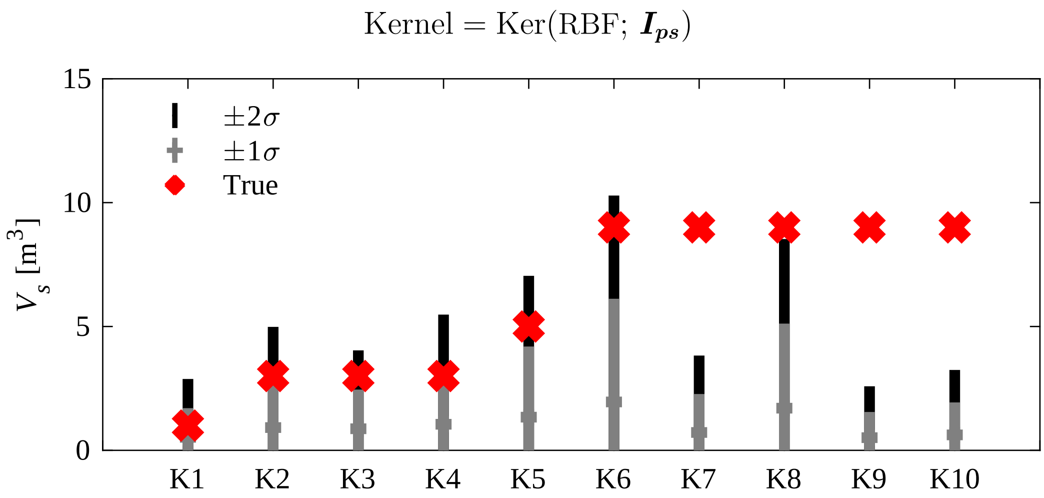

Fig. 6.6 True and estimated total sediment volume V_s at the on-site experiment with Ker(RBF; $\boldsymbol{I_{ps}}$).

Advanced GPR I

In order to cope with the problem above, I added data of flow velocity V and h with them converted to the reciprocal. Further more, same as fig. 6.5, I employed linear kernel with RBF kernel. It is also expected that using all elements of $\boldsymbol{I_{ps}}$ is redundant for sediment transport rate estimate because not the distribution but the scale of signal magnitude is enough. Therefore, I introduced ARD kernel instead of a simple RBF kernel for $\boldsymbol{I_{ps}}$. This mitigated the underestimation as in fig. 6.7, but still underestimated.

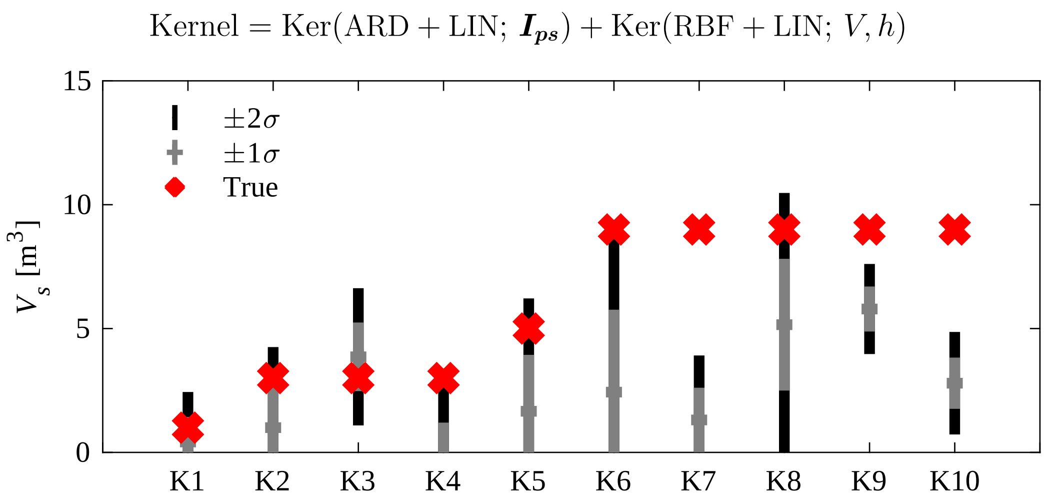

Fig. 6.7 True and estimated total sediment volume V_s at the on-site experiment with Ker(ARD + LIN; $\boldsymbol{I_{ps}}$) + Ker(RBF + LIN; V, h).

Advanced GPR II

In order to include gravel hop length, the following formula was introduced with estimated D_{50}, $\hat{D_{50}}$ (Auel et al., 2017a):

$$\frac{L_p}{\hat{D_{50}}} = 2.3 \left(\frac{\theta}{\theta_c} - 1 \right)^{0.8} \tag{6.44}$$

where L_p = saltation length, θ = Shields' parameter, and θ_c = critical Shields' parameter (in this study, $\theta_c = 0.005$ was chosen, in accordance with the study conducted by Auel et al. (2017a)).

Figure 6.8 shows that the mean gets closer to the truth values. In particular, `K7` is improved significantly. Test `K7` is with a grain size $D_s = 10$ mm and discharge $Q = 20$ m^3/s which might be rather easier to be underestimated due to a combination of high flow velocity and small grain size. This improve seems to be attributed to the introduction of L_p.

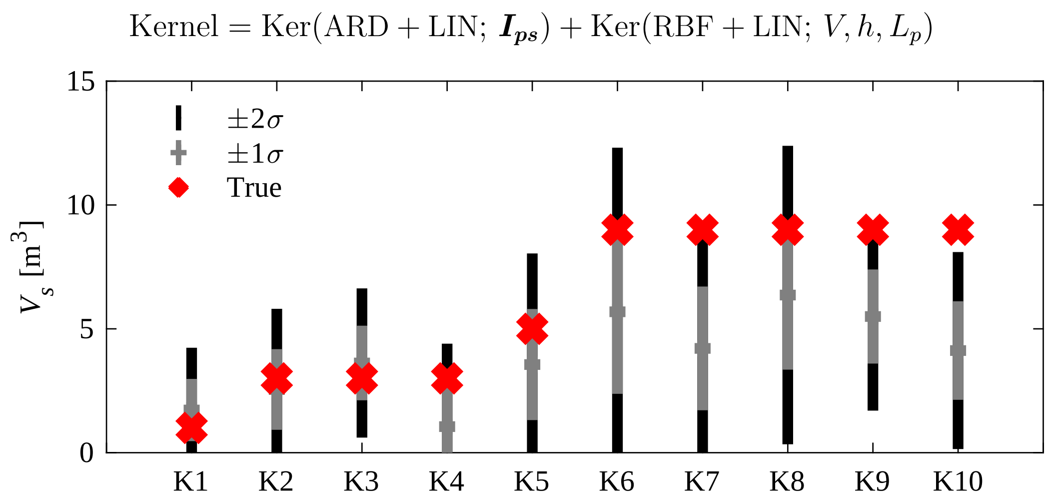

Fig. 6.8 True and estimated total sediment volume V_s at the on-site experiment with Ker(ARD + LIN; $\boldsymbol{I_{ps}}$) + Ker(RBF + LIN; V, h, L_p).

Advanced GPR III

Finally, through several try and errors, I selected the kernel in fig. 6.9. Still some underestimation is found, all truth data are in a range of $\pm 2\sigma$ and the estimate bias are acceptable in terms of bypass tunnel management.

Kernel = Ker(ARD + LIN; $\boldsymbol{I_{ps}}$) + Ker(RBF + LIN; V, L_p) + Ker(RBF + LIN; V, L_p)

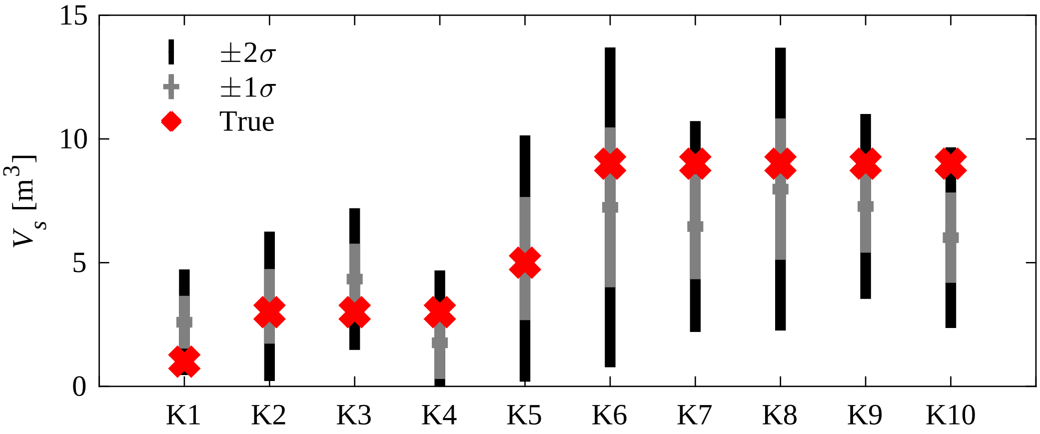

Fig. 6.9 True and estimated total sediment volume V_s at the on-site experiment with Ker(ARD + LIN; $\boldsymbol{I_{ps}}$) + Ker(RBF + LIN; V, L_p) + Ker(RBF + LIN; V, L_p).

Chapter 7

Application to the Koshibu Dam SBT Operation

In this chapter, the Koshibu Dam SBT and the history of the operations are introduced. Then the signal cleaning, feature extraction, and GPR model introduce and developed in chapter 5 and chapter 6 are applied for four operations.

7.1 The Koshibu SBT operations in 2016 - 2019

Since the first operation in September 2016, the Koshibu SBT was operated for eight times as a testing period. Table 7.1 shows the list of operations with the period, operation duration, maximum inflow discharge, and maximum bypass discharge. The consequent maximum flow velocity and water depth were given assuming uniform flow and a roughness length of 0.013 $m^{1/3}s^{-1}$. As of present, the SBT was operated 2-3 times in a year. Also, the inflow discharge in this three years and the bypass discharge are shown in fig. 7.1. First several operations were relatively small scale because their main purpose was to evaluate the SBT for the downstream and structural impacts. Contrary, recent bypassed discharges were as large as inflow discharges, thus the sediment might have been effectively bypassed. In particular, `Op5`, `Op7`, and `Op8` completely include the flood peak periods. Overall, bypass operations did not last until the end of a flood event in order to mitigate sediment deposition inside the tunnel and to start storing water in the reservoir.

Table 7.1 The Koshibu SBT operations in 2016 - 2018.

Operation No.	Date [-]	Duration [hours]	$Q_{bypass,max}$ [m^3/s]	V_{max} [m/s]	h_{max} [m]
Op1	21-22/09/2016	16	80	9.14	1.28
Op2	23/09/2016	5.8	60	8.31	1.06
Op3	04-05/07/2017	3.1	120	10.39	1.67
Op4	22-23/10/2017	9.7	180	11.75	2.18
Op5	29-30/10/2017	48.8	90	9.49	1.83
Op6	04-05/07/2018	10.7	150	11.13	1.93
Op7	04-05/09/2018	44.2	175	11.65	2.14
Op8	01-02/10/2018	69.5	200	12.11	2.34

Some of the sediment monitoring apparatuses were damaged or not able to record data well. Table 7.2 summarizes the condition of all sediment monitoring devises. JPMs were completely destroyed during the second operation. In general, JPMs are not robust against strong impacts, having high sensitivity though, because the half of the pipe is out of bed surface. According to the fact that three IPs are still working after experiencing large bypass operations such as 6, 7, and 8, IPs might be much more robust than JPMs.

Table 7.2 Condition of bedload monitoring apparatuses at the Koshibu SBT.

Operation	IP1	IP2	IP3	IP4	IP5	IP6	IP7	JPM1	JPM2
Op1	✓✓	✓✓	✓✓	✓✓	✓✓	✓✓	✓✓	✓✓	✓✓
Op2	✓✓	✓✓	✓✓	✓✓	✓✓	✓✓	✓✓	✓✓*	✓✓*
Op3	✓	✓	✓	✓	✓	✓	✓	×	×
Op4	✓	✓	✓	✓	✓	✓	✓	×	×
Op5	✓	✓	✓	✓	✓	✓	✓	×	×
Op6	✓✓	✓✓	✓✓	✓✓	✓✓	✓	✓	×	×
Op7	✓	✓	✓	✓	✓	✓	✓	×	×
Op8	✓✓	✓✓	✓✓*	✓✓	✓✓	×	×	×	×

✓✓ Both impulses and raw signals were recorded.
✓ Only impulses were recorded.
× Neither impulses nor raw signals were recorded.
* Broken during the operation.

7.2 Application

The signal cleaning with DWT, feature extraction by impulse count, and GPR were applied for Op1, Op2, Op6, and Op8, which raw signals were recorded, to obtain spatiotemporal information of grain size and bedload transport rate. As in the preceding

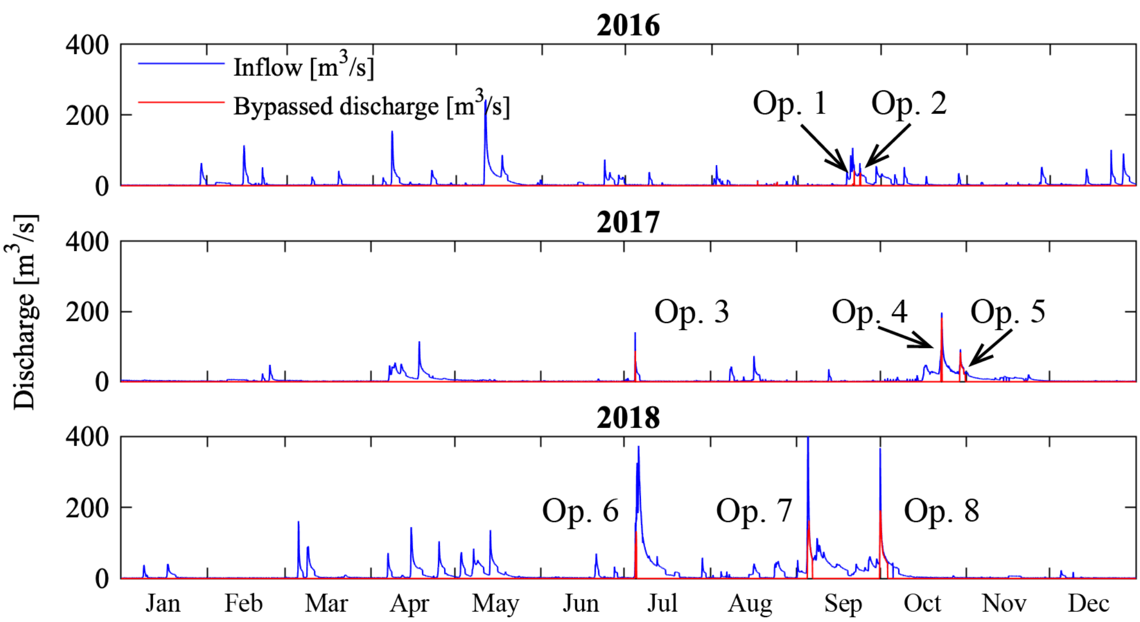

Fig. 7.1 The inflow discharge into the Koshibu reservoir, and the bypassed discharge by the Koshibu SBT in 2016 - 2019

chapter, signals were denoised to `WT1011` and use kernels for gran size and bedload transport rate estimation are Ker(RBF + LIN; $\boldsymbol{I_{ps}}, V^{-1}$) and Ker(ARD + LIN; $\boldsymbol{I_{ps}}$) + Ker(RBF + LIN; V, L_p) + Ker(RBF + LIN; V, L_p) respectively. Their hyperparameters were also those optimized in the preceding chapter using experimental data.

Results of `Op1`, `Op2`, `Op6`, and `Op8` are fig. 7.2, fig. 7.3, fig. 7.4, and fig. 7.5 respectively. Every figure consists of five plots with time in abscissa:

- Top row
  Bypassed discharge Q [m^3/s] and accumulated estimated bedload volume $V_{s,acc}$ [m^3]. The blue shaded area stands for the range of the mean estimate $\pm 1\sigma$(standard deviation).

- Second row
  Estimated D_{50} [mm]. The blue shaded area stands for the range of the mean estimate $\pm 1\sigma$.

- Middle row
  Mean of estimated D_{50} [mm] for each plate (`IP1 - IP5`).

- Forth row

Bedload transport rate BTR V_s [m^3/s]. The blue shaded area stands for the range of the mean estimate $\pm 1\sigma$.

- Bottom row
  Mean of estimated bedload transport rate BTR per a second per a plate width V_s [m^3/s / plate width] for each plate (`IP1 - IP5`).

Note that in fig. 7.5, `IP3` was broken during the operation. Consequently, the grain size and bedload transport rate are underestimated. Also, `IP5` in fig. 7.4 seems to be broken during the operation.

All operation with impulses are in chapter A.

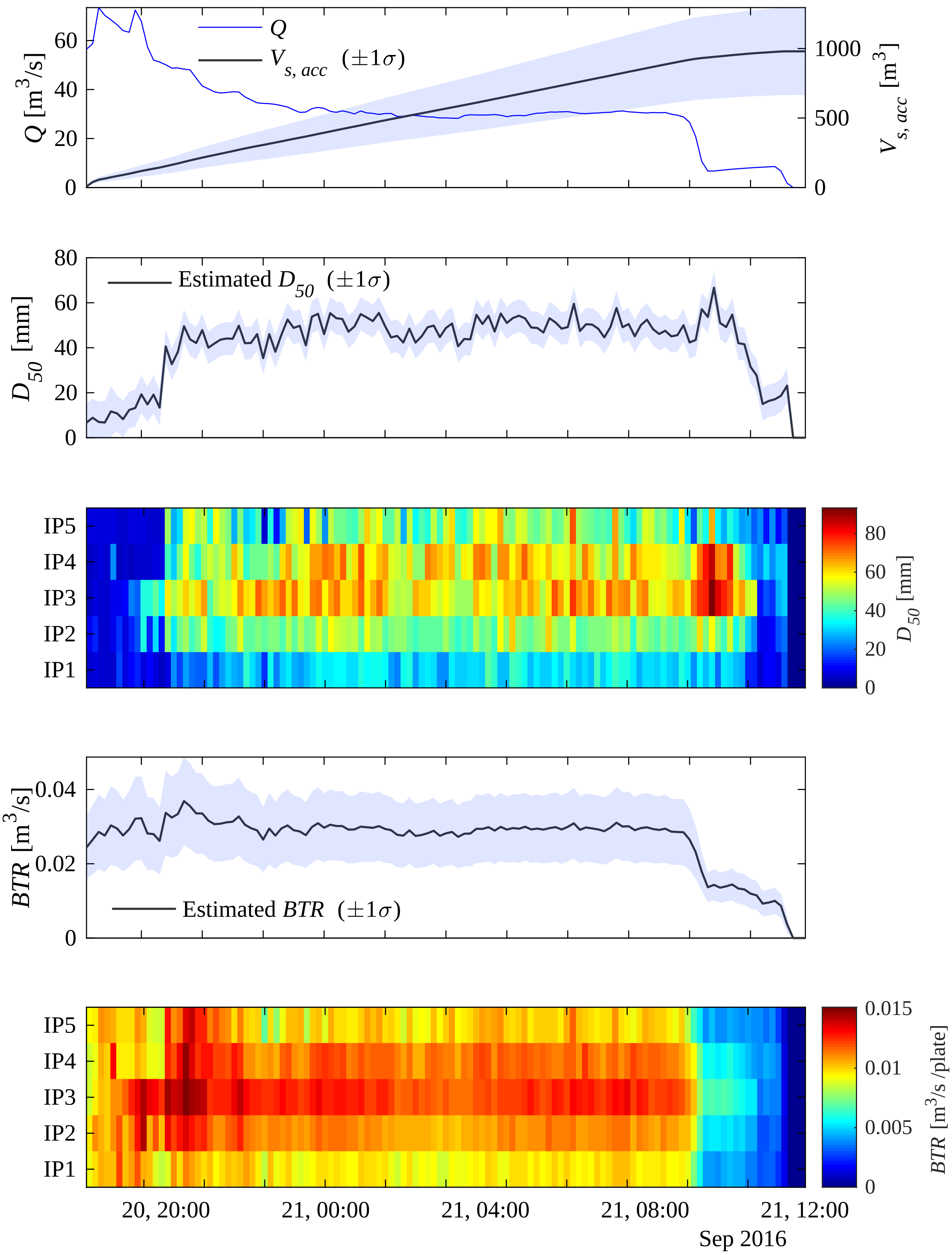

Fig. 7.2 Estimated grain size and bedload transport rate in `Op1`

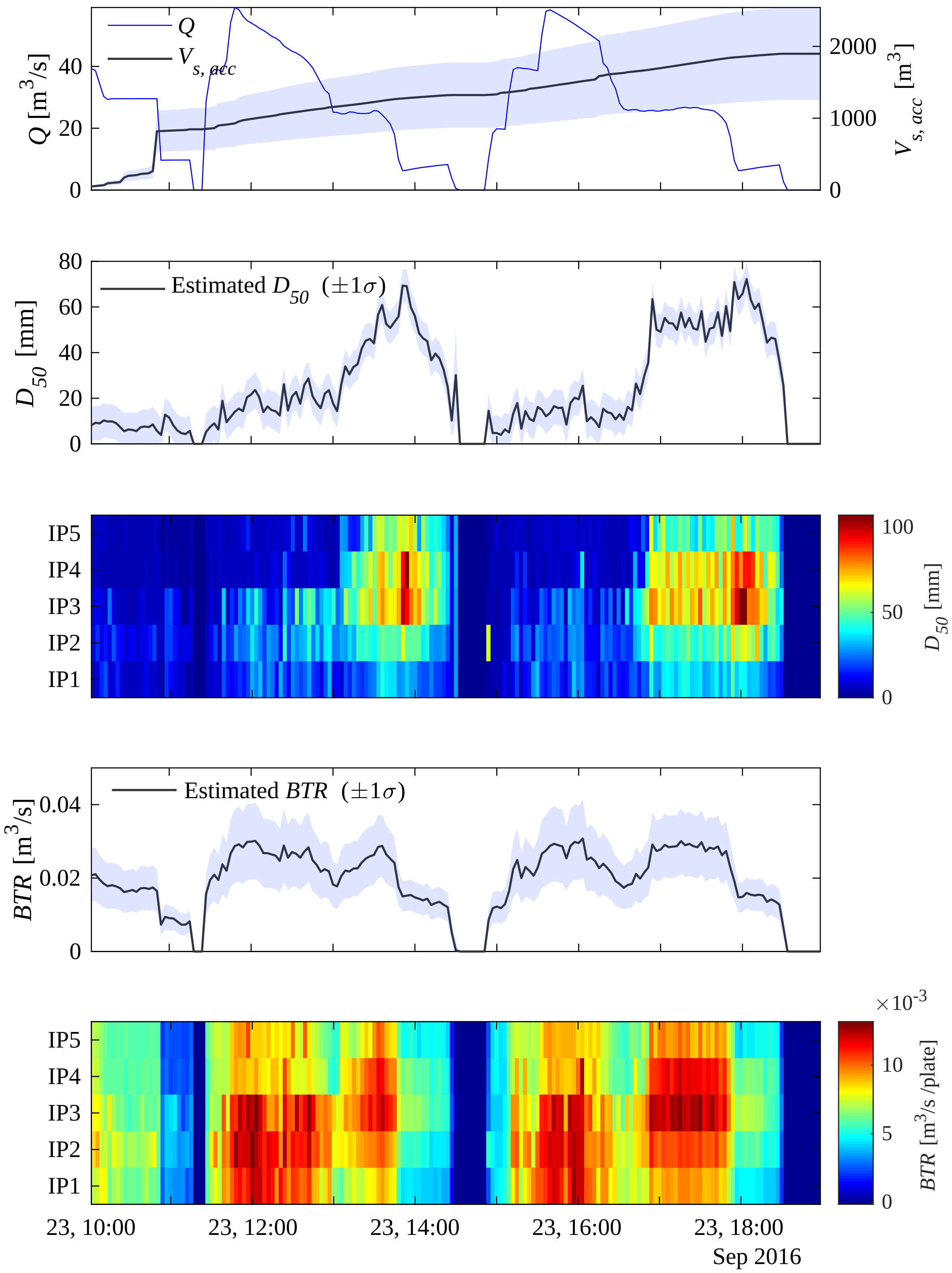

Fig. 7.3 Estimated grain size and bedload transport rate in `Op2`

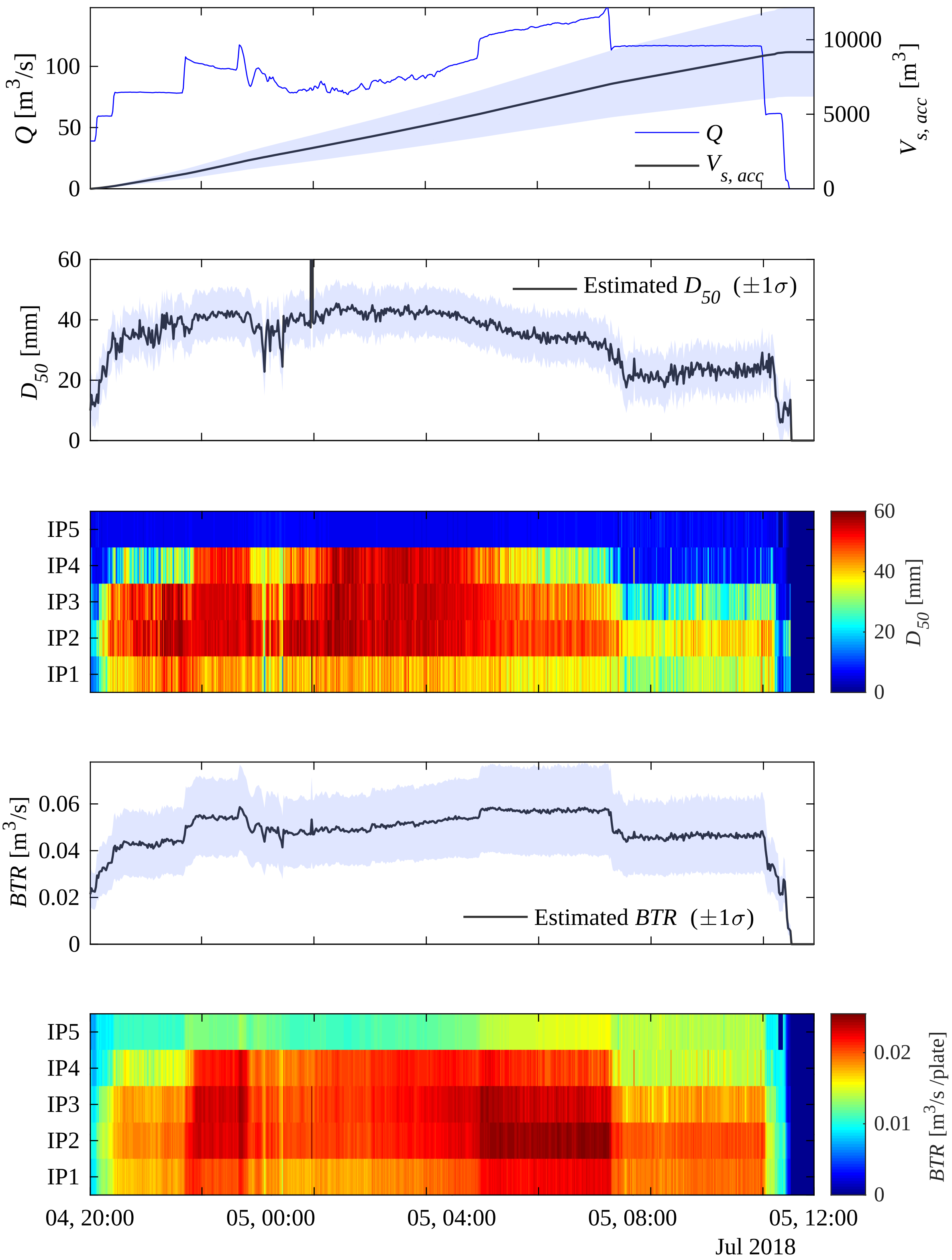

Fig. 7.4 Estimated grain size and bedload transport rate in `Op6`

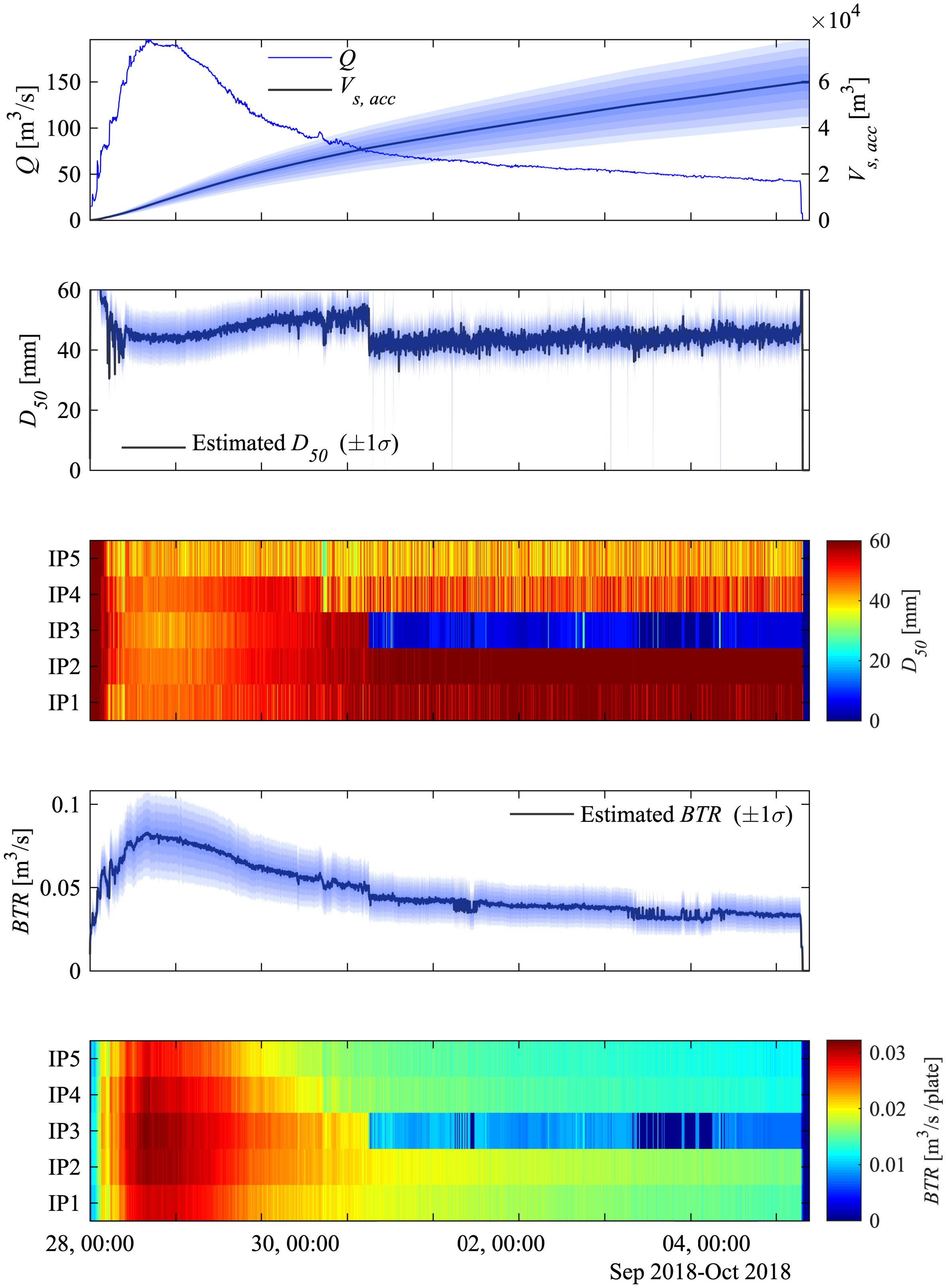

Fig. 7.5 Estimated grain size and bedload transport rate in `Op8`

7.3 Findings

I give findings in `Op2` where a complicated operation was done for a test operation. The discharge presents bimodal shape. This was to test with frequent gate open and close to confirm smooth gate open and close during a flood event.

The results were provided with mean and standard deviation. This is one advantage of using GPR. The method outputs prediction with a probability distribution, thus we can know the uncertainty of the results. Overall, bedload transport was output with higher variance than D_{50}. This is because the D_{50} observed in the field was the same order as that used in laboratory experiments conducted for making the model. In contrast, the bedload transport rate observed in the field was sometimes much higher than that in experiments, thus the variance for bedload transport rate tends to be relatively large.

Estimated D_{50} was less than 100 mm. To consider that the maximum designed sediment grain size to be bypassed at the Koshibu Dam SBT is 100 – 200 mm, this result is reasonable. Evidently, larger grain sizes were observed when discharge was not the maximum value. It might be caused by the condition at the SBT inlet. In the rising limb of the bypass discharge, the inlet gate was opened gradually and flow state was not in open channel. Contrary, the decreasing part of bypass discharge might be open channel, hence larger drag force occurred to induce larger grain sizes to flow. For the aspect of abrasion mitigation, it is reported that saltating gravels damage inverts much higher than sliding and rolling gravels. Accordingly, it is favorable that larger grain size sediment flowed under relatively low discharge period where flow velocity was also low.

Bedload transport was constant in both operations despite of the drastic change of D_{50}. This might be because large grain size was observed in lower discharge and vice versa. It should be noted that bedload concentrated on `IP1` – `IP3` in the first half of each operation. This is caused by secondary flow (secondary flows of Prandtl's second kind) occurred due to the tunnel curvature. Also, this result is consistent with abrasion observation at the Asahi Dam SBT in Japan (fig. 7.6) where abrasion concentrated on tunnel curve inner side. However, the concentration was not as significant as that of abrasion at the Asahi Dam SBT. Even in other operations with the maximum discharge 200 m^3/s recorded, significant concentration was not confirmed. Considering the secondary flow is proportional to flow velocity/curvature, it might be possible that the large curvature of the Koshibu Dam SBT would not make severe abrasion in tunnel curve inner side. Moreover, sediment transport concentrated on the middle in the tunnel width direction in the latter half of each operation. Considering the existence of large grain sizes in these periods, I expect the force caused by secondary flow was not adequately large to move sediment to the inner side. Therefore, at least in the Koshibu Dam SBT or larger SBTs, it might be important to carry out abrasion mitigation measures on the center of tunnels.

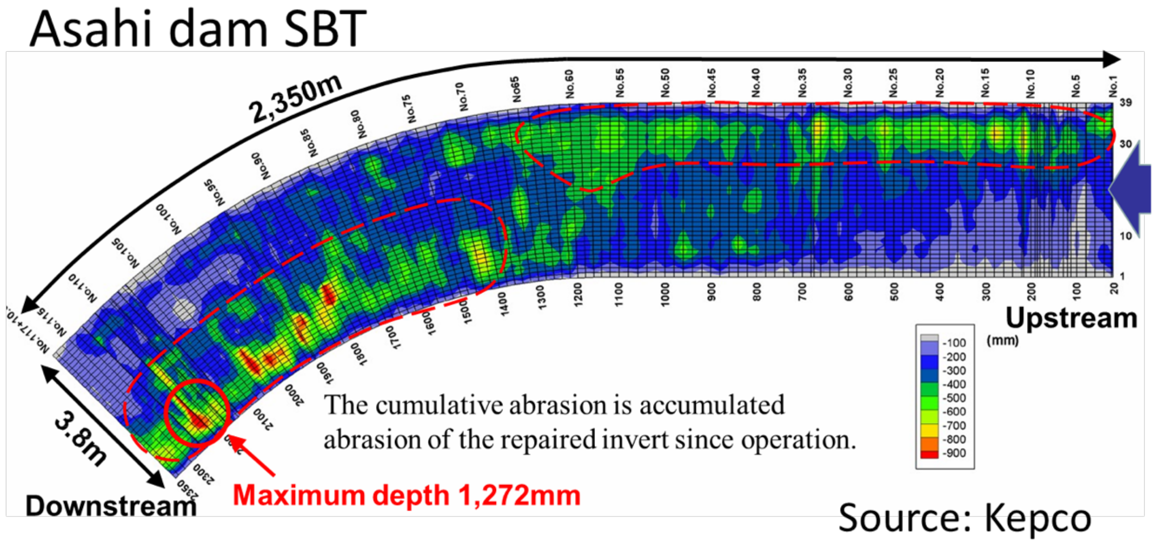

Fig. 7.6 Accumulated abrasion depth (1998 to Nov.2011) at the Asahi dam SBT (adapted from Nakajima et al. (2015)).

Chapter 8

Discussion

This chapter discusses my approaches and results. The discussion consists of two sections, one is on signal analyses and the other is on SBT based on the results obtained in chapter 7. The former section is separated into three subsections on signal cleaning, feature extraction, and modeling.

8.1 Discussion on signal analysis

I systematically conducted signal analysis and statistical modelling for concerting signals obtained from a surrogate monitoring system to grain size and bedload transport rate. It was one achievement that I was able to make a model to estimate grain size and bedload transport rate without giving information on specific observation sites but only from raw signals. However, still I have questions and ideas to improve the accuracy of their prediction as in the following sections.

8.1.1 Signal cleaning

Wavelet selection

I confirmed that the use of DWT much improves the signal denoising than conventional low-pass filtering using FT. The wavelet function (basis function) I used was Daubechies 6 wavelet at level 5, but different from FT, there are many other options available for WT (Rucka and Wilde, 2006). In general, the ability to detect singular property of signals and locality are trade-off, hence no wavelet function can satisfy both requirements.

In other words, different wavelet function gives different balance of the two. In that context, Daubechies 6 wavelet is intermediate wavelet. In future work, I am worth applying other wavelet functions to find the best balance of them for signals obtained from surrogate monitoring systems.

This study used a single combination of decomposed signals. However, it is natural that the best wavelet differs from the source of impacts, e.g., different grain size, impact velocity. In fact, it is reported that the centroidal frequency depends on grain sizes (Barrière et al., 2015; Møen et al., 2010; Thorne, 1986; Wyss et al., 2016a). This implicates the best combination of decomposed signals are also different by grain sizes. Additionaly if one needs to observe sediment of limited range of grain sizes, the specific denoising for the purpose can be designed by using WT.

Singularity detection

One advanced technique using WT is singularity detection using *Lipschitz exponent* (Stephane and Hwang, 1992). Lipschitz exponent computed from CWT can be an indicator of singularity occurrence in a signal. Using this convenient property, Lipschitz exponent is used for anomaly detection such as damage detection (Błaszczuk and Pozorsk, 2007; Hong et al., 2002). Because my interest in signals is at the timing when a gravel hits on the plate, it is possible that Lipschitz exponent directly gives the information on sediment impact.

8.1.2 Feature extraction

Frequency domain

The feature extraction used in this study was impulse count developed in Japan. Originally, the method was developed for greatly decreasing the data volume to be able to store data even in poor computers. Therefore studies that can use raw signals should use more detailed features for improving model precision. Although my study employed 11-dimensional impulses being greater than the conventional one by five dimensions, one important feature I did not use was frequency domain. As noted in the preceding section, grain size depends on frequency spectrum and that is both experimentally and theoretically confirmed. In particular, as long as I use GP, the increase of feature quantity is not a big problem since the computational time of GP is depending on the sample size (Rasmussen and Williams, 2006). However, it should be reminded that the increase of feature quantity can reduce the interpretability of models.

8.1.3 Modeling

Model improvement

This study enabled us to quantify bedload transport information by introducing GPR, which has high expressive power. Even though this approach is rather deductive than existing studies on surrogate monitoring, both approaches do not conflict. I employed some a priori knowledge to kernels, but they are still fundamental relationships: linear relation between impulses and bedload transport rate, underestimation with increasing flow velocity and water depth. Further improvement of the kernels can be achieved by more sophisticated findings proposed by existing studies. In addition, since the GP is non-parametric method, more data may increase the applicability and precision for other applications.

Similar to other statistical models, more data improve GPR more. In particular, my data used were only derived from artificial channel, experimental flumes and SBT. Therefore, I believe that incorporating signals from various natural rivers into the model must improve the model's applicability for any monitoring environment.

One advantage using GPR is that the degree of prediction confidence is explicitly given as $\pm 1\sigma$ depicted in fig. 7.2. By checking the range of variance with various inputs, we can know the data that are far from that the model has experienced. This advantage supports us to plan the next experiments efficiently.

Grain size distribution

The study presented D_{50} prediction, and the next step is grain size distribution. Unfortunately, GPR can not directly applied for multi-output cases. As a solution, the simplest way to compute grain size distribution is making GPR for every grain size fractions. Also, extension of GP for multi outputs cases are proposed by Bonilla et al. (2008).

Phenomena interpretation

My research focused on the better prediction of grain size and bedload transport rate. However, considering GP has high interpretability, we can understand natural phenomena from good kernels found heuristically in GP.

Several approaches to search appropriate kernels from a number of kernel combinations are proposed (e.g. Bach, 2009; Duvenaud et al., 2011). These techniques search the best combination of kernels through and through by certain efficient approach. Then by seeing the kernels used in the model and the selected features, we can infer the structure of data. Interestingly, the attempt to describe the model structure with natural language is proposed by Lloyd et al. (2014). We can say that ARD kernel used in this study is attributed to a similar idea. Optimizing the kernel is equivalent to evaluate the importance of each feature to estimate the target.

8.2 Discussion on sediment bypass tunnels

Spatiotemporal transient of grain size and bedload transport in the Koshibu Dam SBT operations were revealed section 7.2. A particular point of the results is that the values are given as distribution hence mean and $\pm 1\sigma$ are depicted. Because other popular techniques including linear regression, multiple linear regression, Neural Networks do not provide the information, it is hard to know how much certain the results is. This advantage might be valuable particularly in the field of civil engineering that involves high cost and human safe and secure.

According to figures in section 7.2, the standard deviation of D_{50} is generally small. In contrast, that of bedload transport rate is relatively high, thus involves higher uncertainty. It might be attributed to the water depth which used for bedload transport rate estimate but did not for grain size. The flow velocity and impulses, used both for bedload transport rate and grain size, observed in SBT operations were mostly in the range of that observed in flume experiments. While, water depth, used only for bedload transport rate estimate, observed in the operations was generally much higher than that in flume experiments. I expect that great deal of extrapolation with regard to water depth caused the increase of uncertainty in bedload transport estimate. In order to reduce the uncertainty, it is needed to conduct experiments with higher water depths or give some additional physical relationships to the model.

Spatial distribution

Observation with five IPs along the tunnel width direction enables us to know the spatial distribution of bedload transport. Overall, the middle three IPs, `IP2`, `IP3`, and `IP4`, observed the most. Comparing `IP1` and `IP5`,I see bedload transport rate on `IP1` is slightly higher than that on `IP5`. This is natural if secondary flow (secondary flows of Prandtl's second kind) occurred due to the tunnel curvature. Also, this result is consistent with abrasion observation at the Asahi Dam SBT in Japan (Nakajima et al., 2015). It is also reported that the volume of abrasion is proportional to bedload transport rate (Auel et al., 2018). To consider the study and the abrasion observation in the Asahi Dam SBT, the difference of bedload transport rate at `IP1` and `IP5` are too small.

For answering the question, in the future work, two things should be investigated: to confirm the linear relation between estimated bedload transport rate and measured abrasion volume at the Koshibu Dam SBT; bedload monitoring operations with higher bypass discharge because the degree of secondary flow is proportional to flow velocity.

8.3 Summary of signal processing and modelling in this study

Finally, I summarize the process of signal analysis for surrogate monitoring system. I hope this would help surrogate monitoring system users in applying the method proposed in this study. In the following algorithm,
$\mathbf{X} = \{\mathbf{x}_1, \mathbf{x}_2, \cdots, \mathbf{x}_N\}$: raw signals obtained from experiments,
$\mathbf{y} = \{y_1, y_2, \cdots, y_N\}$: targets, grain size or bedload transport rate,
$\mathbf{x}_\star$: new raw signal to be analyzed,
$y_\star$: predicted target corresponding to $\mathbf{x}_\star$,
I_n^j: the number of impulses with jth threshold,
$\mathbf{I} = \{\mathbf{I}_1, \mathbf{I}_2, \cdots, \mathbf{I}_N\}$,
th_{dwt}^i: threshold for Discrete Wavelet Transform (threshold for ith level),
th_{ips}^j: threshold for pulse counting (jth threshold),
k: kernel function with the hyperparameters $\boldsymbol{\theta}$.

In this study, Discrete Wavelet Transform was processed with `MALTAB Wavelet Toolbox`. The Gaussian Process Regression was processed with `GPML software package` (Rasmussen and Nickisch, 2010).

Algorithm 1

Input: $\mathbf{X}$, $\mathbf{y}$, $\mathbf{x}_\star$, th^{i}_{dwt}, th^{j}_{ips}, k
Output: $\Pr(y^\star|\mathbf{x}^\star, \mathbf{y}, \mathbf{X})$

step:1 Signal Cleaning
for $n = 1$ to N **do**
  Remove DC components $\mathbf{x}_n = \mathbf{x}_n - \mathrm{mean}(\mathbf{x}_n)$
  Decompose $\mathbf{x}_n$ with Discrete Wavelet Transform as $\mathbf{x}_n = d_1 + \cdots + d_5 + a_5$
  Thresholding as $d_i(d_i < th) = 0$ and $d_i(d_i > th) = d_i(d_i > th) - th\ (= d'_i)$
  Reconstruct the signal as $\mathbf{x}^{denoised}_n = d'_1 + \cdots + d'_5$
end for

step:2 Feature Extraction
for $n = 1$ to N **do**
  $\mathbf{x}^{abs}_n = \mathrm{abs}(\mathbf{x}^{denoised}_n)$
  $\mathbf{x}^{env}_n = \mathrm{envelope}(\mathbf{x}^{abs}_n)$
  I^{j}_n = the number of times that $\mathbf{x}^{env}_n$ being over th^{j}_{ips}
end for

step:3 Model Optimization
Optimizing $\boldsymbol{\theta}$ by maximizing marginal likelihood $\Pr(\mathbf{y}|\mathbf{X}, \boldsymbol{\theta}))$

step4 Prediction
Process **step:1** and **step:2** for $\mathbf{x}_\star$ to obtain $I^\star$
$\mathbf{K} = k(\mathbf{I}_n, \mathbf{I}_{n'})$
$\mathbf{k}_\star = (k(\mathbf{I}^\star, \mathbf{I}_1), k(\mathbf{I}^\star, \mathbf{I}_2), \cdots, k(\mathbf{I}^\star, \mathbf{I}_N))^\mathsf{T}$
$k_{\star\star} = k(\mathbf{I}^\star, \mathbf{I}^\star)$
$\Pr(y^\star|\mathbf{I}^\star, \mathbf{y}, \mathbf{I}) = \mathcal{N}(\mathbf{k}_\star^\mathsf{T}\mathbf{K}^{-1}\mathbf{y},\ k_{\star\star} - \mathbf{k}_\star^\mathsf{T}\mathbf{K}^{-1}\mathbf{k}_\star)$
return $\Pr(y^\star|\mathbf{x}^\star, \mathbf{y}, \mathbf{X}) = \Pr(y^\star|\mathbf{I}^\star, \mathbf{y}, \mathbf{I})$

Chapter 9

Conclusion

I made a model to quantify grain size and bedload transport rate in sediment bypass tunnels with surrogate bedload monitoring. The model was systematically constructed through signal cleaning, feature extraction, and statistical modeling. My primal contribution is employment of Gaussian process regression for modeling which gives us high intractability and expressive power, quantification of grain size and bedload transport rate in high accuracy with the uncertainty provided. Although this model was made for sediment bypass tunnels monitoring, this is applicable for any natural rivers without giving specific field information, but purely from obtained signals and several fundamental information such as flow velocity and water depth.

Our achievement and findings are following:

- I highlighted the importance of bedload monitoring during SBTs to make appropriate measures against invert abrasion. For that, a surrogate bedload monitoring system called an impact plate was employed. This system presented enough robustness and sensitivity for bedload monitoring in SBTs. The Koshibu Dam SBT in Japan was selected as the study field and impact plates were installed.

- Data used for making a model to predict bedload transport rate and grain size were collected through laboratory flume and on-site experiments.

- I segmented the process of signal analysis into three steps, namely, signal cleaning, feature extraction, and modeling. Then, existing studies on surrogate bedload monitoring was summarized on the basis of the methods used in the each step. Considering the fact that the studies do not focus on signal cleaning well, and use highly deductive approaches, I attempted to use advanced signal processing method for signal cleaning and a relatively inductive (data driven) approach for modeling.

- To consider particular properties of signals obtained from impact plates, i.e., non-periodicity and abrupt change appearance, Discrete Wavelet Transform was exploited for denoising. As the result, it was confirmed that noise was removed better than that done with conventional low-pass filter, consequently the distinguishability of grain size improved.

- For modeling, a non-parametric Gaussian process regression, which has both high expressive power and high interpretability was employed. In addition, because application of models based on flume experiments to real field data involves extrapolation, my models were created only using flume experiment data with integrating background knowledge. Then, the models were evaluated in terms of their prediction accuracy (RMSE) for on-site experiment data where the application also presents extrapolation. At last, I was able to make a model which provides good prediction accuracy for on-site experimental data albeit the model was optimized only from flume experimental data.

- The best model was utilized for estimating spatiotemporal transition of grain size and bedload transport rate during the Koshibu Dam sediment bypass tunnel operations. In addition, I found consistency between the observed bedload and abrasion distribution measured in another sediment bypass tunnel.

I hope this study accelerate not only sediment bypass tunnel design, operation, and maintenance, but also the studies of surrogate bedload monitoring.

References

P. S. Addison. *The illustrated wavelet transform handbook: introductory theory and applications in science, engineering, medicine and finance*. CRC press, 2017. (pages 42 and 43)

H. Akaike. On the role of statistical reasoning in the process of identification. In G. Sawaragi and S. Sagara, editors, *SYSID'97, 11th IFAC Symposium on System Identification*, volume 1, pages 1–8, 1997. (page 36)

H. Akaike, S. Amari, Y. Kabashima, G. Kitagawa, and H. Shimodaira. *Akaike Information Criterion AIC*. Kyoritsu Shuppan Co., Ltd., 2007. (in Japanese). (page 36)

I. Albayrak, M. Mueller-Hagmann, and R. M. Boes. Calibration of Swiss Plate Geophone System for bedload monitoring in a sediment bypass tunnel. In T. Sumi, editor, *2nd International Workshop on Sediment Bypass Tunnels*, page FP16. Kyoto University, Kyoto, Japan, 2017. (page 10)

C. Auel. *Flow characteristics, particle motion and invert abrasion in sediment bypass tunnels*. PhD thesis, ETH Zürich, 2014. (pages 2, 10, 17, and 19)

C. Auel and R. M. Boes. Sediment bypass tunnel design–review and outlook. *Dams and reservoirs under changing challenges*, 40312, 2011a. (page 8)

C. Auel and R. M. Boes. Sediment bypass tunnel design–hydraulic model tests. In *Proc. Hydro 2011- practical solutions for a sustainable future*, volume 29, Prague, Czech Republic, 2011b. Aqua-Media International Ltd. (pages 19 and 29)

C. Auel and R. M. Boes. Sustainable reservoir management using sediment bypass tunnels. In *Proc. 24th ICOLD Congress*, page 224–241, Kyoto, Japan, 2012. (pages 8 and 10)

C. Auel, S. A. Kantoush, and T. Sumi. Positive effects of reservoir sedimentation management on reservoir life – examples from Japan. In *Proc. 84th ICOLD Annual Meeting*, pages 4_11 – 4_20, Johannesburg, South Africa, 2016. (page 9)

C. Auel, I. Albayrak, T. Sumi, and R. M. Boes. Sediment transport in high-speed flows over a fixed bed: 1. particle dynamics. *Earth Surface Processes and Landforms*, 42 (9):1365–1383, 2017a. (page 65)

C. Auel, S. Kobayashi, Y. Takemon, and T. Sumi. Effects of sediment bypass tunnels on grain size distribution and benthic habitats in regulated rivers. *International journal of river basin management*, 15(4):433–444, 2017b. (page 11)

C. Auel, R. M. Boes, and T. Sumi. Abrasion prediction at Asahi sediment bypass tunnel based on Ishibashi's formula. *Journal of Applied Water Engineering and Research*, 6(2):125–138, 2018. (pages 10, 13, 21, and 80)

F. Bach. High-dimensional non-linear variable selection through hierarchical kernel learning. *arXiv preprint arXiv:0909.0844*, 2009. (page 79)

J. Barrière, A. Krein, A. Oth, and R. Schenkluhn. An advanced signal processing technique for deriving grain size information of bedload transport from impact plate vibration measurements. *Earth Surface Processes and Landforms*, 40(7):913–924, 2015. (pages 35 and 78)

A. Baumer and R. Radogna. Rehabilitation of the Palagnedra sediment bypass tunnel (2011-2013). In R. M. Boes, editor, *1st International Workshop on Sediment Bypass Tunnels*, pages 235–245. VAW-Mitteilung 232, ETH Zürich, Switzerland, 2015. (page 10)

N. Baydar and A. Ball. Detection of gear failures via vibration and acoustic signals using wavelet transform. *Mechanical Systems and Signal Processing*, 17(4):787–804, 2003. (page 41)

A. A. Beylich and K. Laute. Combining impact sensor field and laboratory flume measurements with other techniques for studying fluvial bedload transport in steep mountain streams. *Geomorphology*, 218:72–87, 2014. (pages 18, 22, and 35)

C. M. Bishop. *Pattern recognition and machine learning*. Springer Science+ Business Media, 2006. (page 33)

J. Błaszczuk and Z. Pozorsk. Application of the Lipschitz exponent and the wavelet transform to function discontinuity estimation. *Scientific Research of the Institute of Mathematics and Computer Science*, 6(1):23–30, 2007. (page 78)

R. M. Boes, editor. *Proc.Ecological effects of SBT operations on a First International Workshop on Sediment Bypass Tunnels*, VAW-Mitteilungen 232, Zürich, Switzerland, 2015. Laboratory of Hydraulics, Hydrology and Glaciology (VAW), ETH Zürich, Switzerland. (page 11)

R. M. Boes, C. Auel, M. Hagmann, and I. Albayrak. Sediment bypass tunnels to mitigate reservoir sedimentation and restore sediment continuity. *Reservoir sedimentation*, pages 221–228, 2014. (page 9)

E. V. Bonilla, K. Chai, and C. Williams. Multi-task gaussian process prediction. In *Advances in neural information processing systems*, pages 153–160, 2008. (page 79)

K. Bunte, S. R. Abt, J. P. Potyondy, and S. E. Ryan. Measurement of coarse gravel and cobble transport using portable bedload traps. *Journal of Hydraulic Engineering*, 130(9):879–893, 2004. (page 17)

D.J. Buttle and C.B. Scruby. Characterization of particle impact by quantitative acoustic emission. *Wear*, 137(1):63–90, 1990. (page 34)

G. D. Cesare, A. Schleiss, and F. Hermann. Impact of turbidity currents on reservoir sedimentation. *Journal of Hydraulic Engineering*, 127(1):6–16, 2001. doi: 10.1061/(ASCE)0733-9429(2001)127:1(6). (page 2)

I. Daubechies. *Ten lectures on wavelets*, volume 61. Siam, 1992. (pages 41 and 42)

A. Dell'Agnese, L. Mao, and F. Comiti. Calibration of an acoustic pipe sensor through bedload traps in a glacierized basin. *Catena*, 121:222–231, 2014. (page 35)

U. Depczynski, K. Jetter, K. Molt, and A. Niemöller. The fast wavelet transform on compact intervals as a tool in chemometrics. i. mathematical background. *Chemometrics and intelligent laboratory systems*, 39(1):19–27, 1997. (page 41)

D. L. Donoho and I. M. Johnstone. Threshold selection for wavelet shrinkage of noisy data. In *16th Annual International Conference of the IEEE Engineering in Medicine and Biology Society*, volume 1, pages A24–A25. IEEE, 1994. (page 43)

D. Duvenaud. *Automatic Model Construction with Gaussian Processes*. PhD thesis, Computational and Biological Learning Laboratory, University of Cambridge, 2014. (page 50)

D. Duvenaud, H. Nickisch, and C. E. Rasmussen. Additive gaussian processes. In *Advances in neural information processing systems*, pages 226–234, 2011. (page 79)

M. Facchini, A. Siviglia, and R. M. Boes. Downstream morphological impact of a sediment bypass tunnel-preliminary results and forthcoming actions. In R. M. Boes, editor, *1st International Workshop on Sediment Bypass Tunnels*, pages 137–144. VAW-Mitteilung 232, ETH Zürich, Switzerland, 2015. (pages 10 and 11)

T. Figlus, Š. Liščák, A. Wilk, and B. Łazarz. Condition monitoring of engine timing system by using wavelet packet decomposition of a acoustic signal. *Journal of mechanical science and technology*, 28(5):1663–1671, 2014. (page 41)

H. Fukuroi. Damage from Typhoon Talas to civil engineering structures for hydropower and the effect of the Sediment Bypass System at Asahi Dam. In *Proc. Int. Symposium on Dams for a changing World—Need for Knowledge Transfer across the Generations and the World*, Kyoto, Japan, 2012. (pages 9 and 10)

S. Gaillot and H. Piegay. Impact of gravel-mining on stream channel and coastal sediment supply: example of the Calvi Bay in Corsica (France). *Journal of Coastal Research*, pages 774–788, 1999. (page 2)

T. Geay, P. Belleudy, C. Gervaise, H. Habersack, J. Aigner, A. Kreisler, H. Seitz, and J.B. Laronne. Passive acoustic monitoring of bed load discharge in a large gravel bed river. *Journal of Geophysical Research: Earth Surface*, 122(2):528–545, 2017. (pages 34 and 35)

K. Goto, T. Itoh, T. Nagayama, M. Kasai, and T. Marutani. Experimental and theoretical tools for estimating bedload transport using a Japanese pipe hydrophone. *International Journal of Erosion Control Engineering*, 7(4):101–110, 2014. (pages 20 and 35)

P. E. Grams, J. C. Schmidt, and D. J. Topping. The rate and pattern of bed incision and bank adjustment on the Colorado River in Glen Canyon downstream from Glen Canyon Dam, 1956–2000. *Geological Society of America Bulletin*, 119(5-6):556–575, 2007. (page 2)

J. R. Gray, J. B. Laronne, and J. D. G. Marr. *Bedload-surrogate monitoring technologies*. US Department of the Interior, US Geological Survey, 2010. (pages 18 and 19)

M. Hagmann, I. Albayrak, and R. M. Boes. Field research: Invert material resistance and sediment transport measurements. In R. M. Boes, editor, *1st International Workshop on Sediment Bypass Tunnels*, pages 123–135. VAW-Mitteilung 232, ETH Zürich, Switzerland, 2015. (pages 10 and 19)

N. Hakoishi and T. Sakurai. Countermeasures against sedimentation for extending service life of reservoirs. *Civil engineering journal*, 55(1):28–31, 2013. (in Japanese). (page 3)

M. Harada. Planning and hydraulic design of bypass tunnel for sluicing sediment past Asahi Reservoir. In *Proc. 19th ICOLD Congress*, 1997. (page 10)

E. J. Helley and W. Smith. *Development and calibration of a pressure-difference bedload sampler*. US Dept. of the Interior, Geological Survey, Water Resources Division, 1971. (page 17)

J. Hensman, N. Fusi, and N. D. Lawrence. Gaussian processes for big data. *arXiv preprint arXiv:1309.6835*, 2013. (page 59)

T. Higuchi. The innovation of research and development by dig data, 2012. URL https://www.rieti.go.jp/jp/events/bbl/12051401.pdf. (Presentation slide in Japanese). (pages 36 and 37)

J. Hong, Y. Kim, H. Lee, and Y. Lee. Damage detection using the Lipschitz exponent estimated by the wavelet transform: applications to vibration modes of a beam. *International journal of solids and structures*, 39(7):1803–1816, 2002. (page 78)

ICOLD. Challenges and needs for dams in the 21st century, bulletin 185. Paris, France, 2019a. (page 2)

ICOLD. Role of Dams, 2019b. URL https://www.icold-cigb.org/GB/dams/dams.asp. (page 2)

T. Ishibashi. A hydraulic study on protection for erosion of sediment flush equipments of dams. *Civil Engineers Process*, 334(6):103–112, 1983. (in Japanese). (page 21)

F. Jacobs and M. Hagmann. Sediment bypass tunnel Runcahez: Invert abrasion 1995-2014. In R. M. Boes, editor, *1st International Workshop on Sediment Bypass Tunnels*, pages 211–221. VAW-Mitteilung 232, ETH Zürich, Switzerland, 2015. (page 10)

S. A. Kantoush, T. Sumi, A. Kubota, and T. Suzuki. Impacts of sediment replenishment below dams on flow and bed morphology of river. In *Proc. Coastal Zone Management of River Deltas and Low Land Coastlines*, pages 285–303, Alexandria, Egypt, 2010. (page 8)

S. A. Kantoush, T. Sumi, and M. Murasaki. Evaluation of sediment bypass efficiency by flow field and sediment concentration monitoring techniques. *Journal of Japan Society of Civil Engineers, Ser. B1 (Hydraulic Engineering)*, 67(4):I_169–I_174, 2011. (page 10)

J. Kashiwai and S. Kimura. Hydraulic examination of Koshibu dam's intake facilities for sediment bypass. In R. M. Boes, editor, *1st International Workshop on Sediment Bypass Tunnels*, pages 45–53. VAW-Mitteilung 232, ETH Zürich, Switzerland, 2015. (page 10)

J. Kashiwai, T. Sumi, and T. Honda. Hydraulic study on diversion facilities required for sediment bypass systems. In *Proc. 19th ICOLD Congress*, Florence, Italy, 1997. (page 8)

K. Kataoka. Sedimentation management at Asahi dam. In *Proc. The 3rd world water forum, Session "Challenges to the sedimentation management for reservoir sustainability"*, pages 197–207, Kyoto-Shiga, Japan, 2003. (page 11)

C. Kim and R. Aggarwal. Wavelet transforms in power systems. Part 1: General introduction to the wavelet transforms. *Power Engineering Journal*, 14(2):81–87, 2000. (page 41)

G. M. Kondolf. Profile: hungry water: effects of dams and gravel mining on river channels. *Environmental management*, 21(4):533–551, 1997. (page 2)

G. M. Kondolf, Y. Gao, G. W. Annandale, G. L. Morris, E. Jiang, J. Zhang, Y. Cao, C. Paul, K. Fu, Q. Guo, R. Hotchkiss, C. Peteuil, T. Sumi, H. Wang, Z. Wang, Z. Wei, B. Wu, C. Wu, and C. T. Yang. Sustainable sediment management in reservoirs and regulated rivers: Experiences from five continents. *Earth's Future*, 2 (5):256–280, 2014. (page 2)

T. Koshiba, C. Auel, D. Tsutsumi, S. A. Kantoush, and T. Sumi. Application of an impact plate–Bedload transport measuring system for high-speed flows. *International journal of sediment research*, 33(1):35–46, 2018. (pages 20, 22, 25, 35, 40, and 97)

A. Krein, H. Klinck, M. Eiden, W. Symader, R. Bier, L. Hoffmann, and L. Pfister. Investigating the transport dynamics and the properties of bedload material with a hydro-acoustic measuring system. *Earth Surface Processes and Landforms*, 33(1): 152–163, 2008. (pages 34 and 35)

Y. Kubota. *Improvement and application of sediment movement prediction in reservoirs*. PhD thesis, Kyoto University, 2017. (in Japanese). (page 12)

C. Kung, M. Tsai, Y. Chen, S. Huang, and M. Liao. Sediment sluicing tunnel at Nanhua Reservoir in Taiwan. In R. M. Boes, editor, *1st International Workshop on Sediment Bypass Tunnels*, pages 71–83. VAW-Mitteilung 232, ETH Zürich, Switzerland, 2015. (page 10)

J. Kurihara and K. Miyamoto. Equipment for sediment discharge with acoustic sensor. *Japan Society of Erosion Control Engineering*, 44(5):26–31, 1992. (in Japanese). (pages 20 and 21)

J. Lai, F. Lee, C. Wu, Y. Tan, and T. Sumi. Sediment bypass tunnels of the Shihmen Reservoir in Taiwan. In R. M. Boes, editor, *1st International Workshop on Sediment Bypass Tunnels*, pages 55–70. VAW-Mitteilung 232, ETH Zürich, Switzerland, 2015. (page 10)

J. Lin. Feature extraction of machine sound using wavelet and its application in fault diagnosis. *NDT & E International*, 34(1):25–30, 2001. (page 41)

Y. Lin, M. Lee, H. Chiang, T. Chang, and B. Tsai. Design concepts of desilting tunnel at Shimen Reservoir in Taiwan. In T. Sumi, editor, *2nd International Workshop on Sediment Bypass Tunnels*, page FP10. Kyoto University, Kyoto, Japan, 2017. (page 10)

J. R. Lloyd, D. Duvenaud, R. Grosse, J. Tenenbaum, and Z. Ghahramani. Automatic construction and natural-language description of nonparametric regression models. In *28th AAAI conference on artificial intelligence*, 2014. (page 80)

H. Lodhi, C. Saunders, J. Shawe-Taylor, N. Cristianini, and C. Watkins. Text classification using string kernels. *Journal of Machine Learning Research*, 2(2):419–444, 2002. (page 56)

Y. Ma, H. Huang, G. C. Nanson, Y. Li, and W. Yao. Channel adjustments in response to the operation of large dams: The upper reach of the lower Yellow River. *Geomorphology*, 147:35–48, 2012. (page 2)

L. Mao, R. Carrillo, C. Escauriaza, and A. Iroume. Flume and field-based calibration of surrogate sensors for monitoring bedload transport. *Geomorphology*, 253:10–21, 2016. (pages 18, 34, and 35)

S. M. Markalous, S. Tenbohlen, and K. Feser. Detection and location of partial discharges in power transformers using acoustic and electromagnetic signals. *IEEE Transactions on Dielectrics and Electrical Insulation*, 15(6):1576–1583, 2008. (page 41)

E. J. Martín, M. Doering, and C. T. Robinson. Ecological effects of sediment bypass tunnels. In R. M. Boes, editor, *1st International Workshop on Sediment Bypass Tunnels*, pages 147–156. VAW-Mitteilung 232, ETH Zürich, Switzerland, 2015. (pages 10 and 11)

E. J. Martín, M. Doering, and C. T. Robinson. Ecological effects of SBT operations on a residual river: Solis SBT case-study. In T. Sumi, editor, *2nd International Workshop on Sediment Bypass Tunnels*, page FP21. Kyoto University, Kyoto, Japan, 2017. (page 10)

T. Mizuyama, M. Nonaka, and N. Nonaka. Observation of sediment discharge rate using a Hydrophone. *Japan Society of Erosion Control Engineering*, 49(4):34–37, 1996. (in Japanese). (page 20)

T. Mizuyama, M. Nonaka, and M. Fujita. Sediment measurement with a hydrophone at Tsuno-ura Karyu sabo dam in the Joganji River. *Japan Society of Erosion Control Engineering*, 55(3):56–59, 2002. (in Japanese). (page 20)

T. Mizuyama, M. Matsuoka, and M. Nonaka. Bedload measurement by acoustic energy with hydrophone for high sediment transport rate. *Japan Society of Erosion Control Engineering*, 61(1):35–38, 2008. (in Japanese). (page 21)

T. Mizuyama, J. B. Laronne, M. Nonaka, T. Sawada, Y. Satofuka, M. Matsuoka, S. Yamashita, Y. Sako, S. Tamaki, M. Watari, et al. Calibration of a passive acoustic bedload monitoring system in japanese mountain rivers. In *Bedload-surrogate monitoring technologies*, volume 5091, pages 296–318. US Department of the Interior, US Geological Survey, 2010a. (pages 18, 19, 20, 35, 44, and 97)

T. Mizuyama, A. Oda, J. B. Laronne, M. Nonaka, and M. Matsuoka. Laboratory tests of a Japanese pipe geophone for continuous acoustic monitoring of coarse bedload. In *Bedload-surrogate monitoring technologies*, volume 5091, pages 319–335. US Department of the Interior, US Geological Survey, 2010b. (pages 19, 20, 35, and 40)

K. M. Møen, J. Bogen, J. F. Zuta, P. K. Ade, and K. Esbensen. Bedload measurement in rivers using passive acoustic sensors. In *Bedload-surrogate monitoring technologies*, volume 5091, pages 336–351. US Department of the Interior, US Geological Survey, 2010. (pages 22, 23, 35, and 78)

G. L. Morris and J. Fan. *Reservoir sedimentation handbook: design and management of dams, reservoirs, and watersheds for sustainable use.* McGraw Hill Professional, 1998. (page 7)

B. Müller and M. Walker. The Pfaffensprung sediment bypass tunnel: 95 years of experience. In R. M. Boes, editor, *1st International Workshop on Sediment Bypass Tunnels*, pages 247–258. VAW-Mitteilung 232, ETH Zürich, Switzerland, 2015. (page 10)

N. Nakajima, Y. Otsubo, and Y. Omoto. Abrasion and corrective measures of a sediment bypass system at Asahi Dam. In R. M. Boes, editor, *1st International Workshop on Sediment Bypass Tunnels*, pages 21–32. VAW-Mitteilung 232, ETH Zürich, Switzerland, 2015. (pages 10, 12, 76, and 80)

H. Nakatani. Statistical bed load analysis of small-scale floods based on hydrophone observation. *Japan Society of Erosion Control Engineering*, 61(5):4–11, 2009. (in Japanese). (page 21)

S. Narusawa and H. Nishimoto. Outline and present of Matsukawa Dam redevelopment project. In T. Sumi, editor, *2nd International Workshop on Sediment Bypass Tunnels*, page FP26. Kyoto University, Kyoto, Japan, 2017. (page 10)

C. Oertli and C. Auel. Solis sediment bypass tunnel: First operation experiences. In R. M. Boes, editor, *1st International Workshop on Sediment Bypass Tunnels*, pages 223–233. VAW-Mitteilung 232, ETH Zürich, Switzerland, 2015. (page 10)

M. Okano. *An Application of Reservoir Sediment Discharge Technology to Reservoir Sedimentation Management.* PhD thesis, Kyoto University, 2005. (in Japanese). (page 7)

J. Quiñonero-Candela and C. E. Rasmussen. A unifying view of sparse approximate gaussian process regression. *Journal of Machine Learning Research*, 6(12):1939–1959, 2005. (page 59)

C. E. Rasmussen and H. Nickisch. Gaussian processes for machine learning (GPML) toolbox. *Journal of machine learning research*, 11(Nov):3011–3015, 2010. (pages 59 and 81)

C. E. Rasmussen and C. K. I. Williams. *Gaussian Processes for Machine Learning*, volume 38. The MIT Press, Cambridge, MA, USA, 2006. (pages 50, 56, and 78)

I. Reid, J. T. Layman, and L. E. Frostick. The continuous measurement of bedload discharge. *Journal of Hydraulic Research*, 18(3):243–249, 1980. (page 17)

S. C. Reid, S. N. Lane, J. M. Berney, and J. Holden. The timing and magnitude of coarse sediment transport events within an upland, temperate gravel-bed river. *Geomorphology*, 83(1-2):152–182, 2007. (pages 18 and 22)

D. Rickenmann. Bedload transport measurements with geophones, hydrophones and underwater microphones (passive acoustic methods). In D. Tsutsumi and J. B. Laronne, editors, *Gravel bed rivers and disasters*, pages 185–208, 2017a. (page 19)

D. Rickenmann. Bed-load transport measurements with geophones and other passive acoustic methods. *Journal of Hydraulic Engineering*, 143(6):03117004, 2017b. (pages 18, 19, 22, 33, and 39)

D. Rickenmann and B. W. McArdell. Continuous measurement of sediment transport in the Erlenbach stream using piezoelectric bedload impact sensors. *Earth Surface Processes and Landforms: The Journal of the British Geomorphological Research Group*, 32(9):1362–1378, 2007. (page 18)

D. Rickenmann, J. M. Turowski, B. Fritschi, A. Klaiber, and A. Ludwig. Bedload transport measurements at the Erlenbach stream with geophones and automated basket samplers. *Earth Surface Processes and Landforms*, 37(9):1000–1011, 2012. (pages 19, 35, and 97)

D. Rickenmann, J. M. Turowski, B. Fritschi, C. Wyss, J. Laronne, R. Barzilai, I. Reid, A. Kreisler, J. Aigner, H. Seitz, et al. Bedload transport measurements with impact plate geophones: comparison of sensor calibration in different gravel-bed streams. *Earth Surface Processes and Landforms*, 39(7):928–942, 2014. (pages 19, 23, and 35)

D. Rickenmann, G. Antoniazza, C. R. Wyss, B. Fritschi, and S. Boss. Bedload transport monitoring with acoustic sensors in the Swiss Albula mountain river. In *Proc. IAHS*, volume 375, pages 5–10, 2017. https://doi.org/10.5194/piahs-375-5-2017. (page 22)

D. L. Roth, E. E. Brodsky, N. J. Finnegan, D. Rickenmann, J. M. Turowski, and A. Badoux. Bed load sediment transport inferred from seismic signals near a river. *Journal of Geophysical Research: Earth Surface*, 121(4):725–747, 2016. (page 23)

M. Rucka and K. Wilde. Application of continuous wavelet transform in vibration based damage detection method for beams and plates. *Journal of Sound and Vibration*, 297(3-5):536–550, 2006. (pages 42 and 77)

T. Sakurai and K. Kobayashio. Operations of the sediment bypass tunnel and examination of the auxiliary sedimentation measure facility at Miwa Dam. In R. M. Boes, editor, *1st International Workshop on Sediment Bypass Tunnels*, pages 33–44. VAW-Mitteilung 232, ETH Zürich, Switzerland, 2015. (page 10)

J. C. Schmidt and P. R. Wilcock. Metrics for assessing the downstream effects of dams. *Water Resources Research*, 44(4), 2008. (page 2)

M. Schwalt and W. H. Hager. Die strahlbox (the jetbox). *Schweizer Ingenieur und Architekt*, 110(27-28):547–549, 1992. (in German). (page 26)

M. B. Singer. Transient response in longitudinal grain size to reduced gravel supply in a large river. *GeophysicalResearch Letters*, 37(18), 2010. (page 2)

S. Stephane and W. Hwang. Singularity detection and processing with wavelets. *IEEE transactions on information theory*, 38(2):617–643, 1992. (page 78)

T. Sumi. Reservoir sedimentation database and selecting suitable sediment management options in Japan. In *Proc. 81st ICOLD Annual Meeting*, pages 1717–1727, Seattle, USA, 2013. (page 8)

T. Sumi. Comprehensive reservoir sedimentation countermeasures in Japan. In R. M. Boes, editor, *1st International Workshop on Sediment Bypass Tunnels*, pages 1–20. VAW-Mitteilung 232, ETH Zürich, Switzerland, 2015. (page 10)

T. Sumi and S. A. Kantoush. Comprehensive sediment management strategies in Japan: Sediment bypass tunnels. In *Proc. 34th IAHR World Congress*, pages 1803 – 1810, Brisbane, Australia, 2011. Engineers Australia. (page 2)

T. Sumi, M. Okano, and Y. Takata. Reservoir sedimentation management with bypass tunnels in Japan. In *Proc. 9thInternational Symposium on River Sedimentation*, pages 1036–1043, Yichang, China, 2004. (pages 3, 7, 8, 9, and 10)

T. Sumi, S. A. Kantouch, and S. Suzuki. Performance of Miwa Dam sediment bypass tunnel: Evaluation of upstream and downstream state and bypassing efficiency. In *Proc. 24th ICOLD Congress*, pages 576–596, Kyoto, Japan, 2012. (page 10)

H. Suzuki, T. Kinjo, Y. Hayashi, M. Takemoto, K. Ono, and Y. Hayashi. Wavelet transform of acoustic emission signals. *Journal of acoustic emission*, 14:69–84, 1996. (page 41)

T. Suzuki, H. Mizuno, N. Osanai, R. Hirasawa, and Y. Hasegawa. Basic study on sediment rate measurement with a hydrophone on the basis of sound pressure data. *Japan Society of Erosion Control Engineering*, 62(5):18–26, 2010. (in Japanese). (page 21)

T. Suzuki, T. Uchida, A. Okamoto, K. Takahashi, S. Yamashita, Y. Kosuge, and A. Fukumoto. Applicability of bedload observation method using sound pressure data obtained by a hydrophone. *Japan Society of Erosion Control Engineering*, 66 (1):4–14, 2013. (in Japanese). (page 21)

H. Takeuchi, K. Ishida, M. Hayashi, and C. Wakahara. Monitoring scheme for sediment bypass tunnel at Koshibu Dam. In T. Sumi, editor, *2nd International Workshop on Sediment Bypass Tunnels*, page FP6. Kyoto University, Kyoto, Japan, 2017. (page 10)

S. Taniguchi, Y. Itakura, K. Miyamoto, and J. Kurihara. A new acoustic sensor for sediment discharge measurement. In J. Bogen, D. E. Walling, and T. J. Day, editors, *Erosion and sediment transport monitoring in river basins*, pages 135–142, Oslo, Norwahy, 1992. IAHS Publication No. 210. (pages 20, 35, and 61)

TATA & HOWARD. A History of Dams: From Ancient Times to Today, 2019. URL https://tataandhoward.com/2016/05/a-history-of-dams-from-ancient-times-to-today/. (page 1)

P. D. Thorne. Laboratory and marine measurements on the acoustic detection of sediment transport. *The Journal of the Acoustical Society of America*, 80(3):899–910, 1986. (page 78)

A. G. Tsakiris, A. T. N. Papanicolaou, and T. J. Lauth. Signature of bedload particle transport mode in the acoustic signal of a geophone. *Journal of Hydraulic Research*, 52(2):185–204, 2014. (pages 18, 22, and 35)

T. Tsunoda, K. Sano, O. Tsuneoka, and T. Morioka. Acceleration signal characteristics for loose part impact. *Journal of Nuclear Science and Technology*, 23(11):968–978, 1986. (page 34)

D. Tsutsumi, R. Hirasawa, T. Mizuyama, M. Shida, and M. Fujita. Bed load observation in a mountainous watershed by hydrophone equipments. Technical report, Annuals of Disaster Prevention Research Institute, Kyoto University, 2010. (in Japanese). (page 19)

D. Tsutsumi, M. Fujita, and M. Nonaka. Transport measurement with a horizontal and a vertical pipe microphone in a mountain stream: taking account of particle saltation. *Earth Surface Processes and Landforms*, 43(5):1118–1132, 2018. (page 20)

T. Uchida, A. Okamoto, S. Hayashi, T. Suzuki, A. Fukumoto, S. Yamashita, and S. Tagata. Hydrophone observations of bedload transport in mountainous rivers of japan. *Advanced river sediment research*, pages 1749–1796, 2013. (page 20)

M. Uher and P. Beneš. Measurement of particle size distribution by the use of acoustic emission method. In *2012 IEEE International Instrumentation and Measurement Technology Conference Proceedings*, pages 1194–1198. IEEE, 2012. (page 34)

D. Vischer, W. H. Hager, C. Casanova, B. Joos, P. Lier, and O. Martini. Bypass tunnels to prevent reservoir sedimentation. In *Proc. 19th ICOLD Congress*, pages 605–624, Florence, Italy, 1997. (page 8)

A. Wilson and H. Nickisch. Kernel interpolation for scalable structured gaussian processes (kiss-gp). In *International Conference on Machine Learning*, pages 1775–1784, 2015. (page 59)

C. R. Wyss, D. Rickenmann, B. Fritschi, J. M. Turowski, V. Weitbrecht, and R. M. Boes. Laboratory flume experiments with the Swiss plate geophone bed load monitoring system: 1. Impulse counts and particle size identification. *Water Resources Research*, 52(10):7744–7759, 2016a. (pages 19, 23, 34, 35, 78, and 97)

C. R. Wyss, D. Rickenmann, B. Fritschi, J. M. Turowski, V. Weitbrecht, and R. M. Boes. Measuring bed load transport rates by grain-size fraction using the swiss plate geophone signal at the Erlenbach. *Journal of Hydraulic Engineering*, 142(5): 04016003, 2016b. (page 19)

A. Zheng and A. Casari. *Feature engineering for machine learning: principles and techniques for data scientists.* O'Reilly Media, Inc., 2018. (page 33)

Appendix A

Analysis with conventional impulses

This appendix gives the number of impulses observed at the Koshibu SBT operations. Except for `Op8`, `IP1` to `IP5` output impulses successfully for all operations.

In addition, the transported sediment volume at each operation is also exhibited here. These volumes were computed from the number of impulses on the basis of data obtained by the on-site experiment section 4.1.3. Here, we briefly explain the obtained formula to convert impulses to transported sediment volume at the Koshibu SBT. Considering the following findings, we made eq. (A.1) with water discharge Q and impulses I_{ps}^{1024} chosen as the explanatory variables: impulses I_{ps}^{1024} increases as bedload transport rate increases Mizuyama et al. (2010a); Rickenmann et al. (2012); impulses I_{ps}^{1024} decreases as discharge Q increases as the probability that gravels jump over the plate increases Koshiba et al. (2018); Wyss et al. (2016a).

$$\frac{I_{ps}^{1024}}{V_s} = 6.4 \times 10^4 \cdot Q^{-0.98}. \tag{A.1}$$

Hence, the sediment volume transported in a unit time goes as follows:

$$V_s = r_p \sum_{\text{Plate}} \frac{I_{ps}^{1024}}{6.4 \times 10^4 \cdot Q^{\text{-}0.98}}, \tag{A.2}$$

where r_p is the reciprocal of the ratio of the total plates width to the tunnel width, r_p = 2.7 at the Koshibu Dam SBT, the sum total is for five IPs.

The relation between accurate sediment volume and the predicted one with using eq. (A.2) is shown in fig. A.1.

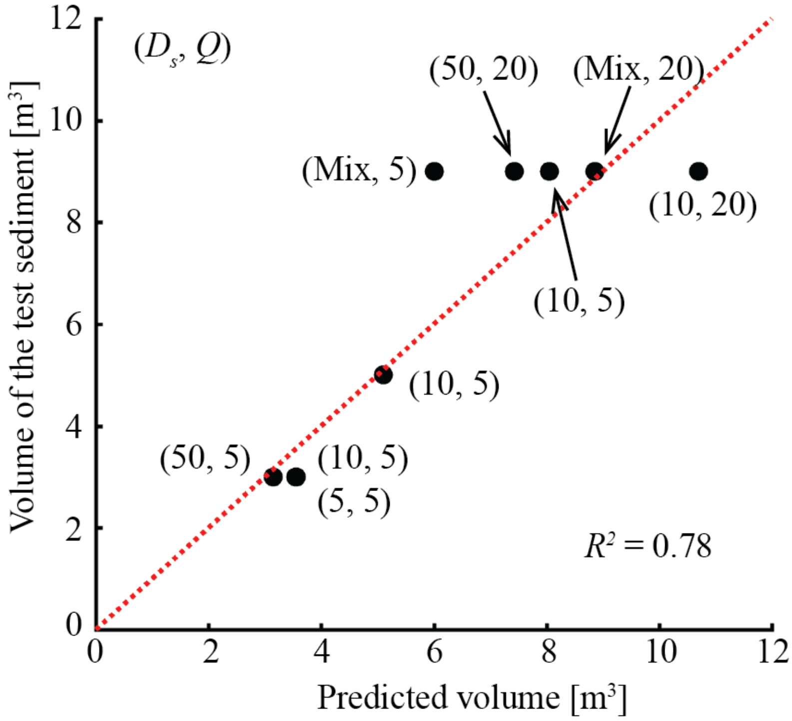

Fig. A.1 The accurate and predicted sediment volume using conventional impulses in the on-site experiments. Each point data is plotted with discharge Q and grain size D_s .

Information on every operation consists of three figures. The top one is temporal I_{ps}^{1024} for `IP1` to `IP5`. The numbers depicted on the left side are corresponding with the IP numbers (see, fig. 4.4(a)). These figures exhibit, aside the temporal information, the spacial sediment distribution along the width direction. The middle figure shows the number of impulses with five amplification factors I_{ps}^{4}, I_{ps}^{16}, I_{ps}^{64}, I_{ps}^{256}, I_{ps}^{1024} obtained from `IP3`, and the bypassed discharge Q_{bypass}. The predicted accumulated bedload transport rate by eq. (A.2) is given in the bottom figure.

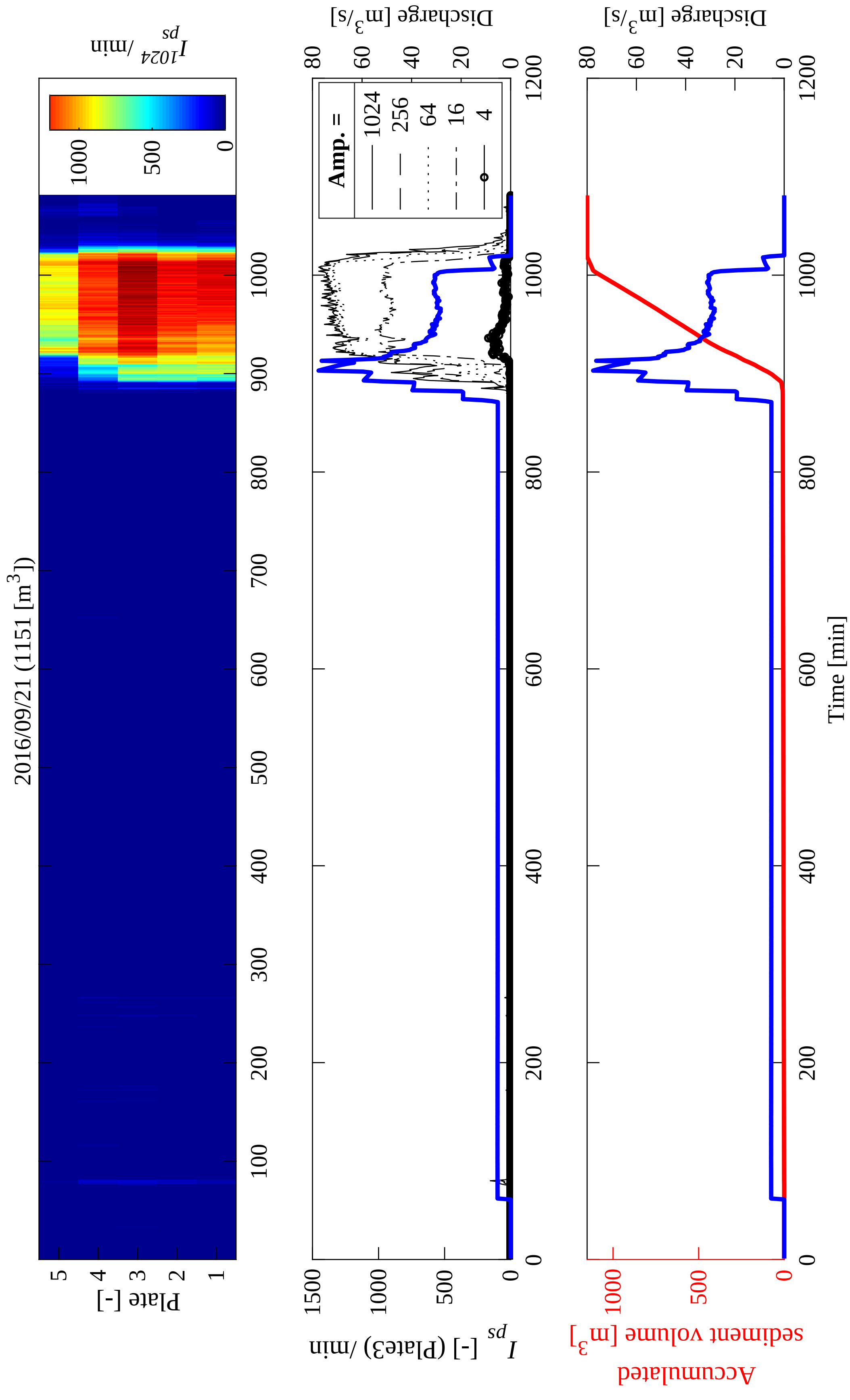

Fig. A.2 The Koshibu Dam SBT operation 1

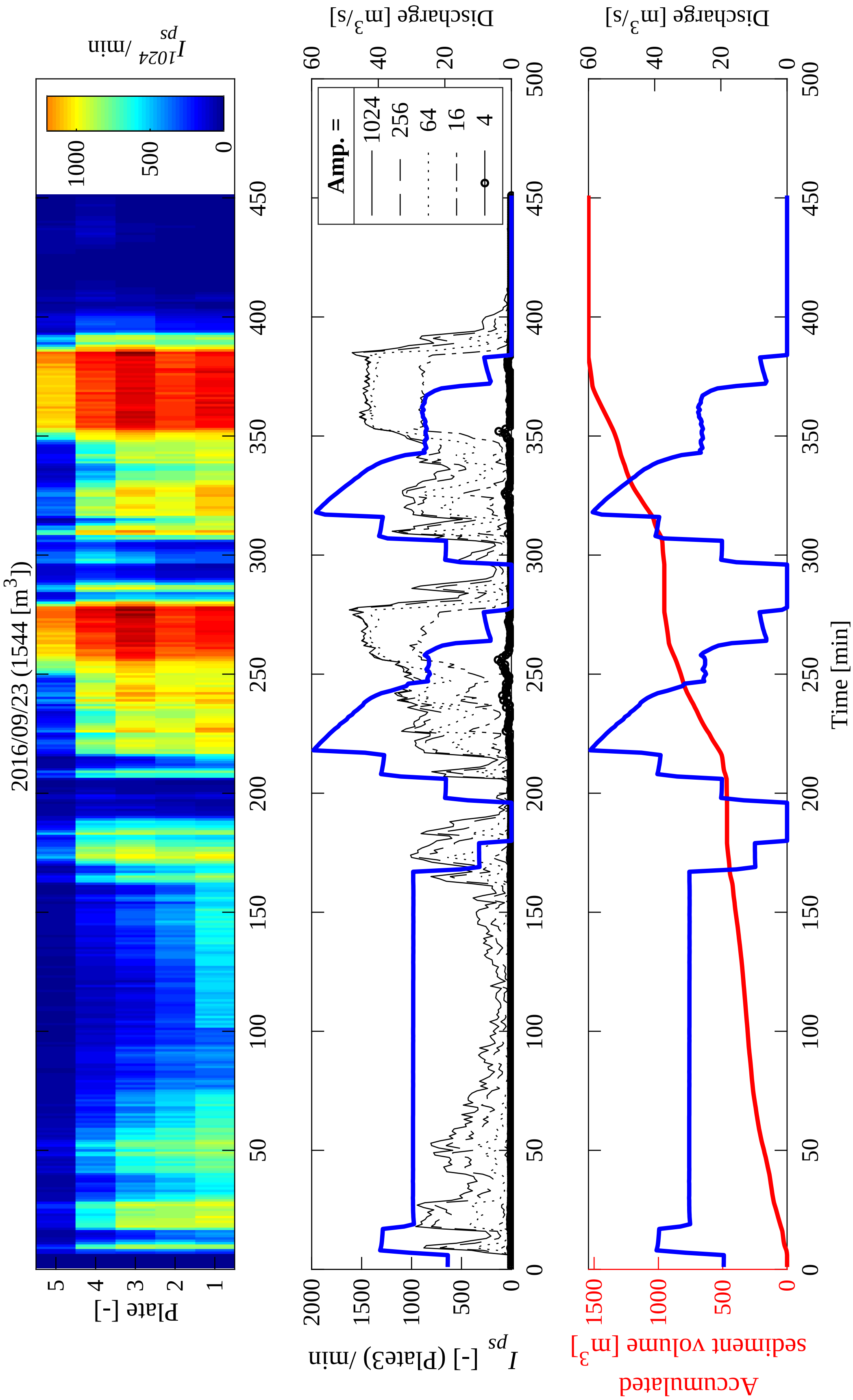

Fig. A.3 The Koshibu Dam SBT operation 2

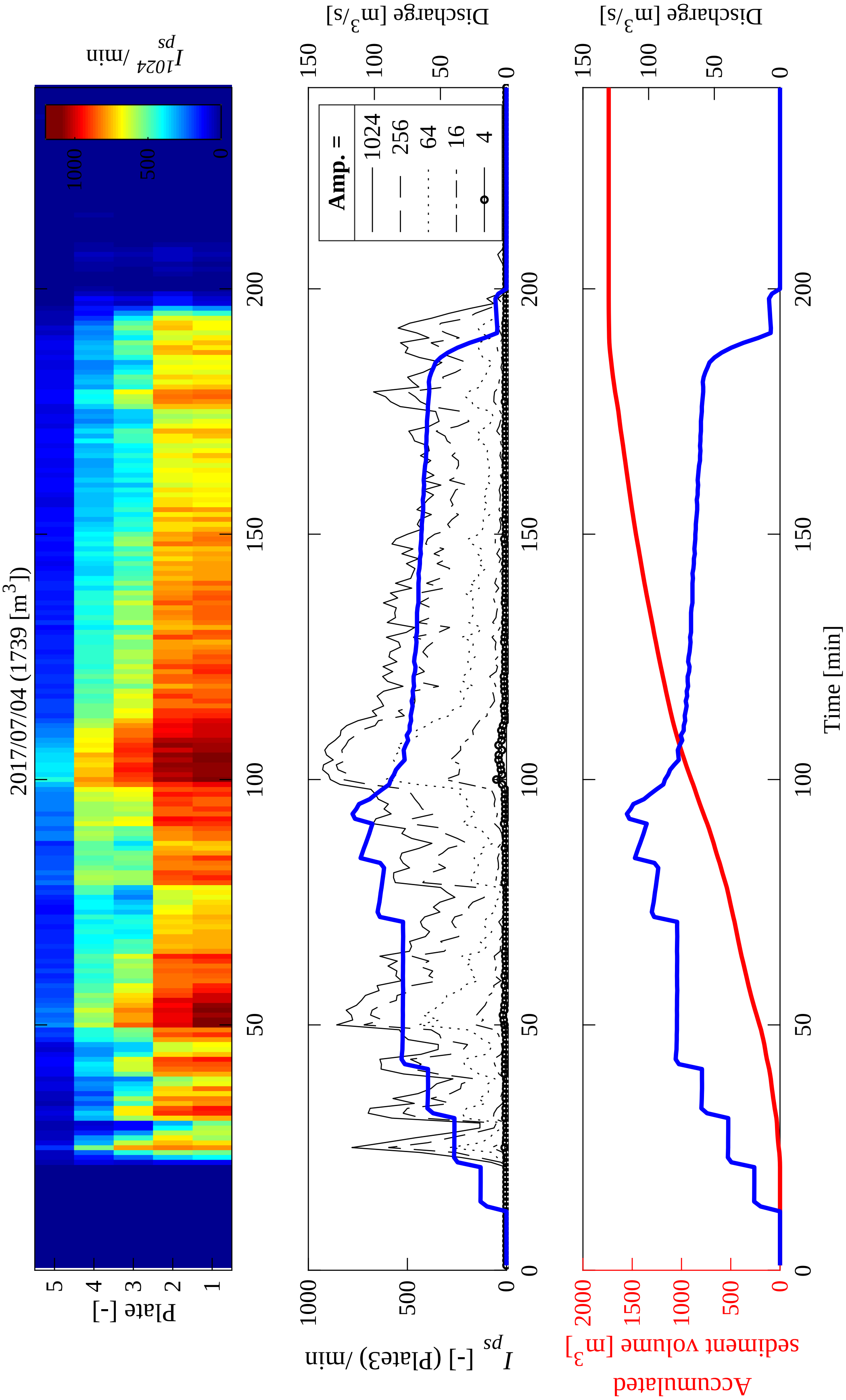

Fig. A.4 The Koshibu Dam SBT operation 3

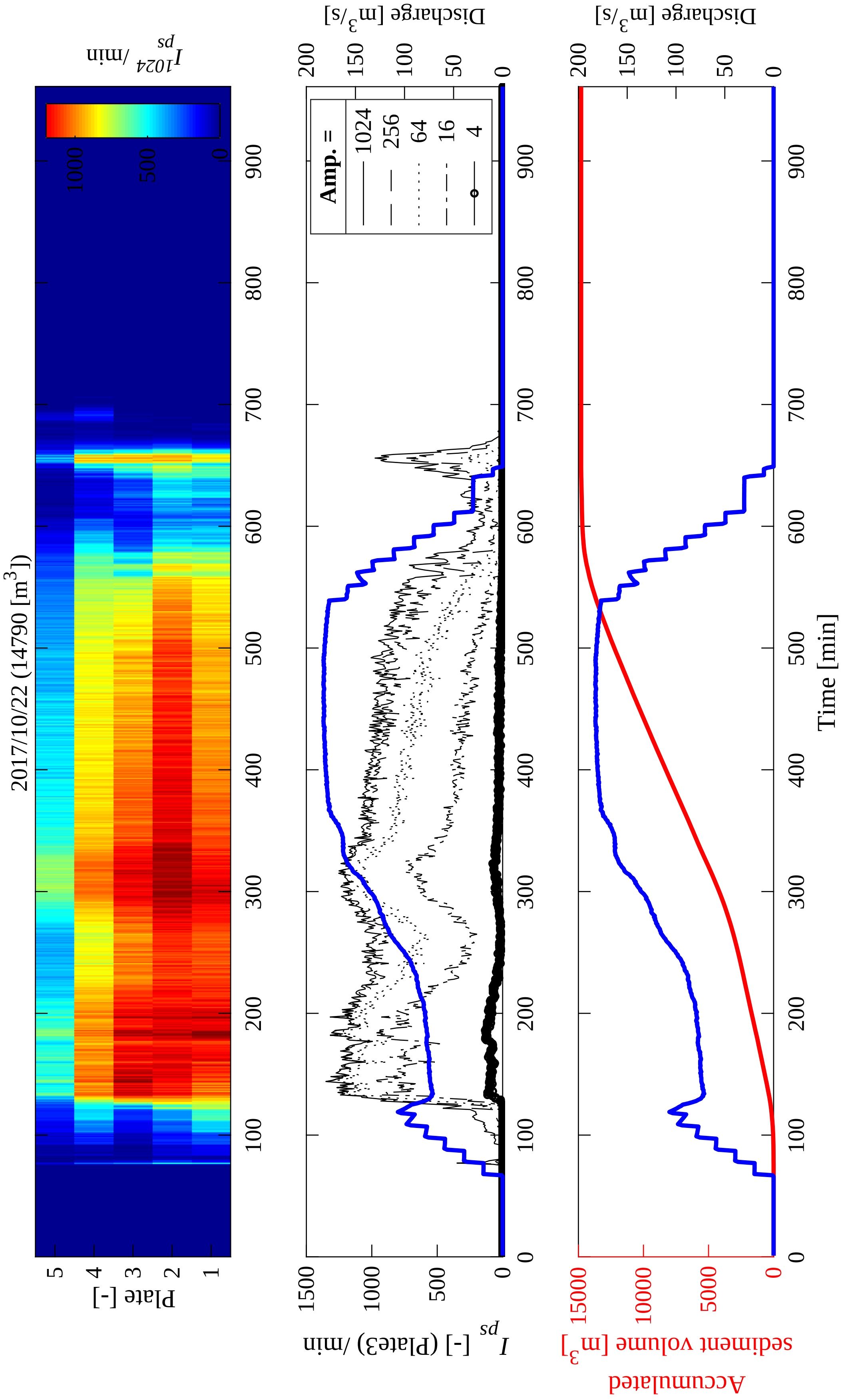

Fig. A.5 The Koshibu Dam SBT operation4

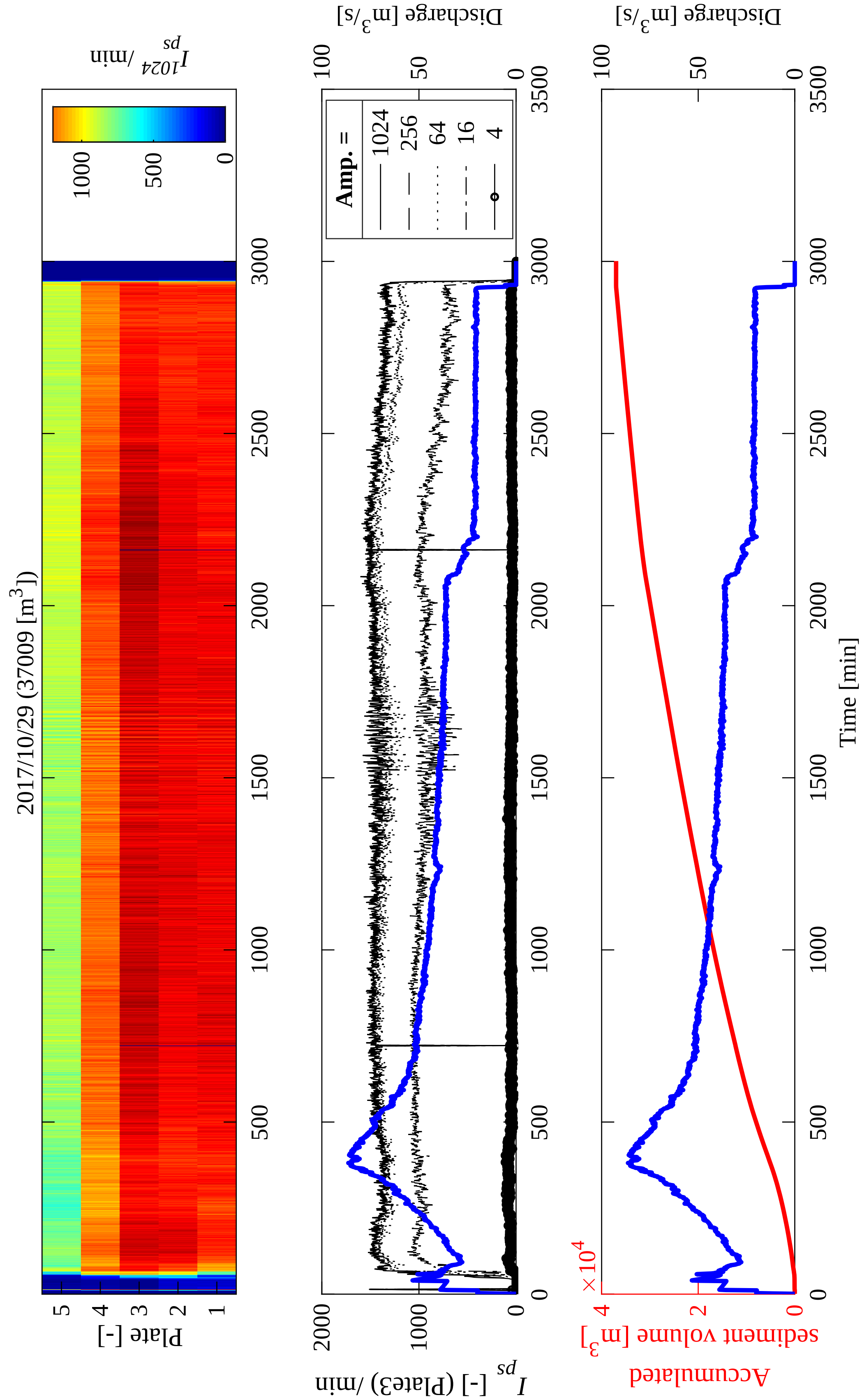

Fig. A.6 The Koshibu Dam SBT operation 5

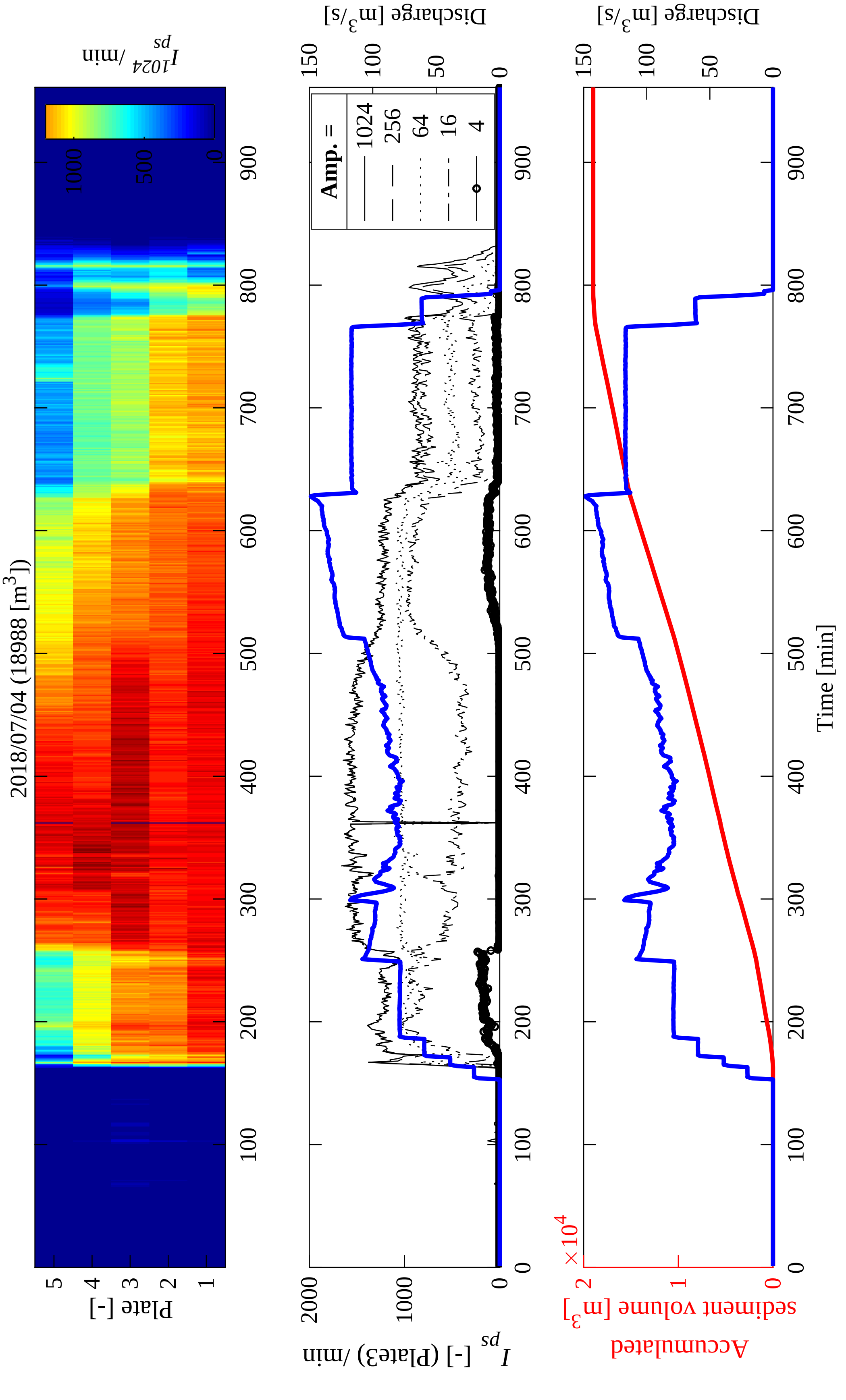

Fig. A.7 The Koshibu Dam SBT operation 6

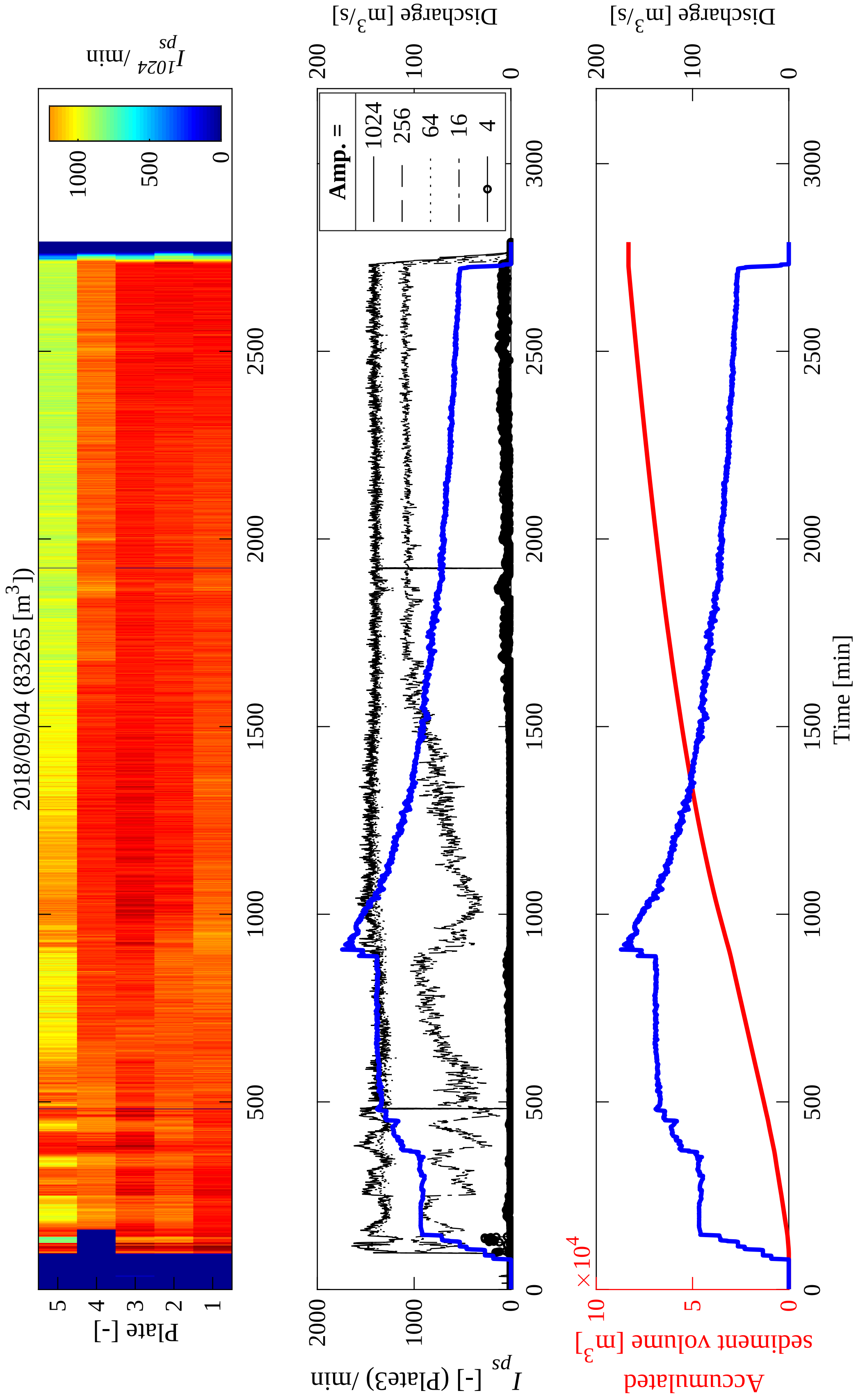

Fig. A.8 The Koshibu Dam SBT operation 7

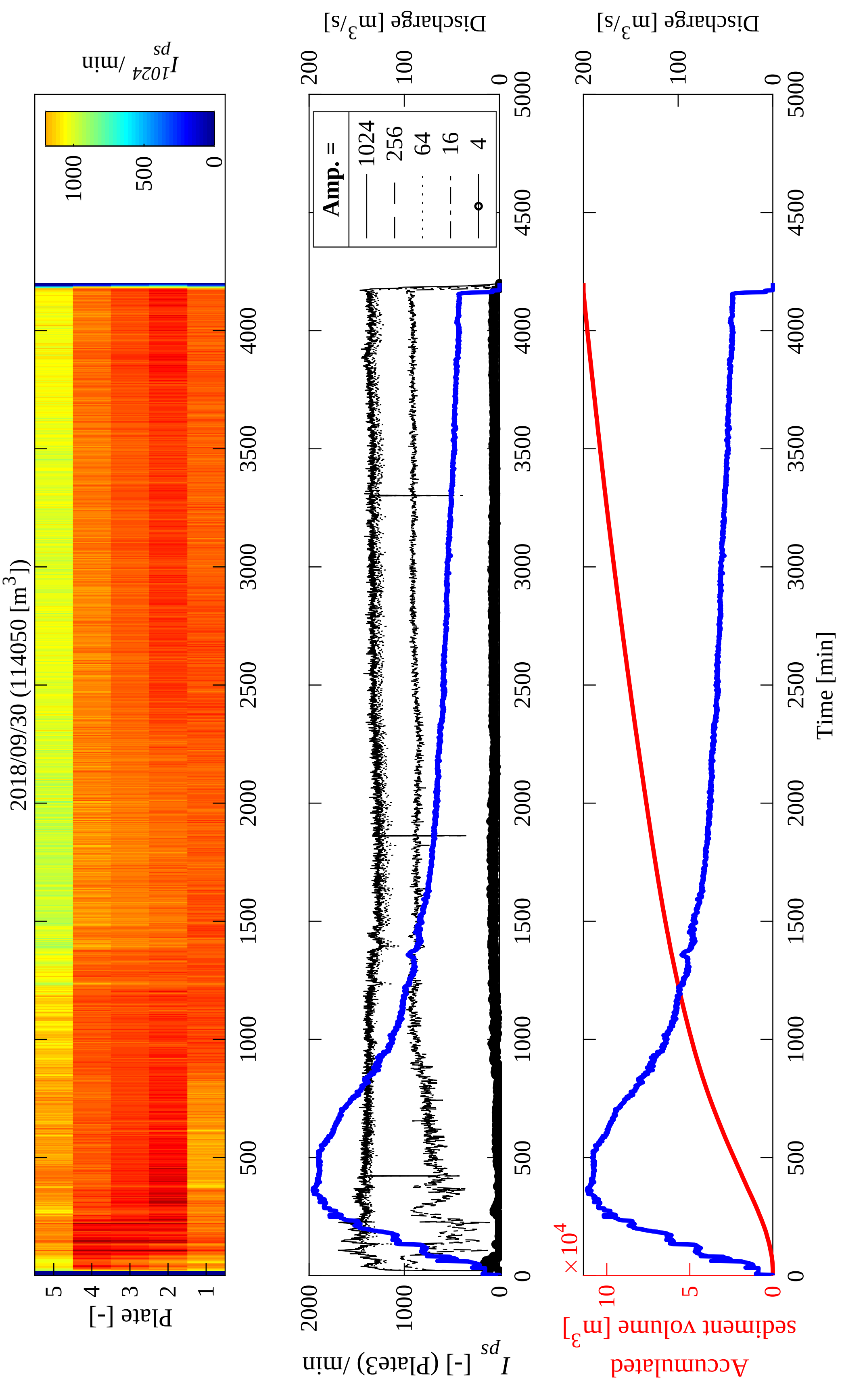

Fig. A.9 The Koshibu Dam SBT operation 8